Dissertation

submitted to the
Combined Faculties for the Natural Sciences and for Mathematics
of the Ruperto-Carola University of Heidelberg, Germany
for the degree of

Doctor of Natural Sciences

presented by
Diplom-Chemikerin Maria Knaub
Born in: Luganskoje (Russia)
Oral-examination: 11th September 2019

Molecular downstream mechanisms of the oncogenic transcriptional regulators YAP/TAZ in hepatocarcinogenesis

Referees:
Prof. Dr. Ralf Bartenschlager
Prof. Dr. Kai Breuhahn

Table of Contents

List of Abbreviations

A	
AACR	American Association for Cancer Research
ABCA1	ATP binding cassette subfamily A member 1
aCGH	array comparative genomic hybridization
AEC	3-amino-9-ethylcarbazole
AMOT	α-catenin and Angiomotin
APOC3	apolipoprotein C3
AR	androgen receptor
ASH	alcoholic steatohepatitis
B	
BMI	body mass index
BrdU	5-bromo-2’-deoxyuridine
C	
Cas	CRISPR-associated
CCNB1	cyclin B1
CDC	cell division cycle
CDK	cyclin dependent kinases
CDT1	chromatin licensing and DNA replication factor 1
CEC	capillary endothelial cell
ChIP	chromatin-immunoprecipitation
CIN	Chromosome instability
CMG	CDC45, MCM2-7, and GINS complex
Col1A1	collagen type I alpha 1 chain
CREB	cAMP responsive element binding protein
CRISPR	clustered regularly interspaced short palindromic repeats

CSC	cancer stem cell
CTGF	connective tissue growth factor
CYR61	cysteine-rich angiogenic inducer 61
D	
DDK	Dbf4-dependent kinase
DZNep	3-Deazaneplanocin A
E	
E2F1	E2F transcription factor 1
ECM	extracellular matrix
EED	embryonic ectoderm development
EZH1	enhancer of zeste 1 polycomb repressive complex 2 subunit
EZH2	enhancer of zeste 2 polycomb repressive complex 2 subunit
F	
FDA	Food and Drug Administration
FDR	false discovery rate
FOXM1	forkhead box M1
G	
GASL	German Association of the Study of the Liver
GINS	GINS complex subunit 1-4
GPCR	G-protein coupled receptors
H	
H3K27me3	trimethylation of lysine 27 of histone H3
HBV	hepatitis B virus
HCC	hepatocellular carcinoma
HCV	hepatitis C virus
Hpo	Hippo

I

IBF	Interfakultäre Biomedizinische Forschungseinrichtung
IHC	Immunohistochemistry
IPA	Ingenuity Pathway Analysis

L

LAP	liver activator protein
LATS1/2	large tumor suppressor kinases 1 and 2
LSEC	liver sinusoidal endothelial cells

M

Mats	mob as tumor suppressor
MCM	minichromosome maintenance complex component
MOB1	Mps one binder kinase activator-like 1
MST1/2	mammalian Ste20-like kinases 1 and 2

N

NAFLD	non-alcoholic fatty liver disease
NASH	non-alcoholic steatohepatitis
NF-κB	nuclear factor kappa B
NF2	neurofibromatosis 2
NTC	nonsense siRNA

O

ORC	origin recognition complex subunit

P

PBS	phosphate buffered saline
PcG	polycomb group
PCR	polymerase chain reaction
PD-1	programmed cell death protein-1
PHx	partial hepatectomy

PMSF	phenylmethylsulfonyl fluorid
POLY	polyprotein;protein F
PRC	polycomb repressive complex
pre-RC	pre-replicative complex
PTPN	protein tyrosine phosphatase non-receptors
Q	
qPCR	semi-quantitative real-time PCR
R	
RBBP4	RB binding protein 4, chromatin remodeling factor
RBBP7	RB binding protein 7, chromatin remodeling factor
RPL41	ribosomal protein L41
RT	RevertAid H Minus Reverse Transcriptase
S	
Sav	salvador
SAV1	salvador family WW domain-containing protein 1
Sd	scalloped
SDS-PAGE	SDS-polyacrylamide gel electrophoresis
sgRNA	single-guide RNA
siRNA	RNA interference
SUZ12	suppressor of zeste 12 polycomb repressive complex 2 subunit
T	
TAZ	transcriptional co-activator with PDZ-binding motif
TBS	Tris-buffered saline
TEAD	TEA domain transcription factor
TERT	telomerase reverse transcriptase
TMA	tissue microarray
TP53	p53 gene

tTA	tetracycline transactivator
V	
VEGF	vascular endothelial growth factor
W	
WT	wildtype
Wts	warts
Y	
YAP	yes-associated protein
YAPS127A	S127A-mutated YAP
Yki	yorkie
Ø	untreated

List of Figures

List of Tables

Summary

Cancer is worldwide the leading cause of death in the 21st century. Liver cancer represents the fourth most common cancer with hepatocellular carcinoma (HCC) being the most frequent primary liver cancer. HCC is the second most common cause of cancer-related deaths with a 5-year survival rate below 12% in the US. These sobering numbers illustrate the need for bio-medical research to identify novel target structures and to develop respective therapeutic strategies. The evolutionarily conserved Hippo signaling pathway is frequently deregulated in human hepatocarcinogenesis. Indeed, overexpression of the transcriptional co-activators yes-associated protein (YAP) and transcriptional co-activator with PDZ-binding motif (TAZ) is associated with pro-proliferative and anti-apoptotic effects in liver tumor cells. However, among the identified direct YAP/TAZ target genes, no functional groups or protein families have been described, which facilitate the biological properties of YAP and TAZ in HCC cells. Since these groups may represent relevant molecular hubs that mediate the tumor-supporting properties of the Hippo pathway, this study aimed to define YAP/TAZ-regulated protein families, which may represent promising therapeutic target structures.

Based on comprehensive transcriptome analysis after siRNA-mediated inhibition of YAP and TAZ in HCC cells, the *minichromosome maintenance* (MCM) protein family, which is crucial for DNA replication, and members of the *polycomb repressive complex 2* (PRC2), which inserts epigenetic repression marks (trimethylation of histone H3; H3K27me3), were identified as YAP and/or TAZ target genes. For the MCM family members (MCM2-7), different molecular approaches confirmed the direct transcriptional regulation *via* YAP/TAZ and the transcription factor TEA domain transcription factor 4 (TEAD4) in independent liver cancer lines. In contrast, the PRC2 components *Enhancer Of Zeste 2* (EZH2) and *Suppressor Of Zeste 12 Protein Homolog* (SUZ12) were predominantly regulated by YAP and TEAD4. Functionally, RNAi-mediated MCM reduction as well as YAP and TAZ perturbations decreased cell proliferation *in vitro*. Additionally, YAP induces the expression of PRC2 components and their epigenetic mark H3K27me3 *in vitro*, leading to the repression of target gene transcription. In a YAP-dependent HCC mouse model (inducible expression of constitutively active $YAP^{S127A)}$) a clear positive association between YAP overexpression and especially abundance of MCM family members confirmed the *in vitro* results. Statistical correlations between tumor progression, YAP expression and MCM2-7, EZH2, and SUZ12 abundance in primary patient tissues supported the hypothesis that both protein groups are cooperatively induced by YAP and TEAD4 in human HCC.

Together, these results illustrate that the Hippo pathway contributes to tumor progression *via* the regulation of protein groups that induce biological functions. The transcriptional regulation of MCM helicase by the Hippo pathway introduces a promising surrogate marker for YAP driven proliferation. Furthermore, YAP induced transcription of PRC2 members illustrates a new

possibility of YAP mediated gene silencing and offers a novel approach to understand oncogenic Hippo/YAP feedback loops. Interestingly, both YAP and TAZ are important for the regulation of all MCM family members, while data for PRC2 constituents point to a predominant role of YAP. This differential dependency of target genes might represent a molecular mechanism of how the Hippo pathway regulates specific biological processes, as epigenetic changes and replication. This is of special importance since direct perturbation of the Hippo/YAP/TAZ-axis could also inhibit pro-regenerative properties (e.g. proliferation), which might be of relevance for patients with chronically damaged livers. Thus, targeting these important downstream hubs could represent one strategy to selectively impair YAP and/or TAZ-dependent HCC cell functionality while saving physiological hepatocellular proliferation in regenerative livers, which could maintain residual liver function. Still, further studies are needed to test if MCM proteins and PRC2 are suitable points-of-interference in HCC patients with YAP and/or TAZ activation.

Zusammenfassung

Weltweit sind Krebserkrankungen die häufigste Todesursache im 21. Jahrhundert. Die vierthäufigste Krebsart ist Leberkrebs, wobei das Hepatozelluläre Karzinom (*hepatocellular carcinoma;* HCC) der häufigste primäre Leberkrebs ist. Außerdem ist das HCC weltweit die zweithäufigste krebsbedingte Todesursache mit einer 5-Jahres-Überlebensrate von unter 12 % in den USA. Diese ernüchternden Zahlen verdeutlichen die Notwendigkeit neue therapeutische Strategien zu entwickeln. Hierzu müssen zunächst relevante Zielstrukturen identifiziert werden. In der humanen Hepatokarzinogenese liegt der evolutionär konservierte Hippo-Signalweg häufig dereguliert vor, wobei die Überexpression der transkriptionellen Co-Aktivatoren yes-associated protein (YAP) und Transcriptional Co-Activator With PDZ-Binding Motif (TAZ) mit pro-proliferativen und anti-apoptotischen Effekten in Lebertumorzellen einhergehen. Bisher wurden keine funktionellen Gruppen oder Proteinfamilien unter den identifizierten direkten Zielgenen beschrieben, die die biologischen Eigenschaften von YAP und TAZ in HCC-Zellen vermitteln. Da diese Gruppen relevante molekulare Knotenpunkte bei der Vermittlung tumorunterstützenden Eigenschaften des Hippo-Signalwegs darstellen können, war es das Ziel dieser Studie vielversprechende therapeutische Zielstrukturen unter den YAP/TAZ-regulierten Proteinfamilien zu definieren.

Basierend auf einer umfassenden Transkriptomanalyse, nach siRNA-vermittelter Reduktion von YAP und TAZ in HCC-Zellen, wurden zwei Proteinfamilien als YAP- und/oder TAZ-Zielgene identifiziert. Der für die DNA-Replikation relevante *minichromosome maintenance* (MCM)-Komplex wurde durch YAP, TAZ und den Transkriptionsfaktor *TEA Domain Transkriptionsfaktor 4* (TEAD4) transkriptionell reguliert, was durch verschiedene molekularbiologische Methoden in unabhängigen HCC-Zelllinien bestätigt wurde. Weiterhin wurden die Mitglieder des *polycomb repressive complex 2* (PRC2), der epigenetische Repressionsmarkierungen (Trimethylierung des Histons H3; H3K27me3) einfügt, überwiegend durch YAP und TEAD4 reguliert

Funktionell führte die RNAi-vermittelte MCM-Reduktion, sowie die YAP- und TAZ-Reduktion, zu einer verringerten Zellproliferation *in vitro*. Darüber hinaus induziert YAP die Expression der PRC2-induzierten epigenetischen Markierung H3K27me3 *in vitro* und unterdrückt so potentiell die Transkription der Zielgene. In einem YAP-abhängigen HCC-Mausmodell (induzierbare Expression von konstitutiv aktivem YAP^{S127A}) bestätigte sich eine klare Assoziation zwischen YAP-Überexpression und vor allem einer erhöhten Konzentration an MCM-Familienmitgliedern. Statistische Korrelationen zwischen dem Tumorwachstum, der YAP-Expression und der Überexpression von MCM2-7 und den PRC2 Komponenten *Enhancer Of Zeste 2* (EZH2) und *Suppressor Of Zeste 12 Protein Homolog* (SUZ12) unterstützten die Hypothese, dass beide Proteingruppen im humanen HCC durch YAP induziert werden.

Gemeinsam zeigen diese Ergebnisse, dass der Hippo-Signalweg durch die Regulation ganzer Proteinfamilien zur Tumorprogression beiträgt. Die transkriptionelle Regulation der MCM-Helikase durch den Hippo-Signalweg stellt einen vielversprechenden Marker für die YAP-abhängige Proliferation dar. Darüber hinaus ist die YAP-induzierte Transkription von PRC2-Komponenten ein neuer Modus der YAP-vermittelten Genrepression und bietet einen Ansatz zur Untersuchung potentieller onkogener Hippo/YAP-Feedback-Mechanismen. Interessanterweise sind sowohl YAP als auch TAZ für die Regulierung aller MCM-Familienmitglieder wichtig, während Daten für die PRC2-Komponenten auf eine dominante Rolle von YAP hinweisen. Diese unterschiedliche Abhängigkeit von Zielgenen könnte einen molekularen Mechanismus des Hippo-Signalwegs darstellen um spezifische biologische Eigenschaften in verschiedenen Zellphasen zu regulieren. Dieses Wissen ist von besonderer Bedeutung, da eine direkte Perturbation der Hippo/YAP/TAZ-Signalachse auch regenerative Eigenschaften beeinflusst, welche essentiell für Patienten mit chronisch geschädigten Lebern sein können. Somit könnte die Fokussierung auf diese wichtigen nachgelagerten Knotenpunkte eine mögliche Strategie darstellen, um selektiv die YAP- und/oder TAZ-abhängige onkogene HCC-Zellfunktionalität zu beeinträchtigen und gleichzeitig die physiologische hepatozelluläre Proliferation in regenerativen Lebern zu erhalten. Dennoch sind weitere Studien erforderlich, um zu testen, ob MCM-Proteine und PRC2 geeignete therapeutische Angriffspunkte bei HCC-Patienten mit YAP- und/oder TAZ-Aktivierung sind.

1 Introduction

1.1 Liver and Liver Cancer

1.1.1 Anatomy and Physiology of the Liver

The liver is the major metabolic organ of the human body, located in the upper right abdomen and accounts for about 2% of the body weight. It has a unique blood supply with 20-25% of oxygenated blood afflux being provided by the hepatic artery (1). The remaining 75-80% of the blood supply is provided by the hepatic portal vein, perfusing the liver with nutrient-rich blood directly from the gastrointestinal tract. Microscopically, the liver is formed by small, hexagonal lobules of 1-2 mm in diameter (2). The junctions of the lobules comprise periportal fields, which contain vessels of the portal vein, the hepatic artery, and the biliary tract. Due to this structure and the permanent contact with oxygenated and nutrient-rich blood, the liver is central for carbohydrate, protein, and lipid metabolism, substance storage (e.g. glycogen and vitamin A) and synthesis (e.g. amino acids, coagulation factors). Newly synthesized molecules are transported through the central vein located in the center of each lobule to the *vena hepatica* into the *vena cava inferior*, thereby efficiently distributed in the body (1).

In addition, the liver is the main detoxifying organ responsible for the elimination of toxic metabolites along with bile salts *via* the bile duct and the gallbladder (3). Metabolic functions are mainly mediated by hepatocytes, which account for about 60% of all liver cells. These cells are frequently binucleated, parenchymal cells and play a key role in carbohydrate, lipoprotein, and cholesterol metabolism (2). Nonparenchymal cells include capillary endothelial cells (CECs), liver sinusoidal endothelial cells (LSECs), Kupffer cells, and stellate cells. CECs and LSECs separate hepatocytes from the bloodstream and facilitate the so-called porto-central blood flow. Kupffer cells represent liver-specific macrophages and localize in the sinusoids acting as central sensors for immunogenic substances and regulators of immune responses. Lastly, hepatic stellate cells are located in the *Space of Disse* between hepatocytes and LSECs, where they produce collagen and extracellular matrix (ECM) material.

1.1.2 Pathophysiology of Liver Cancer

Epidemiology, Risk Factors, and Pathogenesis

Worldwide, cancer is the leading cause of death in the 21st century with estimated 18.1 million new cases and 9.6 million deaths in 2018. In Europe harboring only 9% of the global population, 23% of all new cancer cases were diagnosed (4). Primary liver cancer represents the fourth most common cancer and the second most common cause of cancer-related deaths worldwide with over 780,000 estimated deaths per year (4). The gender difference in liver cancer susceptibility is comparable to other tumor entities with a 2-fold higher incidence in men than in women (4).

The most frequent primary liver cancer diagnosis with 75-85% of all cases is hepatocellular carcinoma (HCC), developing in most cases from hepatocytes, while only 10-15% represent intrahepatic cholangiocarcinoma mainly arising from cholangiocytes of the biliary tree (4). About 90% of all HCCs develop on the basis of fibrosis and cirrhosis due to chronic liver damage (5). The reasons for this permanent insult are diverse and include infections with viruses, alcohol abuse, hereditary diseases, uptake of mycotoxins, non-alcoholic steatohepatitis (NASH), obesity and type 2 diabetes.

Chronic hepatitis upon hepatitis B (HBV) and C virus (HCV) infection accounts for 50% and 30% of all global HCC cases, respectively, most of them located in high-risk countries in Asia and Africa (5). The developement of HBV vaccines reduced infection rates upon mass vaccination in Asia followed by reduced HCC rates (6). However, a HCV vaccine does not exist, but novel Food and Drug Administration (FDA)-approved strategies for the treatment of patients with chronic HCV infections have been developed since 2013. These modern 'direct antiviral agents' target several aspects of virus biology including its replication (e.g. by sofosbuvir) and the activity of viral proteins such as polyprotein;protein F (POLY) (e.g. by ledipasvir). Clinical studies showed a 90% response rate, which led to the expectation that this multi-modal drug cocktail will reduce the incidence of chronic HCV hepatitis and HCV-associated HCC development in the future (7). In Western countries, alcoholic steatohepatitis (ASH) and non-alcoholic fatty liver disease (NAFLD) followed by NASH are the most frequent underlying diseases for HCC development with increasing incidence (8). In addition, there are several other risk factors leading to cirrhosis and HCC such as type 2 diabetes and obesity (Figure 1), which increase the risk to develop HCC about 1.8 to 4-fold and 1.5 to 4-fold (9).

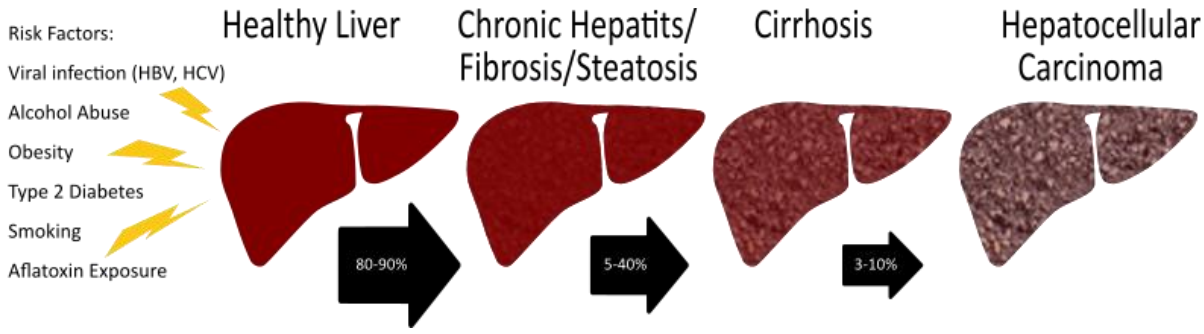

Figure 1: Schematic illustration of hepatocarcinogenesis.
The scheme illustrates the progression from risk factor exposure over chronic liver disease and cirrhosis to HCC development. The arrows indicate the percentage of patients progressing to the next pathological stage over time (10).

Pathogenesis of liver cancer is a multi-step and long-lasting process starting with prolonged exposure to risk factors, which leads to chronic diseases such as chronic virus hepatitis, ASH or NAFLD/NASH. Over months and years, continuous cycles of liver damage (hepatocellular damage and apoptosis) and regeneration (hepatocellular proliferation) could eventually result in cirrhosis (11). It is characterized by the excess formation of fibrous connective tissue (fibrosis)

separating regenerating nodules and thereby perturbating blood flow and normal liver function. HCCs arising on the basis of cirrhosis are characterized by chronic inflammation, one of the hallmarks of cancer (12). During inflammation, activated stellate and infiltrating immune cells produce pro-inflammatory cytokines, which could enhance hepatocellular proliferation. This leads to replicative stress, shortening of telomeres and genomic instability causing precancerous lesions and eventually tumor formation (12). It is assumed that replicative stress, usually defined as replication fork stalling induced by oncogenes or dysfunction of DNA-damage checkpoint, interferes with regulatory pathways, which control the timing and progression of the replication machinery (13). However, the exact mechanisms are not fully understood yet. Permanent cell division is the basis for an accumulation of genetic mutations and chromosomal alterations, promoting the outgrowth of hepatocytes with abnormal proliferating capacities and resulting in dysplastic nodules as well as malignant transformation (12).

Treatment Options and Prognosis

Liver cancer presents as the second leading cause of cancer-related deaths worldwide with mortality to incidence ratio of 0.95 (14). The 5-year overall survival rate for a patient diagnosed with HCC in the US is below 12%, emphasizing the need for improvement in current therapy (5). The established treatment options for HCC can be grouped into three approaches: surgical intervention, percutaneous treatment, and pharmaceutical drugs. The surgical approach includes tumor resection and liver transplantation, which is limited by organ availability and severity of the patient's liver damage. It is so far the only curative approach, increasing the 5-year survival rate of early-stage HCC patients to 75% (5). The second treatment option can reduce tumor load by percutaneous interventions, which includes ethanol injection, radiofrequency or thermal ablation and transarterial interventions (embolization, chemoperfusion, or chemoembolization). Until now, systemic pharmaceutical approaches for the first-line treatment of HCC comprises of two FDA-approved therapies (sorafenib and lenvatinib). The SHARP trial illustrated that the first established multikinase inhibitor sorafenib prolonged the average survival of HCC patients by about 3 months (10.7 months with drug vs. 7.7 months with placebo) (15). A decade later the REFLECT trial demonstrated that the tyrosine-kinase inhibitor lenvatinib showed comparable effects on median overall survival (13.6 months with lenvatinib vs. 12.3 months with sorafenib) (16). Recently other systemic therapies have been FDA-approved, as second-line treatment in patients with disease progression after sorafenib treatment. Besides the multi-kinase inhibitor regorafenib (15) and the tyrosine-kinase inhibitor cabozantinib (17), which perturbates c-MET, VEGFR1/2/3, FLT3, and c-KIT, the programmed cell death protein-1 (PD-1) immune checkpoint inhibitor nivolumab (18) is the first attempt targeting viral related HCC. However, all these therapies only moderately improve the overall survival of HCC patients, which illustrates the need to develop alternative therapeutic approaches.

1.1.3 Molecular Carcinogenesis of HCC

Molecular Classification

HCCs are characterized by a high genetic and phenotypic heterogeneity, partly due to a diverse etiology, late diagnosis, and complexity of hepatocyte function (19). In order to understand the underlying mechanisms in distinct HCC subgroups and to identify subgroups of patients who may benefit from targeted therapies, intense research was done on the molecular classification of HCCs. During tumorigenesis, genetic and epigenetic alterations are frequently observed, which results in deregulated expression of oncogenes and tumor suppressor genes (19). The most frequent mutations found in HCCs are activating mutations in the gene promoter of the *telomerase reverse transcriptase* (TERT) enzyme (20). In about 30-60% HCC cases, these mutations lead to the re-expression of TERT providing cells with indefinite proliferative capacity by circumventing DNA damage checkpoint-induced senescence.

A well-accepted scheme to classify HCCs was published by Boyault et al. in 2007, using a 16 gene-signature to cluster HCCs with distinct molecular and functional features (21). A further characterization was performed in 2017 by Calderaro et al., investigating 343 HCC samples by pathological assessment, immunohistochemistry, gene expression profiling, and DNA sequencing (22). Based on these data, HCCs can be clustered in even more subgroups (G1-G6) with molecular, biological and clinical characteristics (Figure 2).

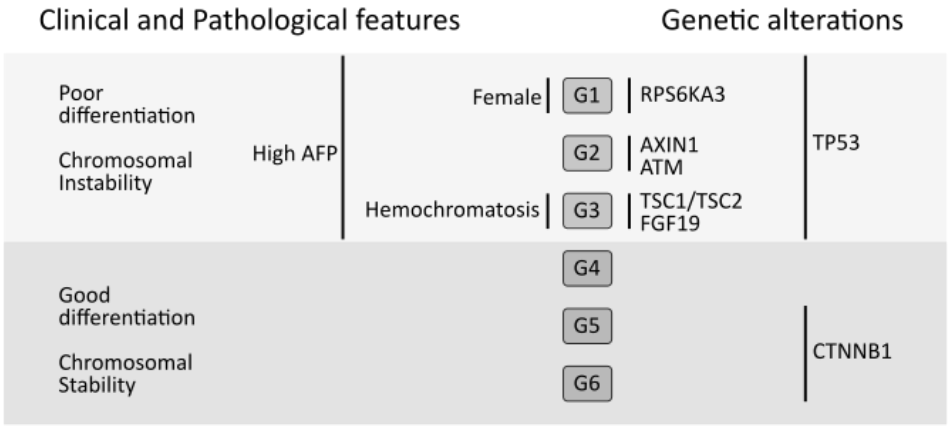

Figure 2: Molecular classification of HCC.
Scheme modified after Calderaro et al. classifying HCCs groups (22).

The G1/G2/G3-groups are characterized by high cell proliferation, chromosomal instability, poor tumor differentiation, and the presence of p53 mutations. In 18-50% of all HCC cases, gene mutations in the p53 gene (TP53) were found, prohibiting the induction of cell cycle arrest and apoptosis upon DNA damage (20). Similar effects can be observed upon upregulation of the p53 inhibitor MDM2 or gene silencing of the tumor suppressor p16/CDKN2/INK4A (23). HCCs grouped G4/G5/G6 show better differentiation, do not exhibit p53 mutations and show less cell proliferation as well as chromosomal stability.

In detail, G1 is characterized by high serum AFP levels, female gender and integration of HBV DNA in low copy number. HCCs clustered in that group showed activation of MAP kinase and PI3K/AKT pathway. Mutated RAS family members have been rarely described in HCC, but recent studies showed copy number gains and overexpression of key genes as *B-Raf* and *H-ras* (24). In addition, dysregulation of PI3K signaling leads to permanently activated Akt, which is linked to deregulation of cell growth and differentiation as well as poor prognosis and sorafenib resistance (25). Since this pathway is upregulated in 40-50% of all HCC cases, drugs targeting the PI3K/Akt/mTOR pathway are currently tested in phase I clinical trials (25). G2 tumors show a high copy number of integrated HBV DNA and also PI3K/Akt/mTOR pathway activation.

The G3 subgroup has the worst prognosis due to the association with macrotrabecular-massive HCC-subtype and enhanced vascular invasion. Tumor recurrence and poor prognosis coincide with increased circulating Vascular Endothelial Growth Factor (VEGF) levels, which induce physiological and pathological angiogenesis. During HCC development pathological angiogenesis results in abnormal vascular invasion providing a nutrition rich and hypoxic microenvironment and therefore facilitating therapy resistance, cell proliferation, and tumor growth (26). Recent data indicate that dysregulation of the so-called Hippo pathway, which is associated with chromosomal instability and worse clinical outcome, is especially detectable in G1 and G3 (27).

G4 is a heterogeneous subgroup of tumors including inflammatory and steohepatitic subtype, arising on the basis of fibrotic or cirrhotic livers. This process is associated with elevated infiltration of immune cells and activation of the nuclear factor kappa B (NF-κB) signaling pathway in tumor cells, which induces proliferation and cell cycle progression via activation of cyclin D1 (28). G5 and G6 clustered HCCs show a high rate of activating β-catenin mutations, the third most frequent HCC driver mutation, which leads to Wingless-Type MMTV Integration Site (Wnt) pathway activation. The Wnt-signaling pathway plays an important role in cell differentiation during embryogenesis, cell proliferation, and tumorigenesis. Wnt activation results in nuclear β-catenin accumulation, which is associated with the acquirement of stemness characteristics, high proliferation rate and immortality of HCC cells (11).

1.2 Hippo Pathway

1.2.1 Structure and Regulation of the Hippo Pathway

Hippo Pathway in *Drosophila melanogaster* and Mammals

The Hippo signaling pathway is an evolutionarily highly conserved signaling pathway and has key functions in the regulation of cell proliferation and tissue homeostasis, as first demonstrated in *Drosophila melanogaster* and subsequently in mammals. The first member described in this pathway was the kinase warts (Wts) in 1995, which was identified in a genetic mosaic screen for regulators of tissue growth in *Drosophila melanogaster* (29). Mutational inactivation of *Wts* led to hyperproliferation and overgrowth e.g. of the compound eye, the wing blades, and the wing discs (29). Similar phenotypes were observed for mutations in other pathway constituents such as *hippo* (Hpo), *salvador* (Sav) and *mob as tumor suppressor* (Mats) (30-32). The discovery of the transcriptional co-activator yorkie (Yki) as a negatively regulated downstream effector of the Hippo pathway in 2005 illustrated how the pathway affects the transcriptional machinery (33). Indeed, Yki overexpression and its subsequent interaction with the transcription factor *scalloped* (Sd) showed the same phenotype as observed for Hippo pathway component inactivation such as uncontrolled tissue overgrowth (34).

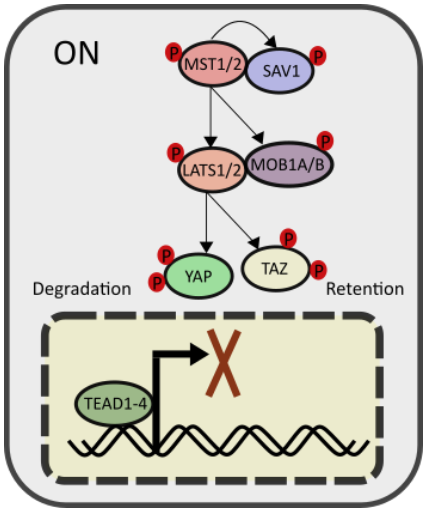

Figure 3: Scheme of the mammalian Hippo pathway.
Activation of the Hippo pathway is characterized by sequential phosphorylation of Mst1/2 and Lats1/2, which leads to phosphorylation of YAP/TAZ and their nuclear exclusion. In contrast, inactivation of the Hippo pathway is associated with the inactive non-phosphorylated form of Mst1/2, Lats1/2, and successive de-phosphorylation of YAP and TAZ. Hypo-phosphorylated YAP and TAZ translocate into the nucleus, where they bind to transcription factors (e.g. TEAD family members) and initiate the transcription of pro-proliferative and anti-apoptotic target genes.

In mammals, the core kinase cassette of the Hippo pathway is composed of two serine-threonine kinases mammalian Ste20-like kinases 1 and 2 (MST1/2; Hippo homologs) and large tumor suppressor kinases 1 and 2 (LATS1/2; Warts homologs), which physically interact with the scaffolding proteins Salvador family WW domain-containing protein 1 (SAV1; Salvador homolog) and Mps one binder kinase activator-like 1A and 1B (MOB1; Mats homologs), respectively (35). Following Hippo pathway activation (Figure 3), MST1/2 facilitate the phosphorylation of SAV1 and MOB1 leading to the recruitment and phosphorylation of LATS1/2. Consequently, the activated kinases LATS1/2 phosphorylate the mammalian orthologues of Yki, Yes-associated protein (YAP) and transcriptional co-activator with PDZ-binding motif (TAZ; also called WWTR1;

paralogue of YAP), at 5 and 4 serine/threonine sites, respectively (36). Especially, phosphorylation at S127 in YAP and S89 in TAZ create 14-3-3 protein-specific binding sites, which prevent YAP and TAZ from being translocated into the nucleus. Additionally, polyphosphorylation is associated with polyubiquitination and proteasomal degradation of both factors, as was reported for S381 (YAP) and S311 (TAZ) phosphorylation (30).

Vice versa, inactivation of the pathway is associated with the hypophosphorylation of YAP/TAZ as well as their nuclear translocation and induction of transcription. Since YAP and TAZ lack specific DNA binding sites, the interaction with transcription factors is needed to facilitate their biological responses. So far, a couple of YAP/TAZ-interacting transcription factors have been described. However, most target genes are regulated by TEA domain transcription factor (TEAD; Scalloped homologs) family members, which makes the YAP/TEAD interaction an interesting target structure for the development of anti-cancer drugs (34, 37). Beside the well-characterized target genes, *connective tissue growth factor* (CTGF) and c*ysteine-rich angiogenic inducer 61* (CYR61), additional downstream effectors involved in proliferation and cell growth have been described, including *forkhead box M1* (FOXM1), *cyclin B1* (CCNB1) and *minichromosome maintenance complex component* (MCM) 2 (38). But, how exactly YAP and TAZ regulate complex processes such as proliferation and organ growth remains poorly understood. In addition, it is not sufficiently elucidated whether the Hippo/YAP/TAZ signaling pathway directly mitosis-related proteins.

Regulation of Hippo Pathway Activity

The Hippo pathway and the subcellular localization of YAP/TAZ are regulated by various cell-autonomous and external stimuli. Interestingly, no distinct ligand/receptor combination has been described that affect the Hippo/YAP/TAZ axis. Instead, cell-cell contacts, interaction with the ECM and cell polarity represent key regulators of this pathway (Figure 4). In this context, cell contact inhibition has been linked to Hippo pathway activity in cell culture models, where nuclear exclusion of YAP/TAZ and Hippo core kinase cassette activation was gradually observed with increasing cell density (39). Cell polarity and cell contact proteins belong to the most potent activators of the Hippo pathway that stimulate LATS1/2 phosphorylation, as well as binding of YAP and TAZ, thereby preventing nuclear translocation. Many upstream regulators of the Hippo pathway are part of adherence junctions (e.g. E-cadherin) and tight junctions (e.g. claudins). Proteins involved in adherence and tight junctions such as *protein tyrosine phosphatase non-receptors* (PTPN), α-catenin and Angiomotin (AMOT), circumvent the Hippo core kinase cassette by sequestrating YAP/TAZ and thereby repressing their transcriptional activity (35). Moreover, the known tumor suppressor *neurofibromatosis 2* (NF2) links cytoskeletal components with membrane proteins and affects Hippo pathway activity. In this case, NF2 associates with the cytoplasmic phosphoprotein Kibra activating the Hippo core kinase cassette by recruiting LATS1/2 to the plasma membrane (40). The cell density-based

activity of YAP/TAZ is not only regulated by junctional proteins, but also by changes in ECM composition. It was reported that Rho-GTPase signaling affects YAP/TAZ localization by combining cell density effects with G-protein coupled receptors (GPCR) signaling, upon growth factor or hormone activation (41).

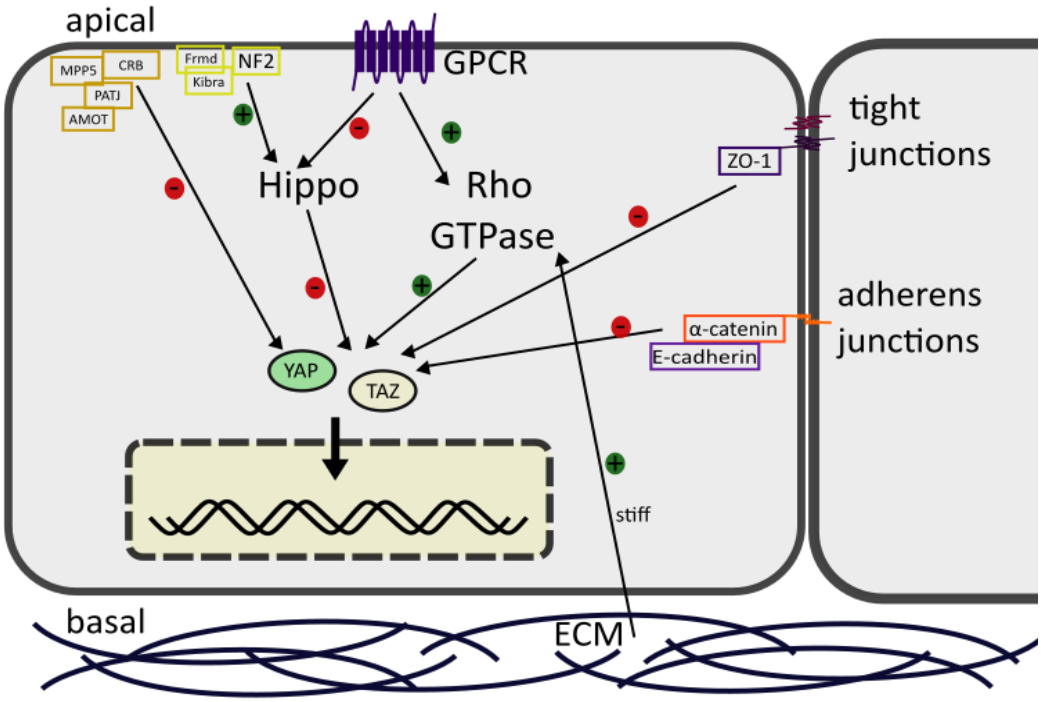

Figure 4: Complex upstream regulation of the Hippo pathway.
Several intrinsic and extrinsic signals regulate the subcellular localization of YAP and TAZ. Cell polarity complexes, e.g. tight junctions, adherence junctions, and Crumbs complex, directly bind YAP/TAZ to the cell membrane. Extracellular matrix (ECM) composition and GPCR signaling transmit extracellular signals via RhoGTPase or Hippo signaling.

1.2.2 The Role of the Hippo Pathway in Cell Proliferation

The functional relevance of the Hippo pathway in embryonic development has been widely studied using different mouse models. It has been shown that mice with systemic TAZ knockout are viable but suffer from diseases resembling human polycystic kidneys and pulmonary emphysema (42). In contrast, systemic YAP knockdown results in embryonic lethality with signs of developmental perturbations as shortened body axis and failure of chorioallantoic fusion (43). These results suggest that YAP and TAZ are not redundant but have independent functions in embryonic development. Interestingly, the homozygous knockouts of upstream Hippo pathway components such as Lats2 (44), Mob1 (45), Sav1 (46), and Mst1/2 (47) also cause an embryonic lethality. In addition, these data illustrate that organ- or even cell-type-specific mouse models are required for a detailed analysis of Hippo/YAP/TAZ pathway constituents under different conditions.

Consistently with *in vitro* data, the liver-specific and inducible knockout of MST1/2 in newborns led to increased proliferation and tissue overgrowth, which resulted in tumor formation after 6

months (48). Interestingly, these mice showed increased nuclear YAP accumulation due to reduced phosphorylation and elevated protein levels. In contrast, reduced phosphorylation and overall protein levels had no effects on the nuclear presence of TAZ (49). This suggests that YAP plays a more important role in the induction of proliferation in the liver than TAZ. The relevance of YAP on mitosis has been confirmed using inducible and liver-specific overexpression of S127A-mutated YAP (YAP^{S127A}), which cannot be phosphorylated and therefore efficiently translocates into the nucleus. Mutant hyperactive YAP expression in murine hepatocytes induced proliferation of cells with a so-called oval cell phenotype and led to increased cell number and hepatomegaly (4-5-fold increase of liver size) (50). Withdrawal of YAP^{S127A} reversed the phenotype by reducing cell number suggesting the activation of intrinsic control mechanisms (50). Interestingly, the effects of Hippo deregulation on organ size had only slight effects on other organs in mice (48). Furthermore, YAP also controls liver growth under regenerative conditions. Following partial hepatectomy (PHx), a living organ donation in humans or a mouse model, organ size is restored within 8-15 days in humans and 5-7 days in mice, by increased proliferation of differentiated liver cells (51). Indeed, PHx led to an induction of YAP activation and decreased MST1/2 and LATS1/2 phosphorylation, which returned to basal levels as soon as the livers regained its original size (52). These results illustrate the relevance of a functionally intact Hippo/YAP pathway signaling in embryogenesis and under regenerative conditions in mammalian livers.

The Hippo/YAP Pathway in Cancer/HCC

A hallmark of cancer is the capability of cells to evade growth suppression, which results in unlimited proliferation (53). Due to the central role of the Hippo/YAP pathway in the regulation of cell proliferation, its oncogenic and tumor-supporting properties have been discussed for many different cell-types and organs.

Dysregulation of several Hippo pathway components has been observed in different tumor entities. For example, down-regulation of LATS1/2 and MST1/2 was found in lymphoblastic leukemia (54), HCC (49) and soft tissue sarcomas (55). Reduced expression of the scaffolding protein MOB1 has been reported in nonsmall cell lung cancer (56) and colorectal cancer (57), which correlated with worse clinical outcome. Interestingly, genomic mutations of Hippo pathway components, like genomic deletions or loss-of-function mutations in *NF2*, *LATS1/2*, and *MST1/2*, are rare and have only been observed in meningiomas, schwannomas, and mesotheliomas (58). In contrast, epigenetic modifications affecting Hippo pathway constituents occur already in pre-cancerous lesions and lead to altered gene expression in different tumor types. Exemplarily, the hypermethylation of CpG-islands in *MST1/2* and *LATS1/2* promoter regions resulted in reduced gene expression in human soft tissue sarcomas (55) and aggressive breast cancers (59).

In contrast to the frequent mutations within the Hippo core-cassette, epigenetic or genetic changes of the pathway effectors YAP and TAZ are rare. Amplifications of the YAP locus at 11q22 are hypothesized to be driving mutations, which have been identified in few esophageal cancers and HCC (60). However, alterations in the phosphorylation pattern and subcellular localization of YAP and TAZ are observed more frequently among different tumor types. High YAP levels were reported in multiple tumor entities, including ovarian, lung, prostate cancer, and HCC (61, 62). Furthermore, reduced YAP phosphorylation was ascertained in 70% of all human HCCs and correlated with reduced MST1/2 activity (49). In contrast, nuclear TAZ accumulation was only observed in 20% of analyzed breast cancer patients (63). This either reflects minor biological relevance of TAZ or a scientific focus on YAP-mediated downstream signaling. Nevertheless, YAP and TAZ have been discussed to be involved in the regulation of stemness and evading apoptosis. For example, TAZ protein levels were elevated in isolated cancer stem cells (CSC) (64), which was corroborated by enforced TAZ overexpression in oral cancer cells conferring CSC-like properties (65). Knock-down of YAP in different human cancer cell lines reduced the proliferative capacities of tumor cells and increased DNA damage-induced apoptosis (66).

The dysregulation of Hippo signaling and overexpression of YAP or TAZ have been frequently described in the context of tumorigenesis, especially in HCCs (49) and precancerous lesions such as NASH livers (67). In order to study the mechanisms involved in Hippo pathway induced hepatocarcinogenesis different mouse models have been introduced. In 2007, the first publication of a liver-specific mouse model illustrated that long-term elevated YAP expression led to liver tumor formation (30). Short-term exposure of these ApoE/rtTA-YAP mice to Dox increased the liver size constantly but was reversible upon doxycycline withdrawal (30). Targeting the Hippo pathway, a conditional knockout mouse was generated specifically inactivating the gene for WW45 in the liver, $WW45^{flox/flox}$Albumin-Cre mice (68). Within the first three months, these mice showed only slight changes in development without a detectable malfunction of the liver. Upon aging, the transgenic mice showed expansion of oval cells and nuclear YAP accumulation in the liver. Hepatoma formation in these transgenic mice was detected at the age of 12 months, illustrating that that the Hippo pathway can limit the hyperexpansion of progenitor cells (68).

To confirm the relevance of the Hippo core kinases in HCC different MST knockout mice were generated. Homozygous liver knockout of MST1 and MST2 was lethal, whereas knockout of either MST1 or MST2 had no effects, demonstrating the redundancy of these kinases (49). Consistently, mice with only one wildtype allele of MST1 or MST2, engineered by homozygous knockout of MST1 and heterozygous knockout of MST2 or vice versa, were viable and fertile. Interestingly, these mice eventually developed highly aggressive HCCs with total MST1/2 knockout (49). The intact Hippo pathway in the surrounding liver demonstrated, that spontaneous MST1/2 deletion, equivalent to Hippo pathway inactivation, can be sufficient to

induce HCC formation.

However, the involvement of deregulated Hippo pathway components in human HCC and Hippo pathway downstream effectors responsible for tumor formation are largely unknown. Additionally, the mechanism of YAP and TAZ-induced proliferation and hepatocarcinogenesis in murine and human HCC needs to be further elucidated.

2 Objectives

Worldwide, HCC is the second most common cause of cancer-related death. However, systemic curative options are missing, yet. The Hippo pathway and its downstream effectors YAP and TAZ are critically involved in the initiation and progression of liver cancer and may therefore represent promising therapeutic target structures. Due to the fact that the Hippo/YAP/TAZ signaling axis is also essential for regenerative processes, direct targeting of YAP and/or TAZ may cause unwanted side effects, especially under conditions of chronic liver damage. For this reason, the identification of functionally relevant YAP/TAZ effector mechanisms is crucial to finding alternative and druggable target structures. These factors or protein families could be used for the development of anti-cancer therapies and minimize side effects under regenerative conditions.

Therefore, the aims of this thesis were:

- Identification of functional protein groups, which are regulated by YAP and/or TAZ.
- Description of the molecular YAP and/or TAZ-dependent mechanisms that regulate these functional groups.
- Functional characterization and comparison of identified family members.
- Verification of downstream effectors in a YAP-dependent and liver-specific HCC model.
- Confirmation of gene regulation and YAP/TAZ target genes in cohorts of HCC patients.

3 Materials

3.1 Antibodies

Table 1: Primary antibodies.

Antigen (clone)	Species	Application	Dilution	Blocking agent	Secondary dilution	Company
Actin (C4)	mouse	WB	1:10,000	BSA	1:20,000	MP Biomedicals Germany GmbH, Eschwege, Germany
EZH2 (D2C9) XP®	rabbit	IHC	1:50	-	-	Cell Signaling Technology Europe, B.V., Frankfurt am Main, Germany
		WB	1:500	BSA	1:20,000	
GAPDH	chicken	WB	1:10,000	BSA	1:20,000	Merck Millipore, Darmstadt, Germany
Histone H3 (1B1B2)	mouse	WB	1:800	BSA	1:20,000	Cell Signaling
Ki67	mouse	IHC	1:400	-	-	Dako - Agilent Technologies Sales & Services GmbH & Co. KG, Hamburg, Germany
MCM2 (D7G11) XP®	rabbit	IHC	1:500	-	-	Cell Signaling
		WB	1:2,000	BSA	1:20,000	
MCM3	rabbit	IHC	1:100	-	-	Cell Signaling
		WB	1:1,000	milk	1:20,000	
MCM4 (D3H6N) XP®	rabbit	IHC	1:100	-	-	Cell Signaling
		WB	1:1,000	milk	1:20,000	
MCM5 [EP2682Y]	rabbit	IHC	1:200	-	-	Abcam, Berlin, Germany
		WB	1:500	BSA	1:20,000	
MCM6 [EPR17686]	rabbit	IHC	1:4,000	-	-	Abcam
		WB	1:1,000	milk	1:20,000	

Antigen (clone)	Species	Application	Dilution	Blocking agent	Secondary dilution	Company
MCM7 (D10A11) XP®	rabbit	IHC	1:50	-	-	Cell Signaling
		WB	1:2,000	BSA	1:20,000	
RbAp48	rabbit	WB	1:500	milk	1:20,000	Abcam
SUZ12 (D39F6) XP®	rabbit	IHC	1:100	-	-	Cell Signaling
		WB	1:1,000	BSA	1:20,000	
TAZ (V386)	rabbit	ChIP	2 µg	-	-	Cell Signaling
		WB	1:1,000	BSA	1:20,000	
TEF-3 (N-G2)	mouse	ChIP	2 µg	-	-	SANTA CRUZ biotech., Heidelberg, Germany
Tri-Methyl-Histone H3 (Lys27) (C36B11)	rabbit	IF	1:500	-	1:300	Cell Signaling
		IHC	1:200	-	-	
		WB	1:400	BSA	1:20,000	
YAP	rabbit	WB	1:400	BSA	1:20,000	Cell Signaling
YAP (D8H1X) XP®	rabbit	ChIP	2 µg	-	-	Cell Signaling
		IHC	1:200	-	-	

Table 2: Secondary antibodies.

Antigen	Isotype	Application	Company
anti-rabbit Cy3	donkey IgG	IF	Jackson ImmunoResearch Europe Ltd., Ely, UK
IRDye 680LT anti-mouse	donkey IgG	WB	LI-COR Biosciences, Bad Homburg, Germany
IRDye 800CW anti-chicken	donkey IgG	WB	LI-COR Biosciences
IRDye 800CW anti-rabbit	donkey IgG	WB	LI-COR Biosciences

3.2 Bacteria and Supplements

- Mach1 T1R competent bacteria cells (Invitrogen Ltd, Paisley, UK)
- Ampicillin sodium salt (Sigma-Aldrich, Taufkirchen, Germany)
- LB medium pH 7.0 (1% (w/v) tryptone, 0.5% (w/v) yeast extract, 1% (w/v) NaCl)
- LB agar plates (LB medium + 1.5% (w/v) agar)

3.3 Buffers and Solutions

All chemicals were used in p. a. quality and were purchased from the following manufacturers, if not otherwise indicated:

- AppliChem (Darmstadt, Germany)
- Carl Roth (Karlsruhe, Germany)
- Merck Millipore (Darmstadt, Germany)
- SERVA (Heidelberg, Germany)
- Sigma-Aldrich (Taufkirchen, Germany)

Table 3: Reagents.

Reagent	Company
30% Formamide	Carl Roth
3-Amino-9-ethylcarbazole	DAKO
99% Ethanol	Carl Roth
Acetone	Carl Roth
Agar	BD Biosciences, Heidelberg, Germany
AP-Polymer Detection Line	DCS, Hamburg, Germany
Cell Lysis Buffer 10x	New England Biolabs, Frankfurt, Germany
DAPI Fluoromount-G	Southern Biotech, Birmingham, USA
Dimethylsulfoxide	Sigma-Aldrich
distilled, DNAse/RNAse free water	Gibco/Life Technologies, Darmstadt, Germany
DNA loading dye 6x	Thermo Fisher Scientific, Darmstadt, Germany
dNTP Mix	Thermo Fisher Scientific
Dynabeads® Protein G	Thermo Fisher Scientific
Enhancer Detection Line	DCS

Reagent	Company
Fetal bovine serum	Gibco/Life Technologies
Fisher's EZ Run Pre-Stained Rec Protein Ladder	Fisher Scientific, Schwerte, Germany
Fugene® HD transfection reagent	Promega, Mannheim, Germany
GelRedTM Nucleic Acid Gel Stain	Biotium, Hayward, USA
GeneRulerTM 1kb DNA ladder	Thermo Fisher Scientific, Darmstadt, Germany
H_2O_2 block	DAKO
NEBuffer 1.1	New England Biolabs
NEBuffer 2.1	New England Biolabs
OligofectamineTM	Life Technologies
Opti-MEM	Gibco/Life Technologies
Penicillin/Streptomycin	Sigma-Aldrich
Permanent AP Red	Zytomed, Berlin, Germany
Phenylmethylsulfonylfluorid (PMSF)	Sigma-Aldrich
Phosphate buffered saline	GE Healthcare, Solingen, Germany
PhosStop 10x	Roche, Mannheim, Germany
Protease-Inhibitor Mix G 1000x	SERVA, Heidelberg, Germany
REAL Hematoxylin	DAKO
Resazurin	Sigma-Aldrich
RPMI-1640	Sigma-Aldrich
Salmon sperm DNA	Invitrogen/Thermo Fisher Scientific, Darmstadt, Germany
Streptavidin-HRP	DAKO
Sulfuric acid	Carl Roth
Target Retrieval Solution (pH 6)	DAKO
Target Retrieval Solution (pH 9)	DAKO
Tazemetostat	Biomol, Hamburg, Germany
Tryptone	BD Biosciences

Reagent	Company
Verteporfin	Sigma-Aldrich
Reagent	Company
Xylene	Carl Roth
Yeast extract	BD Biosciences

Table 4: Enzymes.

Enzyme	Company
ABsolute qPCR SYBR Green ROX Mix	Thermo Fisher Scientific, Darmstadt, Germany
BbsI	New England Biolabs
HindIII	New England Biolabs
KpnI	New England Biolabs
Q5® High-Fidelity DNA Polymerase	New England Biolabs
RevertAid H Minus RT	Thermo Fisher Scientific
RPMI-1640	Sigma-Aldrich
SacI	New England Biolabs
T4 DNA Ligase	New England Biolabs
T4 Polynucleotide Kinase	New England Biolabs
Trypsin-EDTA	Sigma-Aldrich

Table 5: Recipes of solutions and buffers.

Solution/Buffer	Recipe
Blocking solution (B)	5% (m/v) BSA in TBST
Blocking solution (M)	5% (m/v) skim milk in TBST
Borate buffer (pH 8.8)	20 mM Boric acid 1.27 mM EDTA
IP wash buffer	100 mM Tris (pH 8.5) 500 mM LiCl 1% Igepal CA 630 1% Na-Desoxycholate

Solution/Buffer	Recipe
Loading buffer (4x) (pH 7.6)	250 mM Tris (pH 8) 8% SDS 40% glycerol 0.04% bromphenol blue 100 mM DTT
Nuclear extraction buffer	10 mM Tris-HCl 10 mM MgCl2 25 mM KCl 1% Triton X-100 8.6% Sucrose 200X protease inhibitor
PBST (pH 7.4)	0.02% Tween-20 in PBS
Phosphate buffered saline (PBS, pH 7.4)	140 mM NaCl 2.7 mM KCl 10 mM Na2HPO4 1.8 mM KH2PO4
Protein isolation buffer	1X Cell Lysis Buffer 1X PhosStop 1X Protease inhibitor
RIPA buffer	150 mM NaCl 0.1% SDS 0.5% Na-Desoxycholate 1% Igepal CA 630 5 mM EDTA 50 mM Tris (pH 8)
RIPAh	150 mM NaCl 0.1% SDS 0.5% Na-Desoxycholate 1% Igepal CA 630 5 mM EDTA 50 mM Tris (pH 8) 1 mM PMSF 10X Protease inhibitor
SDS-Running buffer	25 mM Tris 192 mM Glycin 0.1% (m/v) SDS
TAE-Buffer (pH 8)	40 mM Tris-Acetate 1 mM EDTA

Solution/Buffer	Recipe
Talianidis elution buffer	70 mM Tris (pH 8) 1 mM EDTA 1.5% (w/v) SDS
TBST	0.1% (v/v) Tween-20 in TBS
TE buffer	70 mM Tris (pH 8) 1 mM EDTA
Tris buffered saline (TBS, pH 7.6)	20 mM Tris-HCl 140 mM NaCl

3.4 Consumables

Table 6: Consumables.

Consumables	Company
Amersham Protran 0.45 µm Nitrocellulose Blotting Membrane	GE Healthcare
Microscope cover glasses	Marienfeld, Lauda-Königshofen, Germany
Microscope slides “Menzel-Gläser”	Thermo Fisher Scientific
Nunc™ 96-Well Polypropylene MicroWell™ Plates	Thermo Fisher Scientific
Precellys® Ceramic Kit 1.4 mm	Peqlab, Erlangen, Germany
WhatmanTM 3 mm Chr	GE Healthcare
Sterile stripettes®	Corning, New York, USA
Microcentrifuge tubes (0.2 mL; 1.5 mL; 2 mL)	Eppendorf, Hamburg,Germany Sarstedt, Nümbrecht, Germany Greiner Bio-One, Frickenhausen, Germany
Falcons (15 mL; 50 mL)	
Cell culture plates (15 cm; 10 cm; 6 well, 24 well, 96 well)	
Cell scrapers	

3.5 'Ready to use' Kits

Table 7: Kits.

Name	Company
AP based DCS Detection Line system	DCS, Hamburg, Germany
Avidin/Biotin blocking KIT	Vector, Burlingame, USA
Cell proliferation Biotrak Elisa System, version 2	GE Healthcare
Clariom™ D Assay, human	Applied BiosystemsTM
Dual-Luciferase® Reporter Assay System	Promega
NucleoSpin Gel and PCR Clean-up	Macherey-Nagel, Düren, Germany
NucleoSpin® RNA II kit	Macherey-Nagel
NucleoSpin Plasmid	Macherey-Nagel
PureYieldTM Plasmid Midipred System	Promega
Puregene® Core Kit A	Qiagen

3.6 Equipment

Table 8: Equipment.

Equipment	Company
12-Tube Magnet	Qiagen, Hilden, Germany
Agarose Gel Electrophoresis Systems	von Keutz Labortechnik, Reiskirchen, Germany
AlphaImagerTM gel documentation system	Biozym, Hessisch Oldendorf, Germany
Axiovert 25 microscope	Zeiss, Oberkochen, Germany
Bacteria Incubator	Memmert, Schwabach, Germany
BIOWIZARD Silver Line safety cabinet	Ewald, Bad Nenndorf, Germany
EV231 power supply	Consort, Turnhout, Belgium
FLUOstar Omega Microplatereader	BMG Labtech, Ortenberg, Germany
Hera Cell 150 CO2-Incubator	Heraeus, Hanau, Germany
Intelli-mixer overhead shaker	Neolab, Heidelberg, Germany
Kern EG scale	Kern, Balingen-Frommern, Germany

Equipment	Company
KS15 orbital shaker with TH15 incubation hood	Edmund Bühler, Hechingen, Germany
Megafuge 16R	Thermo Fisher Scientific
Microwave R-208	SHARP, Hamburg, Germany
Mikro 200R	Hettich, Tuttlingen, Germany
Mini Trans-Blot Cell	Bio-Rad, Munich, Germany
Mini-PROTEAN® 3 Cell SDS-gel electrophoresis systems	Bio-Rad
NanoDrop ND-1000 Spectrophotometer	Thermo Fisher Scientific
Neubauer counting chamber	Brand, Frankfurt, Germany
Odyssey Sa Infrared Imaging System	LI-COR Biosciences
Olympus CKX41 microscope	Olympus, Hamburg, Germany
pH 210 Microprocessor pH-Meter	Hanna Instruments, Kehl am Rhein, Germany
Precellys® 24 Homogeniser	Peqlab, Erlangen, Germany
PTC-200 Thermal Cycler	Biozym, Hessisch Oldendorf, Germany
Roll shaker CAT RM5	Neolab, Heidelberg, Germany
S-4000 Sonicator	Qsonica, Newton, USA
Secuflow fume hood	Waldner, Wangen, Germany
StepOnePlusTM Real-Time PCR System	Applied Biosystems, Darmstadt, Germany
Thermomixer compact	Eppendorf, Hamburg, Germany
Transsonic T460/H ultrasound water bath	Elma, Singen, Germany
Universal 32R	Hettich, Tuttlingen, Germany

3.7 Oligonucleotides

DNA Oligonucleotides were purchased from Thermo Fisher Scientific, siRNAs were bought from Eurofins Genomics, Ebersberg, Germany.

Table 9: Oligonucleotides used for RNA interference (siRNA).

siRNA name	Final conc.	Target structure	Sequence (5' - 3')	mRNA accession number	Final conc.
#1EZ	20 nM	EZH2	CAUCGAAAGAGAAAUGGAA-dT-dT	NM_001203247	20 µM
#2EZ	20 nM	EZH2	AUAUUGAACCUCCUGAGAA-dT-dT	NM_001203247	20 µM
#1M2	20 nM	MCM2	UGAGCUGUUGCUCUUCAUA-dT-dT	NM_004526	20 µM
#2M2	20 nM	MCM2	CUACCAGCGUAUCCGAAUC-dT-dT	NM_004526	20 µM
#1M3	20 nM	MCM3	AGACCAUAGAGCGACGUUA-dT-dT	NM_002388	20 µM
#2M3	20 nM	MCM3	GCTTCTGAACAATGCCTTT-dT-dT	NM_002388	20 µM
#1M4	20 nM	MCM4	GAAUUAGCUGAAGCAUUGA-dT-dT	NM_005914	20 µM
#2M4	20 nM	MCM4	GCAGAAGATATAGTGGCAA-dT-dT	NM_005914	20 µM
#1M5	20 nM	MCM5	GGAUGAACUCAAGCGGCAU-dT-dT	NM_006739	20 µM
#2M5	20 nM	MCM5	CCACCAUCUUGUCGCGCUU-dT-dT	NM_006739	20 µM
#1M6	20 nM	MCM6	AGAGGAGCGAGCUUGUUAA-dT-dT	NM_005915	20 µM
#2M6	20 nM	MCM6	CACCUGAUGUCAAUCUAGA-dT-dT	NM_005915	20 µM
#1M7	20 nM	MCM7	GCUCAUGAGGCGUUACAUA-dT-dT	NM_005916	20 µM
#2M7	20 nM	MCM7	GAAGGAGAGAACACAAGGA-dT-dT	NM_005916	20 µM
#1M	40 nM	#1MCM2	UGAGCUGUUGCUCUUCAUA-dT-dT	NM_004526	3.3 µM
		#3MCM3	AGACCAUAGAGCGACGUUA-dT-dT	NM_002388	3.3 µM
		#3MCM4	GAAUUAGCUGAAGCAUUGA-dT-dT	NM_005914	3.3 µM
		#4MCM5	GGAUGAACUCAAGCGGCAU-dT-dT	NM_006739	3.3 µM
		#1MCM6	AGAGGAGCGAGCUUGUUAA-dT-dT	NM_005915	3.3 µM
		#1MCM7	GCUCAUGAGGCGUUACAUA-dT-dT	NM_005916	3.3 µM

siRNA Name	Final conc.	Target structure	Sequence (5' - 3')	mRNA accession Number	Final conc.
#2M	40 nM	#2MCM2	CUACCAGCGUAUCCGAAUC-dT-dT	NM_004526	3.3 µM
		#4MCM3	GCTTCTGAACAATGCCTTT-dT-dT	NM_002388	3.3 µM
		#4MCM4	GCAGAAGATATAGTGGCAA-dT-dT	NM_005914	3.3 µM
		#5MCM5	CCACCAUCUUGUCGCGCUU-dT-dT	NM_006739	3.3 µM
		#3MCM6	CACCUGAUGUCAAUCUAGA-dT-dT	NM_005915	3.3 µM
		#2MCM7	GAAGGAGAGAACACAAGGA-dT-dT	NM_005916	3.3 µM
NTC	-	nonsense	UGGUUUACAUGUCGACUAA-dT-dT	-	20 µM
#1S	20 nM	SUZ12	GGAUGUAAGUUGUCCAAUA-dT-dT	NM_001321207	20 µM
#2S	20 nM	SUZ12	ACAAGCCUGGUUCAGUUAA-dT-dT	NM_001321207	20 µM
#1Y	20 nM	YAP	CCACCAAGCUAGAUAAAGA-dT-dT	NM_006106	20 µM
#2Y	20 nM	YAP	GGUCAGAGAUACUUCUUAA-dT-dT	NM_006106	20 µM
#2T	20 nM	TAZ	AAACGUUGACUUAGGAACUUU-dT-dT	NM_015472	20 µM
#3T	20 nM	TAZ	AGGUACUUCCUCAAUCACA-dT-dT	NM_015472	20 µM
#1YT	40 nM	#1YAP	CCACCAAGCUAGAUAAAGA-dT-dT	NM_006106	10 µM
		#2TAZ	AAACGUUGACUUAGGAACUUU-dT-dT	NM_015472	10 µM
#2YT	40 nM	#2YAP	GGUCAGAGAUACUUCUUAA-dT-dT	NM_006106	10 µM
		#3TAZ	AGGUACUUCCUCAAUCACA-dT-dT	NM_015472	10 µM
#1T14	80 nM	#1 TEAD1	GGACAUUCGUCAGAUUUAUGA-dT-dT	NM_021961	10 µM
		#1 TEAD4	GGGCAGACCUCAACACCAA-dT-dT	NM_201443	10 µM
#2T14	80 nM	#2 TEAD1	GAGCACAACAUCAUAUUUACA-dT-dT	NM_021961	10 µM
		#2 TEAD4	CCGCCAAAUCUAUGACAAA-dT-dT	NM_201443	10 µM

Table 10: PCR primer for chromatin-immunoprecipitation (ChIP).

Genepromoter	Genomic location	Name	Sequence (5‘-3‘)
EZH2	-7q36.1	Forward	CCCCAACAGTTCATAGGTGAC
		Reverse	GTCTCTCCTATTGCTTCATGTGGC
MCM2	+3q21.3	Forward	CCGATATTTGAGCTGGCTTCTATTTG
		Reverse	CTTGTCCTCCAACACACCAAACC
MCM3	-6p12.2	Forward	AGACTCCATAATTCGGCTGC
		Reverse	GGCTTTAAGTCTTGGGTTGCACA
MCM5	+22q12.3	Forward	GGAGAGTCTTTGTCACCATAC
		Reverse	CTTCGGCCTCCCAAAGTGC
MCM6	-2q21.3	Forward	GACAGCAGAAGCGGCTTACTC
		Reverse	GGCTGCTGGAACAAGTTCG
MCM7	-7q22.1	Forward	GGGCCTCACGTTAGCTTTATTTG
		Reverse	CCTCCCAGGACTGGTTCATTG
RBBP7	-Xp22.2	Forward	CCTTCTCTGACCCTCACTG
		Reverse	CGGCTTGGGAGATGATTTGTATC
SUZ12	+17q11.2	Forward	GCAAAGGCTTTGATAAAACCTGTACTTTAGG
		Reverse	GGGTTCTCTATAGTTAACTGCAAAACACTG

Table 11: PCR primer for semi-quantitative real-time PCR (qPCR) for human genes.

Gene	mRNA accession number		Sequence (5‘-3‘)
B2M	NM_004048	Forward	CACGTCATCCAGCAGAGAAT
		Reverse	TGCTGCTTACATGTCTCGAT
EED	NM_001308007	Forward	AAGGAGAAATCCGGTTGTTGC
		Reverse	AGCAGAGGATGGCTCGTATTG
EZH1	NM_001991	Forward	GAGAAGTTCTGCCAGTGCAACC
		Reverse	TGACTGAACAGGTTGGACACG

Gene	mRNA accession number		Sequence (5‘-3‘)
EZH2	NM_004456	Forward	GAGAGTGTGACCCTGACCTCTG
		Reverse	CGTCAGATGGTGCCAGCAATAG
MCM2	NM_004526	Forward	GAAATCGTGGCCGAGTTCTTC
		Reverse	AATGCTGTTGATGCCGAATG
MCM3	NM_002388	Forward	TGTGTGGAGGGCATTGTCACT
		Reverse	CCACCAGGGTGGTGAGATCAG
MCM4	NM_005914	Forward	CAGCCCTCCCCAAATGCATTC
		Reverse	GTGTGCCCCTAACACCACTTC
MCM5	NM_006739	Forward	TTGTACAAGCAGCCAGCCGA
		Reverse	CAGGCTACGAATGCTGGAAGG
MCM6	NM_005915	Forward	CTTACCTGTGTCGGGCCTTGA
		Reverse	ACTGTCTGACAGTCCAAGCACA
MCM7	NM_005916	Forward	AGTGCCAAACCAACCGCTCA
		Reverse	CTCCTTCTACCAGCACCGTGA
PPIA	NM_021130	Forward	CCGCCGAGGAAAACCGTGTA
		Reverse	TCTTTGGGACCTTGTCTGCAA
RBBP4	NM_005610	Forward	TCTCCTGGAATCCCAATGAACC
		Reverse	TTCTGGATCCACGCTTCCTTC
RBBP7	NM_002893	Forward	TACCGTTCAGTGGCTTCCTG
		Reverse	ACTCGAGCAACCACCAGATG
RPL41	NM_001035267	Forward	AAACCTCTGCGCCATGAGAG
		Reverse	AGCGTCTGGCATTCCATGTT
SUZ12	NM_015355	Forward	GGACCAGTTAAGAGAACACC
		Reverse	AGACATGCTTGCTTTTGTTCG
TEAD1	NM_021961	Forward	GACAGTCACCTGTTCCACCAAAG
		Reverse	CCATTCTCAAACCTTGCATACTCCG

Gene	mRNA accession number		Sequence (5‘-3‘)
TEAD2	NM_001256658	Forward	CTCACCTGTTCCTCCAAGGTC
		Reverse	CACCAGGTACTCGCACATGG
TEAD3	NM_003214	Forward	TTCATGGAGGTGCAGCGAGAC
		Reverse	CGCACATCTACTGCCTCCAG
TEAD4	NM_201443	Forward	TGGAGTTCTCTGCCTTCCTG
		Reverse	GGACTGGCCAATGTGCACGA
WWTR1 (TAZ)	NM_015472	Forward	CAGAGAATCCAGATGGAGAG
		Reverse	GTTGACAGCAGCCTGAACTG
YAP1	NM_006106	Forward	CCTGCGTAGCCAGTTACCAA
		Reverse	CCATCTCATCCACACTGTTC

Table 12: PCR primer for semi-quantitative real-time PCR (qPCR) for murine genes.

Gene	mRNA accession number		Sequence (5‘-3‘)
ACTB	NM_007393	Forward	GCTTCTTTGCAGCTCCTTCGT
		Reverse	ACCAGCGCAGCGATATCG
EED	NM_021876	Forward	GAAGGAGACCCTCTGGTGTTTG
		Reverse	CTGCTAATAGAGGGTGGCTGG
EZH1	NM_007970	Forward	TGGGTGACGAGGTGAAGGAAG
		Reverse	CGTCCTCCTCCTCATCAGAGT
EZH2	NM_001146689	Forward	CTGAAACTGGGGGAGAGAAC
		Reverse	GGAGGTTCAATATTTGGCTTC
GAPDH	NM_008084	Forward	TGTCCGTCGTGGATCTGAC
		Reverse	CCTGCTTCACCACCTTCTTG
HPRT	NM_013556	Forward	TCCTCCTCAGACCGCTTTT
		Reverse	CCTGGTTCATCATCGCTAATC

Gene	mRNA accession number		Sequence (5‘-3‘)
MCM2	NM_008564	Forward	CCATTTGAAGATGAGTCTGAGGG
		Reverse	AGACATCGAGCTCCGGAATG
MCM3	NM_008563	Forward	GTGAATGACCTGCGCAGGAAG
		Reverse	CGTAGGTGGCGTCAATGGAG
MCM4	NM_008565	Forward	GGGCAGACACCTCACACTATTG
		Reverse	CAAGGCCATGCAGACGTTT
MCM5	NM_008566	Forward	CCCGTCGAGCATTCGGATTC
		Reverse	GAGTAGCCTTGGCACGGACT
MCM6	NM_008567	Forward	GCCCAAGCTGGTGACAGATG
		Reverse	GATCTCTGACACCAAGGGCC
MCM7	NM_008568	Forward	CCAGGAGTGCCAGACCAATC
		Reverse	GGCTGGGCAATTCTTGTGTTCT
PPIA	NM_008907	Forward	AGCTGTCCACAGTCGGAAAT
		Reverse	GCATACAGGTCCTGGCATCT
RBBP4	NM_009030	Forward	AGTGAGTTCATTCTTGCCACAGG
		Reverse	GAGGTGACCACTGAACTTGGAAT
RBBP7	NM_009031	Forward	AGCTGTTGTAGAGGATGTGGCC
		Reverse	GCTGTAGGGATTGAATGAGAGGC
SUZ12	NM_199196	Forward	GCACTCTGAACTGCCGTAAACTG
		Reverse	CTGCATAGGAGCCATCATAACACTC
TBP	NM_013684	Forward	TTGTCTGCCATGTTCTCCTG
		Reverse	CAGGGTGATTTCAGTGCAGA
TEAD4	NM_011567	Forward	CAAGGCCGCAGCATAGCTAG
		Reverse	CTGGCTGATGTGCACAAACAGG
TPX2	NM_001141977	Forward	GTATGTGCCCATTGCACAGCAG
		Reverse	GTTCACAGATTTGGAGGGTAACAAGC

Gene	mRNA accession number		Sequence (5‘-3‘)
TTK	NM_009445	Forward	GTGTGTTCCAGAACCCTGCTG
		Reverse	GGTGTCTCACAAGCAGACTTTGG
TUBB5	NM_011655	Forward	TCACTGTGCCTGAACTTACC
		Reverse	GGAACATAGCCGTAAACTGC
WWTR1 (TAZ)	NM_001168281	Forward	CCAATGCACTGACCACTCAGC
		Reverse	CTCATATCTGTGCTCATGGCAGG
YAP1	NM_001171147	Forward	GACTCCGAATGCAGTGTCTT
		Reverse	ATCGGAACTATTGGTTGTCA

Table 13: Primer for cloning: luciferase vectors.

Genepromoter	Genomic location	Name	Sequence (5‘-3‘)
MCM7	-7q22.1	Forward1	ATTACACTAGGTACCCCGAG
MCM7	-7q22.1	Forward2	GTGACCACCAAATAGAGGC
MCM7	-7q22.1	Reverse1	CCTTCACTGAGTCCTTCCA
MCM3	-6p12.2	Forward1	CGACTTTGGTGGAGGTAGTTC
MCM3	-6p12.2	Reverse1	GGTCCATGCTGTTATTCCCA

Table 14: Oligonucleotides for cloning: CRISPR plasmids.

Target of guide RNA	Name	Sequence (5‘-3‘)
MCM2	Sense guide	ACCTGAGAACCTGGAGGATCTCAA
MCM2	Antisense guide	AAACTTGAGATCCTCCAGGTTCTC

Table 15: Sequencing Primer.

Name	Sequence (5‘-3‘)
Luc-F	AGTCAAGTAACAACCGCGA
Luc-N Rev	CATAGCCTTATGCAGTTGCTCTCC
Amp_rev	GCTATGTGGCGCGGTATTAT

Table 16: Plasmids.

Name	Function	Backbone	Resistance	Additional feature
CRISPR-MCM2	sgRNA against MCM2	pX458-ΔCas9	Ampicillin, Puromycin	GFP
CRISPR-0	-	pX458-ΔCas9	Ampicillin, Puromycin	GFP
pRL_TK	-	pRL	Ampicillin	Renilla Luciferase
MCM2-Firefly	MCM2 promoter	pGL3	Ampicillin	Firefly Luciferase
MCM3-Firefly	MCM3 promoter	pGL3	Ampicillin	Firefly Luciferase
MCM4-Firefly	MCM4 promoter	pGL3	Ampicillin	Firefly Luciferase
MCM6-Firefly	MCM6 promoter	pGL3	Ampicillin	Firefly Luciferase
MCM7-Firefly	MCM7 promoter	pGL3	Ampicillin	Firefly Luciferase
18ABJOTP	MCM2 promoter	pMK-RQ	Kanamycin	-
18ABJOSP	MCM4 promoter	pMK-RQ	Kanamycin	-
18ABJORP	MCM6 promoter	pMK-RQ	Kanamycin	-

3.8 Software

Table 17: Software.

Name	Company
ApE v2.0.47	www.biologylabs.utah.edu/jorgensen/wayned/ape
Aperio ImageScope v11.0.2.725	Leica Biosystems, Nussloch, Germany
CCTop	https://CRISPR.cos.uni-heidelberg.de/ (69)
CellSens Dimension	Olympus, Hamburg, Germany
COBALT (Constraint-based Multiple Alignment Tool)	https://www.ncbi.nlm.nih.gov/tools/cobalt/ (70)
Inkscape 0.92.3	www.inkscape.org
Fiji (ImageJ v1.46j)	www.fiji.sc
IBM SPSS Statistics 23.0	IBM, Ehningen, Germany
Image Studio v3.1.4	LI-COR Biosciences, Bad Homburg, Germany
JASPAR	http://jaspar.genereg.net/ (71)

Name	Company
Omega v3.00 R2	BMG Labtech, Ortenberg, Germany
R i386 3.2.3	https://www.R-project.org
StepOne software v2.3	Applied Biosystems, Darmstadt, Germany

4 Methods

4.1 Cell Culture

4.1.1 Cultivation of Cells

All cell lines in this study were cultured at 37°C in a 5% CO_2 humid atmosphere, passaged twice a week and discarded after 6 month or 50 passages. The cells were detached using Trypsin-EDTA, 2 mL per plate, and split into new dishes containing the corresponding medium (Table 18) supplemented with 10% FCS and 1% penicillin/streptomycin.

Table 18: Background and culture information of cell lines.

Cell line	Donor Gender	Donor Age [years]	Tissue	Tumor type	Medium	Provider
HepG2	male	15	liver	hepatoblastoma	RPMI	LGC Standards GmbH, Wesel Germany
HepG2-Cas9	male	15	lLiver	hepatoblastoma	RPMI	S. Luiken (AG Roessler), Heidelberg, Germany
Sk-Hep1	male	52	liver/ ascites	adenocarcinoma	DMEM	LGC Standards GmbH
HLF	male	68	liver	non-differentiated hepatoma	DMEM	JCRB Cell Bank, Osaka, Japan

For cryo-conservation, sub-confluent cells from one 10 cm plate dish were trypsinized and resuspended in 2 mL medium supplemented with 10% DMSO. The vials were slowly cooled down to -80°C within 24 h and then transferred to the vapor phase of liquid nitrogen (-196°C). For revitalization, cells were rapidly thawed at 37°C, dissolved in 10 mL medium, centrifuged at 300 x g for 5 min and resuspended in 10 mL medium before being transferred to a 10 cm dish.

4.1.2 Seeding Cells

Cells were seeded according to Table 19 for each experiment. Therefore cells were trypsinized, counted in a Neubauer chamber and resuspended in the respective medium.

Table 19: Seeding cells.

Cell line	6-well-plate	24-well-plate
HepG2	100,000/well	30,000/well 100,000/well
HepG2-Cas9	-	100,000/well
Sk-Hep1	80,000/well	-
HLF	80,000/well	20,000/well

4.1.3 Transfection of siRNAs

For RNAi-experiments cells were seeded into 6-well plates according to section 4.1.2 and used for transfection the following day. Untreated and nonsense siRNA-transfected cells were used as negative controls. Therefore, siRNAs and Oligofectamine™ were each diluted in Opti-MEM according to Table 20. After incubation for 10 min at room temperature, both solutions were mixed and incubated for 15 min. Prior to the addition of respective transfection solution mixtures (A+B), cells were washed with PBS and covered with 800 µL Opti-MEM. After 24 h, the medium was replaced and cells were harvested after an additional culture time of 24 or 48 h.

Table 20: Transfection protocol for siRNAs.

A

Final conc.	20 nM	40 nM	80 nM
Opti-MEM	184 µL	183 µL	181 µL
siRNA(20 µM)	1 µL	2 µL	4 µL

B

Opti-MEM	10 µL
Oligofectamin	5 µL

4.1.4 Substance Treatment

The EZH2 inhibitor Tazemetostat and the YAP/TEAD inhibitor Verteporfin were dissolved in DMSO to prepare 0.2 mM and 2 mM stock solutions, respectively. Cells were seeded into 6-well plates one day prior to treatment and then incubated with the indicated concentrations for 24 h, followed by a medium exchange. After an additional 24 h of cultivation, cells were harvested and DMSO-treated cells served as a negative control.

4.2 Human and Mouse Sample Analysis

4.2.1 Tissue Microarray (TMA)

A HCC TMA was evaluated after immunohistochemical staining for YAP, Ki67, and potential target genes. The TMA contained 105 HCCs (grading: G1: n=10, G2: n=75, G3: n=16, G4: n=4) and 7 normal liver tissues, evaluated by a pathologist (Prof. Dr. S. Singer). For each tissue sample, a score was derived from the scoring system (Table 21) and the product of the qualitative and quantitative parameters was calculated (range: 0-12). The evaluation was performed by two experienced investigators, independently.

Table 21: Scoring system for TMA evaluation.

score	Quality -staining intensity-	Quantity -positive cells-
0	negative	no expression
1	low	< 1%
2	medium	1 - 9%
3	strong	10 - 50%
4	-	> 50%

4.2.2 Statistical and Survival Analysis

Basic statistic tests were performed using SPSS and R software. All data were presented as a mean ± standard deviation. Significance levels were defined as * $p \leq 0.05$, ** $p \leq 0.01$ and *** $p \leq 0.001$. Statistical comparison was conducted using the two-tailed Mann-Whitney U test or the Student's t-test.

Analysis of target gene expression correlation to overall survival and cancer recurrence (Kaplan-Meier) were performed on transcriptome and clinical data of 242 HCC patients (cohort 1)(72) and 370 liver cancer patients (cohort 2)(27). Statistical tests, such as log-rank and Breslow test, were performed using the IBM SPSS Statistics software. Correlation analysis was performed using the Pearson's Chi^2-test and Spearman's rank correlation analysis (rS).

4.2.3 Transgenic Mice

All experiments were approved by the German Regional Council of Baden-Wuerttemberg (Karlsruhe, Germany) and performed in accordance with the institutional regulations of the IBF (Interfakultäre Biomedizinische Forschungseinrichtung, University of Heidelberg). Mouse samples of different experiments were kindly provided by group members (AG Breuhahn, Institute of Pathology, Heidelberg, Germany).

Briefly, transgenic mice (Col1A1-YAPS127A-LAP-tTA)(61) were housed and bred at the IBF and genotyping PCR performed on genomic DNA isolated from tail biopsies. During breeding, the transgene expression (YAP^{S127A}) was suppressed by doxycycline supplementation of the drinking water.

Doxycycline was withdrawn eight weeks after birth to induce hepatic YAP^{S127A} overexpression. Total liver samples for RNA isolation were obtained from liver tissues 8 or 12 weeks after doxycycline deprivation. Hepatocyte isolation of transgenic and wildtype mice was performed 10 weeks after doxycycline withdrawal.

4.3 Methods of Molecular Biology

4.3.1 Luciferase Plasmid Cloning

Isolation of genomic DNA

Total genomic DNA was isolated from cultured HLF cells using the Puregene® Core Kit A according to the manufacturer's instructions.

Polymerase Chain Reaction (PCR)

For amplification of the MCM3 and MCM7 promoter sites, genomic DNA was amplified using Q5-High Fidelity DNA Polymerase. The reaction setup is described in Table 22 and the cycling conditions in Table 23. The PCR product of the first MCM7-PCR (Forward1, Reverse1) was purified employing agarose gel electrophoresis and used as DNA-template for the second MCM7-PCR (Forward2, Reverse1) described in Table 22 and Table 23.

Table 22: PCR master mix for luciferase cloning.

Reagent	Volume	Final concentration
5X Q5® Reaction Buffer	10 µL	1X
dNTPs [10 mM]	1 µL	200 µM
Forward primer [10 µM]	5 µL	0.5 µM
Reverse primer [10 µM]	5 µL	0.5 µM
DNA-Template	100 ng	2 µg/mL
Q5® High-Fidelity DNA Polymerase	0.5 µL	20 U/mL
dH2O	ad 50 µL	

Table 23: Thermocycling conditions for luciferase cloning PCR.

Step	Description	Temperature	Time	Cycles
1	Initial denaturation	95°C	30 s	1 X
2	Denaturation	95°C	30 s	30 X
3	Annealing	66°C (MCM3) 59°C (1. MCM7) 55°C (2. MCM7)	30 s	
4	Elongation	95°C	1 min	
5	Final elongation	72°C	10 min	1X

Restriction enzyme digestion

To introduce the MCM promoters upstream of the firefly luciferase gene in the pGL3_basic plasmid, sticky-end cloning was employed. Therefore the PCR products, pGL3-basic and ordered plasmids (MCM2, MCM4, MCM6) were digested for 1 h at 37°C with the respective enzymes depicted in Table 24 and purified employing agarose gel electrophoresis.

Table 24: Digestion conditions.

	reaction buffer	Enzyme	
MCM2	NEBuffer 2.1	KpnI	HindIII
MCM3	NEBuffer 1.1	SacI	KpnI
MCM4	NEBuffer 2.1	HindIII	HindIII
MCM6	NEBuffer 2.1	KpnI	HindIII
MCM7	NEBuffer 1.1	SacI	KpnI

Agarose gel electrophoresis

PCR products and digested plasmids were visualized and purified using agarose gel electrophoresis. For this purpose, a 1% agarose gel was prepared using melted agarose in TAE buffer, supplemented with 20 µL/L GelRed™ Nucleic Acid Gel Stain as a DNA intercalator for visualization of DNA fragments under to UV light. The agarose solution was poured into gel trays and solidified. DNA was mixed with 6x DNA loading dye and loaded onto the agarose gel next to a DNA size marker (GeneRuler 1 kb DNA ladder). Fragments were separated by applying 100 V for 1 h. PCR products were visualized using the AlphaImager™ gel documentation system. The agarose gel piece containing the desired PCR product was cut out of the gel.

DNA PCR and gel purification

Purification of PCR products or digestion products was performed by using the NucleoSpin® Gel and PCR Clean-up KIT according to the manufacturer's instructions.

Ligation

To ligate the digested fragments, MCM promoter regions with the pGL3-basic backbone, the purified insert (200 ng) was added to the vector (400 ng), together with T4 ligase (5 units) and T4 Buffer and incubated at room temperature for 1 h.

4.3.2 CRISPR Plasmid Cloning

CCTop-software (69) was used to identify specific target sites within the exons 3-6 and corresponding oligonucleotides were ordered. In order to obtain the inserts, the respective oligonucleotides were annealed and phosphorylated with T4 polynucleotide kinase (Table 25), following thermocycling conditions displayed in Table 26.

Table 25: Reaction mix for phosphorylation and annealing.

Reagent	Volume	Final concentration
10X T4 DNA ligase Buffer	1 µL	1 U/µL
T4 Polynucleotide Kinase	1 µL	1 X
Sense guide [10 µM]	1 µL	1 µM
Antisense guide [10 µM]	1 µL	1 µM
dH_2O	6 µL	

Table 26: Thermocycling conditions for phosphorylation and annealing.

Description	Temperature	Time
Phosphorylation	37°C	30 min
Denaturation	95°C	5 min
Annealing	-0.1°C	s^{-1}

The annealed insert was diluted with water (1:10) with water and cloned into the pX458-ΔCas9-vector using the restriction enzyme BbsI according to the protocol shown in Table 27 and using the thermocycling conditions listed in Table 28.

Table 27: Reaction mix for digestion and ligation.

Reagent	Volume	Final concentration
10X T4 DNA ligase Buffer	2 µL	1X
BbsI	1 µL	0.5 U/µL
T4 ligase	1 µL	0.25 U/µL
Insert (annealed and phosphorylated guides, dilution 1:10)	1 µL	
pX458-ΔCas9-Vector	100 ng	5 ng/µL
dH_2O	ad 20 µL	

Table 28: Thermocycling conditions for digestion and ligation.

Description	Temperature	Time	Cycles
Digestion	37°C	10 min	6X
Ligation	22°C	10 min	

4.3.3 Transformation of Competent Bacteria and Plasmid Isolation

Plasmids were transformed into competent bacteria via heat shock. Freshly thawed bacteria were mixed with Ligation-mixture, incubated on ice for 15 min and heat-shocked at 42°C for 45 s. The mixture was cooled on ice, plated on LB-Agar plates with Ampicillin (50 µg/mL), and incubated at 37°C overnight. Single colonies were picked the next day and expanded in 5 mL (Miniprep) or 100 mL LB medium (Midiprep) containing Ampicillin and incubated at 37°C under shaking overnight. For long-term storage, bacteria cultures were mixed 1:1 with 70% glycerol and frozen at -80°C.

Isolation of plasmid DNA was carried out with NucleoSpin® Plasmid kit (Miniprep) or PureYield™ Plasmid Midiprep System kit (Midiprep) according to the manufacturer's instructions.

4.3.4 Sequencing

Sequencing reactions were carried out by the Microsynth AG (Balgach, Switzerland). Sequencing results were analyzed using the software ApE-A plasmid Editor v2.049.10.

4.3.5 Isolation of Total RNA and cDNA Synthesis

Total RNA of cultured cells was isolated using the NucleoSpin® RNA II kit according to the manufacturer's instructions. For isolation of RNA from tissue samples, small tissue pieces were homogenized using the Precellys® Ceramic Kit 1.4 mm and the Precellys® 24 Homogeniser (2X 20 s, 6,000 x g). After centrifugation, the supernatant was used for further RNA isolation with the NucleoSpin® RNA II kit.

Total RNA concentration was determined by measuring the absorption at 260 nm using a spectrophotometer. The ratio of 260 nm to 280 nm of absorbance was used to assess the purity, (ratio ≥1.9 for RNA). Total RNA was transcribed into cDNA by mixing 1 µg of isolated RNA with dNTPs (1 mM) and random Hexamer primer (5 µM). The mixture was first incubated at 75°C for 5 min and then cooled to 25°C. After the addition of 5X reaction buffer and RevertAid H Minus Reverse Transcriptase (RT), the reverse transcription was performed at 42°C for 1 h and stopped at 70°C for 10 min in a thermal cycler.

4.3.6 Semi-Quantitative Real-Time PCR (qPCR)

Real-time PCR was used to analyze mRNA expression. Therefore 2 µL of cDNA (1:50) was mixed with 2X ABsolute QPCR SYBR Green ROX Mix, forward primers (0.3 µM) and reverse primers (0.3 µM). Samples were analyzed in duplicates, water-samples were used as negative control and melting curve analysis was performed to check for PCR specificity. The qPCR was performed on a StepOnePlus™ Real-Time PCR System with the cycling conditions and melting curve program listed in Table 29.

Relative gene expression was calculated using the $\Delta\Delta C_T$-method and normalized to *Ribosomal Protein L41* (RPL41). For the analysis of gene expression in murine tissue samples, a panel of

housekeeping genes (Actb, Gapdh, Hprt, Ppia, Tbp,Tubb5) was evaluated using the geNorm algorithm to find the most stable reference gene (73)

Table 29: Thermocycling conditions for qPCR.

Part	Step	Description	Temperature	Time	Cycles
PCR	1	Initial denaturation	95°C	15 min	1 X
	2	Denaturation	95°C	15 s	40 X
	3	Annealing and elongation	60°C	60 s	
Melting curve	4	Denaturation	95°C	15 s	1X
	5	Annealing	60°C	30 s	
	6	Stepwise dissociation	60-95°C	0.5°C/s	
	7	Final denaturation	95°C	15 s	

4.4 Methods of Protein Biochemistry

4.4.1 Total Protein Isolation and Quantification

Cultured cells were washed two times with PBS and scraped in 60 µL/well protein isolation buffer. The samples were sonicated in an ultrasound water bath three times for 20 s and cooled on ice in between. Centrifugation at 14,000 x g at 4°C for 10 min removed cell debris and protein concentration was determined by measuring the absorption of 2 µL sample at 280 nm using a Nanodrop spectrophotometer.

4.4.2 Protein and Histone Isolation

Cultured cells were washed two times with PBS, scraped in nuclear extraction buffer and incubated on ice for 5 min. Centrifugation at 600 x g for 5 min at 4°C separated chromatin-bound proteins in the pellet from the soluble proteins. The supernatant was collected and protein concentration was determined using a Nanodrop spectrophotometer. The pellet was washed with 200 µL TE buffer (pH 7.4), resuspended in 50 µL 0.2 M sulfuric acid and incubated for one hour on ice. After centrifugation at 10,000 x g for 10 min at 4°C, the supernatant was transferred into a tube containing 500 µL of ice-cold acetone and incubated overnight at -20°C. Precipitated histones were pelleted at 10,000 x g for 10 min at 4°C and resuspended in 20 µL water.

4.4.3 SDS-Polyacrylamide Gel Electrophoresis (SDS-PAGE)

SDS-PAGE was used to separate proteins according to their molecular weight. Therefore, 100 µg of total protein or 5 µL of isolated histones, in 20 µL total volume, were mixed with 7 µL Loading

buffer and denaturated for 10 min at 95°C. The samples were loaded with 2 µL of a protein size marker on polyacrylamide gels, which were prepared as described in Table 30. Electrophoretic separation was carried out at 120 V for 1.5 h.

Table 30: Preparation of SDS-polyacrylamide gel.

Substance	8% separation gel	15% separation gel	stacking gel
Acrylamide	8% (v/v)	15% (v/v)	5% (v/v)
Tris-HCl, pH 8.8	375 mM	375 mM	-
Tris-HCl, pH 6.8	-	-	125 mM
SDS	0.1% (w/v)	0.1% (w/v)	0.1% (w/v)
APS	0.1% (v/v)	0.1% (v/v)	0.1% (v/v)
TEMED	0.06% (v/v)	0.04% (v/v)	0.1% (v/v)

4.4.4 Immunoblotting

Proteins were transferred from SDS-gels to nitrocellulose membranes using a wet blot chamber at 95 V and 450 mA for 1.5 h with ice-cold borate buffer. Membranes were blocked for 30 min in 5% BSA or milk in TBST and primary antibodies added according to Table 1. After overnight incubation at 4°C, membranes were washed three times with TBST and incubated for 1 h at room temperature with suitable secondary antibodies as shown in Table 2. After washing the membranes three times with TBST, the Odyssey Sa Infrared Imaging System was used to detect the fluorescence signals.

4.4.5 Immunofluorescence

Cultured cells were washed with PBS and fixated for 15 min with 4% PFA-solution. After permeabilization with 0.2% TritonX for 12 min, cells were washed two times for 5 min with PBS and blocked for 30 min with 1% BSA in PBS. Incubation with a primary antibody according to Table 1 for 1 h at room temperature was followed by three times washing, each for 5 min in PBS and incubation with secondary antibody for 1 h at room temperature described in Table 2. The samples were sequentially washed for 5 min in PBS (3x), VE-water (1x), 99% Ethanol (1x), airdryed and mounted with DAPI-containing Fluoromount-G™. Slides were stored at 4°C and images were taken at the Olympus CKX41 microscope.

4.4.6 Immunohistochemistry (IHC)

All IHC stains were performed by the central IHC research facility at the Institute of Pathology, Heidelberg. Paraffin-embedded tissues were cut with a microtome to 3 µm sections, which were mounted on microscope slides and dried overnight. Deparaffinization was performed three

times by incubation in xylene for 5 min and followed by rehydration of the tissue. The slides were sequentially submitted to 100% ethanol (2x), 96% ethanol (2x), 70% ethanol (1x), and finally aqua dest for 2 min each. The tissue sections were then incubated in a steamer or pressure cooker in antigen retrieval-buffer according to Table 31. Slides were washed in TBS or TBST, blocked with avidin and biotin (Avidin/Biotin Blocking Kit), and washed with TBS/TBST, followed by primary antibody incubation in a wet chamber at 4°C overnight. After washing twice with TBS/TBST for 5 min, the tissue sections were incubated with biotinylated secondary antibody or Enhancer Detection Line for 25 min, followed by 2x 5 min TBS/TBST washes, H_2O_2 block for 10 min, 2x TBS/TBST washes for 5 min, Streptavidin-HRP or AP-Polymer Detection Line incubation for 20 min, 2x TBS/TBST washes for 5 min and AEC (3-amino-9-ethylcarbazole) or Permanent AP Red development. For nuclear visualization, tissue sections were washed 2x with TBS for 5 min and incubated with REAL Hematoxylin.

Table 31: Antibody retrieval and detection conditions for IHC.

Antigen	Detection	Detection system	Pretreatment	Citrate buffer
EZH2	Permanent AP Red	DCS 2red SuperVision rabbit	pressure cooker	pH 6
SUZ12	Permanent AP Red	DCS 2red SuperVision rabbit	pressure cooker	pH 6
YAP	Permanent AP Red	DCS 2red SuperVision rabbit	pressure cooker	pH 6
Ki67	AEC	Dako 5003	steamer	pH 9
Tri-Methyl-Histone H3 (Lys27)	Permanent AP Red	DCS 2red SuperVision rabbit	steamer	pH 9
MCM4	Fancy Red	DCS 2red SuperVision rabbit	steamer	pH 6
MCM5	Permanent AP Red	DCS 2red SuperVision rabbit	steamer	pH 6
MCM6	Permanent AP Red	DCS 2red SuperVision rabbit	steamer	pH 6
MCM2	Permanent AP Red	DCS 2red SuperVision rabbit	pressure cooker	pH 6
MCM3	Fancy Red	DCS 2red SuperVision rabbit	steamer	pH 9
MCM7	Liquid Permanent Red	DCS 2red SuperVision rabbit	steamer	pH 9

4.5 Functional Assays

4.5.1 5-Bromo-2'-Deoxyuridine (BrdU) Incorporation Assay

BrdU assay was performed to quantify DNA synthesis in proliferating cells. Therefore, cells were seeded in 6-well plates and treated with siRNAs against YAP, TAZ, and MCMs as described in 4.1.3. One day after inhibition, cells were trypsinized and seeded on 96-well plates in quadruplicates. BrdU assay was performed with Cell Proliferation Biotrak Elisa System the following day according to manufacturer's instruction. Briefly, cells were incubated with BrdU for one hour at 37°C, followed by 30 min fixation and 30 min blocking at room temperature. Incubation with BrdU-antibody (1:100) for one hour and three washing steps were performed at room temperature. Addition of TMB-substrate starts the peroxidase reaction, which was stopped after 5 min using 1 M sulfuric acid. Absorbance at 450 nm was measured using a microplate reader (FLUOstar Omega).

4.5.2 Chromatin Immunoprecipitation (ChIP)

For ChIP experiments, 3,000,000 cells were seeded in a 15 cm dish, one day prior to the experiment (one plate per two IPs). After washing with PBS, cells were fixed with 1% formaldehyde/PBS at room temperature for 15 min. The crosslinking was stopped by adding glycine to a final concentration of 125 mM for 5 min and two times washing with cold PBS. Cells were harvested in 1 mL cold RIPAh/15 cm plate and sonicated to generate fragments of genomic DNA (<500 bp). Cell debris were removed by centrifugation at 16,000 x g at 4°C for 15 min and 0.5 mL protein lysates/IP precleared with Dynabeads® Protein G. Therefore, magnetic beads were washed with RIPA buffer and incubated with lysates at 4°C for 1.5 h with rotation. Meanwhile, the Dynabeads for IP were prepared by washing with RIPA buffer and blocking with BSA (1 mg/mL) and salmon sperm DNA (0.3 mg/mL) at 4°C for 1.5 h with rotation. Two percent of precleared lysates were added in Talianidis elution buffer and stored at -20°C until further processing (input sample). After washing with RIPA, the blocked beads were resuspended in 0.5 mL RIPA per IP and added to precleared lysates with 2 µg antibody followed by incubation at 4°C overnight with rotation. The beads were washed successively with RIPA buffer, two times with IP wash buffer and again RIPA buffer, each time with 5 min rotation in between. Subsequently, beads were shortly washed with TE buffer and immunocomplexes were eluted with Talianidis elution buffer at 65°C for 10 min. Crosslinking reversal of the supernatant and input-sample was achieved by adjusting to 0.2 M NaCl and incubation at 65°C for 5 h. Purification of DNA was performed using the NucleoSpin® Gel and PCR Clean-up kit according to the manufacturer's protocol. Promoter binding was finally analyzed with quantitative real-time PCR using IgG-IP as a negative control and input-sample for quantification. In order to identify and quantify the DNA fragments of the respective promoter regions obtained by ChIP, primers were designed based on TEAD4 binding sites predicted by the JASPAR database (74).

4.5.3 Competitor Assay

A competitor assay was performed to analyze the target gene dependency of tumor cells with regards to survival and cell proliferation. The CRISPR/Cas (Clustered Regularly Interspaced Short Palindromic Repeats/CRISPR-associated) system was employed to abolish target gene expression and cell survival was monitored using an immunofluorescence approach. Therefore, HepG2-Cas9 and HepG2 cells were seeded on 24-well plates as described in section 4.1.2. The following morning, cells were transfected with empty CRISPR-plasmids or vectors coding for a single-guide RNA (sgRNA). For each well, 200 ng plasmid was mixed with 1 µL Fugene® HD transfection reagent in 10 µL Opti-MEM. After incubation for 15 min, the transfection solution was spread onto the cells and medium was exchanged 5 h later. One day after transfection, medium was changed to RPMI medium supplemented with Puromycin (0.2 µg/mL). Immunofluorescence pictures were taken at days 2, 3 and 4 after transfection. For each picture, the green fluorescent area was measured using Fiji (75) as a surrogate marker for viability and transfection efficiency.

4.5.4 Dual-Luciferase Reporter Gene Assay

Luciferase gene reporter assay was performed to quantify the regulation of target gene expression. Different MCM promoter constructs were used, containing 0.6 -2 kbp of the promoter sequence identified by ChIP and fused to the firefly luciferase gene as described in section 4.3.1. Cells were seeded into 24-well plates in the morning and transfected the same afternoon. For transfection, 400 ng of the promoter-firefly construct was mixed with 8 ng of Renilla Luciferase (pRL_TK) and 2 µL of Fugene® HD transfection reagent in 50 µL Opti-MEM and incubated for 15 min. The transfection solution was spread onto the cells and incubated overnight. Transfection with siRNA was carried out directly after the medium change as described in section 4.1.3. Briefly, 0.5 µl of siRNAs (final concentration 40 nM) and 1.25 µL of Oligofectamin were diluted in Opti-MEM, then mixed and incubated at room temperature for 15 min. Meanwhile, cells were washed with PBS, covered with 200 µL Opti-MEM/well and supplemented with the transfection solution. Twenty-four hours after transfection the medium was changed. Luciferase activity was measured 48 h after siRNA transfection using the Dual-Luciferase® Reporter Assay System according to the manufacturer's instructions. Therefore, lysates were transferred into dark 96-well plates (Nunc™) and activity was measured using a microplate reader (FLUOstar Omega). Firefly luciferase activity was normalized to Renilla luciferase activity.

4.5.5 Expression Profiling

Identification of differentially regulated genes was assessed by microarray analysis using the Clariom™ D Pico Assay (human) in cooperation with the Medical Research Center of the Medical Faculty Mannheim. Total RNA was isolated from HepG2 cells 48 h after RNAi treatment against YAP, EZH2, and SUZ12, as described in detail in sections 4.3.5 and 4.1.3, respectively. Gene

expression profiling was performed according to the manufacturer's instruction in collaboration with the laboratory of Prof. Norbert Gretz (Med. Fakultät Mannheim). Briefly, RNA was reverse transcribed and then Biotin-labeled and hybridized using a GeneChip Hybridization oven 640. A GeneChip Fluidics Station 450 was used for staining and the microarray scanned with a GeneChip Scanner 3000 (Affymetrix). Arrays were annotated by Custom CDF with Entrez-based gene definitions (76). Raw fluorescence intensity values were normalized by quantile normalization and false discovery rate (FDR) correction performed using the software package SAS JMP7 Genomics. A false-positive rate of 0.05 was taken as the level of significance. Heatmaps were generated using the pheatmap package of R (http://CRAN.R-project.org/package=pheatmap).

4.5.6 Cell Viability Assay

The active reduction of resazurin to resorufin by mitochondrial enzymes is used to determine cell viability. Therefore, cells were seeded in 6-well plates and treated with siRNAs against MCMs as described in section 4.1.3. 48 h after siRNA treatment, media was replaced by 1 mL fresh medium containing 10% Resazurin. After incubating for 1 h at 37°C, the supernatant was transferred on a 96 well plate and the absorbance at 573nm (resorufin) was measured using a microplate reader (FLUOstar Omega).

5 Results

5.1 Gene Families Regulated by the Hippo Pathway Effectors YAP and TAZ

5.1.1 Identification of Potential YAP and TAZ Target Gene Families

Physiologically, the Hippo pathway is crucial for controlling proliferation and apoptosis (77). It has been shown that deregulation of the pathway and overexpression of the co-transcriptional regulator YAP leads to drastic tissue overgrowth and tumor formation *in vivo* (58). Several distinct genes regulated by the Hippo signaling pathway have already been identified. However, it is unclear to which extent the transcriptional co-regulator YAP and its paralog TAZ affect the expression of functionally related gene/protein families.

To identify groups of YAP- and/or TAZ-regulated and functionally related gene families in liver cancer cells, both transcriptional regulators were transiently and individually repressed by two independent siRNAs in HepG2 cells. In addition, YAP- and TAZ-specific siRNAs were combined to jointly silence both factors. Untreated and nonsense siRNA (NTC)-transfected cells served as controls (20 µM and 40 µM siRNA for single and combined siRNA transfection, respectively). Expression profiling analysis using the Affymetrix platform was performed on mRNA, which was isolated 48 h after siRNA transfection. The workflow in Figure 5A summarizes the steps leading to the identification of Hippo pathway target genes, which were further analyzed in this study. In total, 409 genes were consistently and significantly regulated by either both YAP siRNAs, both TAZ siRNAs or both combinations compared to the respective nonsense control. 163 of these genes were significantly downregulated and of these 13 genes were selected for further validation. Five of these genes were consistently downregulated upon YAP and/or TAZ silencing, namely *ajuba LIM protein* (*AJUBA*), *DLC1 Rho GTPase activating protein* (*DLC1*), *MCM2, septin 10* (*SEPTIN10*) and *Suppressor Of Zeste 12 Protein Homolog* (*SUZ12*). As already described in previous work of the group this approach is valid and gave reproducible results.

Since the goal of this study was to identify groups and families of YAP/TAZ-regulated genes, which may cooperate in the regulation of HCC cell biology, literature describing these five genes was systematically screened for gene families. One identified gene frequently associated with proliferation and cell cycle progression was MCM2, which assembles with MCM3-7 to form a ring-shaped hexameric complex, named the MCM helicase (78). Because deregulation of this complex might facilitate tumor growth, it was tempting to test whether the expression of MCM family members MCM2-7 are equally regulated by YAP and/or TAZ in HCC cells. Another gene involved in epigenetic regulation and important for embryonic development and proliferation is SUZ12, a component of the polycomb repressive complex 2 (PRC2) (79). Since epigenetic alterations might influence gene expression in carcinogenesis, PRC2 components were also chosen for further analysis of transcriptional regulation by YAP and/or TAZ.

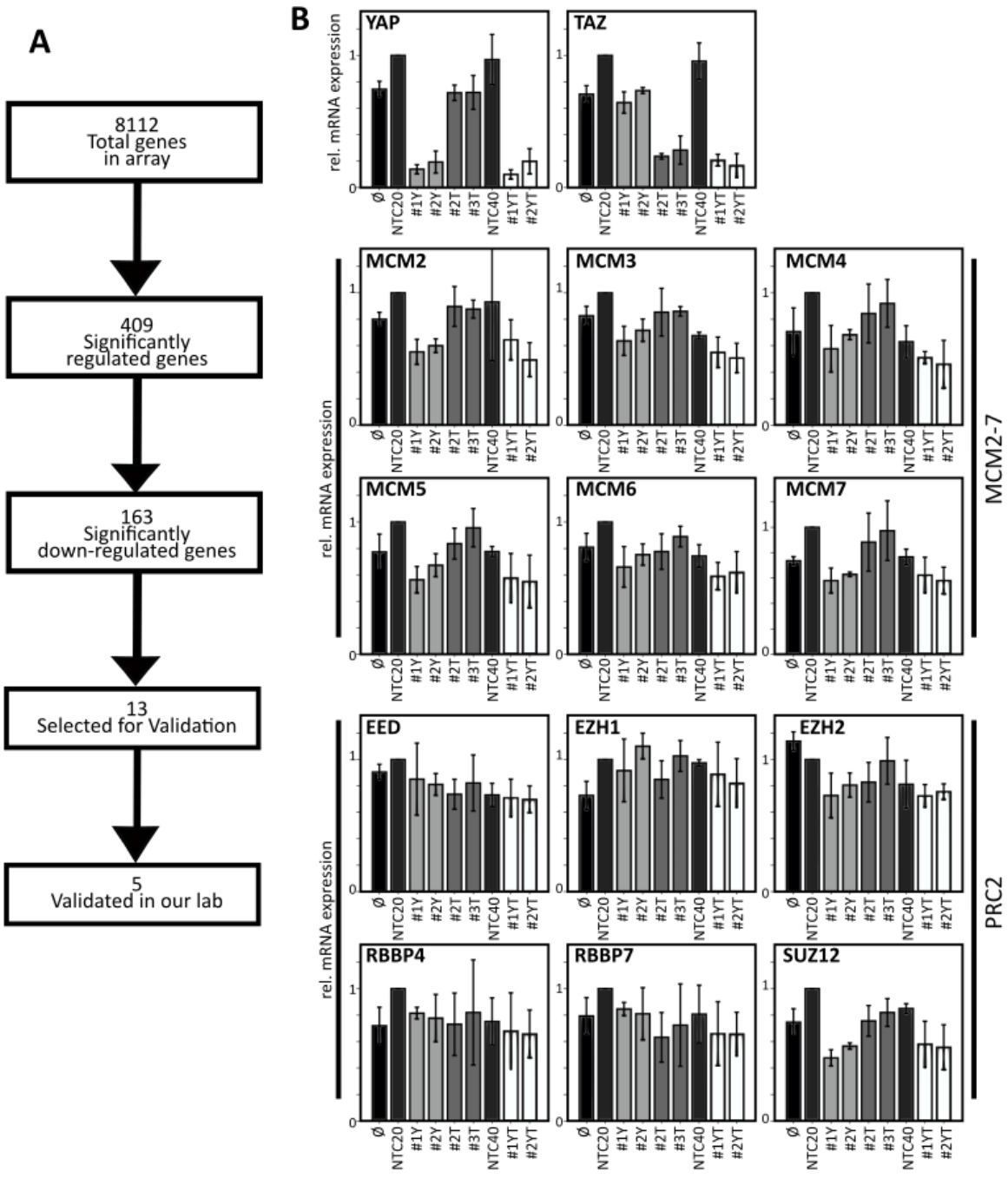

Figure 5: The transcriptional co-activators YAP and TAZ regulate target gene expression *in vitro*.
(A) Scheme depicting YAP/TAZ – target gene selection based on gene expression array analysis. (B) Transient transfection of two independent YAP (#1Y, #2Y) and TAZ (#2T, #3T)-specific siRNAs alone and in combination (#1YT, #2YT) reduced respective mRNA expression levels measured by real-time PCR. Mean ± SD of three independent experiments in HepG2 cells is shown and untreated (Ø) and nonsense siRNA-transfected cells with corresponding siRNA amounts, 20 or 40 nM respectively (NTC20, NTC40). Data were normalized to NTC20 control values.

In order to confirm whether the expression of these two families was affected by the Hippo pathway, the siRNA inhibition experiments were repeated using different liver cancer cell lines (Sk-Hep1, HLF, HepG2). Accordingly, the mRNA expression has been tested for six MCM genes

(*MCM2, MCM3, MCM4, MCM5, MCM6, and MCM7*) and six PRC2 core-component genes (*embryonic ectoderm development (EED), enhancer of zeste 1 polycomb repressive complex 2 subunit (EZH1), enhancer of zeste 2 polycomb repressive complex 2 subunit (EZH2), RB binding protein 4, chromatin remodeling factor (RBBP4), RB binding protein 7, chromatin remodeling factor (RBBP7*), and *SUZ12 polycomb repressive complex 2 subunit* (*SUZ12*) following YAP/TAZ depletion (Figure 5B).

Efficient knockdown of YAP at the mRNA level to less than 20% led to a reduced expression of all analyzed MCM mRNAs. MCM mRNA levels were homogeneously reduced to 60-75% upon YAP inhibition with the weakest effects on MCM6 and the strongest effects on MCM2 expression in HepG2. In contrast, the efficient TAZ inhibition to about 30% alone led to no consistent change on MCM mRNA levels, with a remaining MCM6 mRNA abundance of 80-90% being the strongest observed reduction. Interestingly, the combined inhibition of YAP and TAZ reduced MCM4 mRNA amounts to 45-50% as compared to single YAP inhibition (58-68%), whereas MCM7 was reduced to about 60% for both treatments. Additionally, single YAP inhibition in Sk-Hep1 cells reduced all MCM mRNA levels as low as 45-85% (MCM7 and MCM6; data not shown). Furthermore, combined YAP and TAZ inhibition led to consistently diminished MCM expression to 20% for MCM7 and 40% for MCM3. Moreover in HLF cells, combined reduction of YAP and TAZ to below 20% and 40%, respectively, decreased MCM2-7 abundance to 30-80% (datanot shown). Thus the combined inhibitions had in most cases either comparable or enhanced effects as compared to single inhibition, which indicated that YAP and TAZ cooperate in the transcriptional regulation of MCMs. For this reason, all further experiments concerning MCM helicase were conducted using combined YAP and TAZ inhibition.

As indicated by the expression array data, some PRC2 components were reduced upon efficient YAP knockdown. SUZ12 showed the most prominent effects, with a reduction to approximately 55% following YAP reduction, whereas EZH1 abundance was not drastically affected in HepG2 cells. In contrast, TAZ inhibition neither had reproducible effects on PRC2 components when silenced individually nor any additional effects in combination with YAP. Similar effects were observed in Sk-Hep1 cells, showing a reduced mRNA expression of EED, EZH2, SUZ12 and RBBP4/7 to 50-80% upon single YAP and combined YAP/TAZ inhibition. These results pointed to an exclusive regulatory role of YAP on PRC2 constituents. Therefore, all further experiments focusing on PRC2 factors were conducted after single YAP inhibition.

Taken together, these results show that mRNA expression of MCM helicase family members and PRC2 complex components were positively regulated by the Hippo pathway effectors YAP (MCMs and PRC2 complex) and TAZ (MCMs) in liver cancer cells (HLF, HepG2, Sk-Hep1). In the following, this study focuses first on the effects of YAP and TAZ on MCM expression and later on the regulation of PRC2 by YAP.

5.2 MCM Protein Family

5.2.1 YAP and TAZ Regulate MCM Expression via TEAD

Pursuing the previous findings, showing that YAP and TAZ knockdown reduced MCM mRNA expression, immunoblotting analysis was performed. Therefore, different liver cancer cell lines were treated with a combination of YAP and TAZ-specific siRNAs for 48 h (HLF, HepG2, Sk-Hep1). Efficient combined YAP and TAZ knockdown was associated with reduced protein abundance of MCM2-7 as shown exemplary for HLF cells in Figure 6. YAP and TAZ knockdown to about 5% and 30% respectively, reduced MCM6 protein levels to 60-65% and MCM4 protein levels to 50-70%. Although MCM5 and MCM7 abundance decreased moderately to 80-95%, the effects on MCM2 and MCM3 with a reduction to 50-80% and 70-80%, respectively, were more diverse but consistent. Similar changes in protein abundance were observed in HepG2 cells and by 10-20% enhanced in Sk-Hep1 cells.

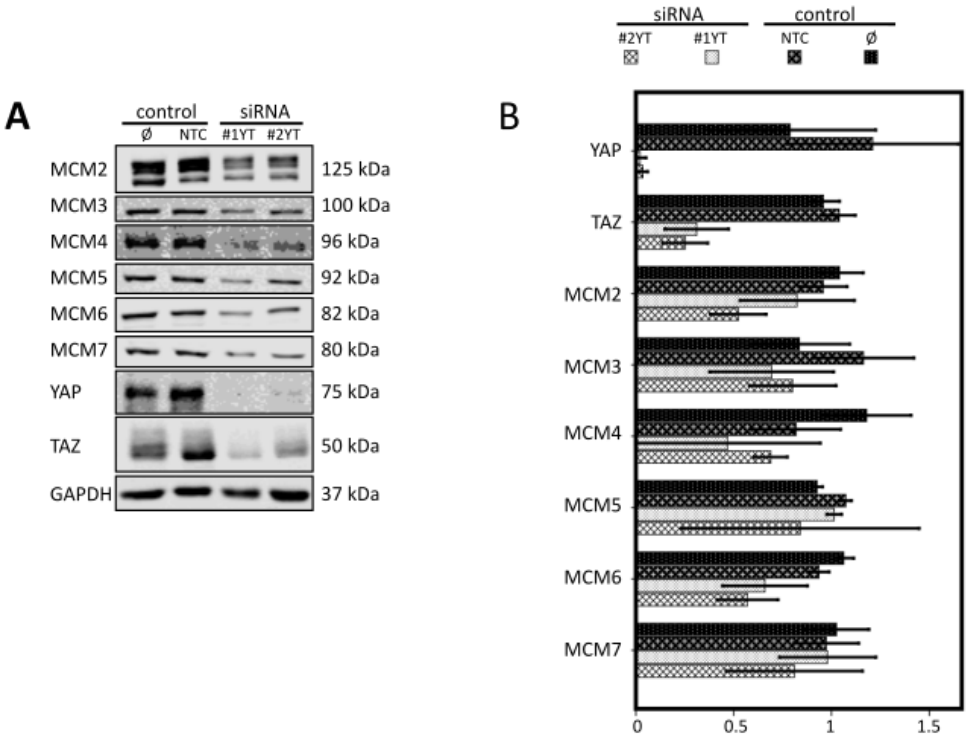

Figure 6: The transcriptional co-activators YAP and TAZ regulate MCM gene expression *in vitro*.
(A) Transient transfection with two YAP and TAZ-specific siRNAs led to reduced levels of MCM proteins as exemplarily illustrated by Western Blot analysis in HLF cells. Untreated (Ø) and nonsense siRNA (NTC) transfection served as controls. GAPDH was used as a loading control. (B) Protein quantification of MCM proteins relative to GAPDH expression of two independent experiments. Comparable results were achieved for Sk-Hep1 and HepG2 cells (not shown).

The Hippo pathway effectors YAP and TAZ are transcriptional coactivators lacking a DNA binding site (80). Indeed, several transcription factors have been reported to interact with YAP and TAZ to regulate the transcription of different target genes. A well-described protein group of YAP/TAZ-binding transcription factors is the TEAD-family, consisting of four family members

(TEAD1-4) (34). In order to assess whether these transcription factors are also involved in the regulation of MCM expression, TEAD family members were inhibited by RNAi in liver cancer cell lines (Sk-Hep1, HLF). Initial data showed expression of TEAD2 and TEAD3 only at low levels in the used cell lines (data not shown). Therefore, a combined siRNA-mediated knockdown of TEAD1 and TEAD4 expression was performed. Figure 7A illustrates the reduced mRNA expression of TEAD1, TEAD4, and all MCM family members in Sk-Hep1 cells. The strongest effects were observed on MCM2 and MCM7 mRNA levels upon combined TEAD1 and TEAD4 inhibition with a reduction to 25-40% and 20-30%, respectively. In sum, a reduction of TEAD1/4 mRNAs below 20% was accompanied by a reduction of MCM2-7 mRNA by 50 to 80%.

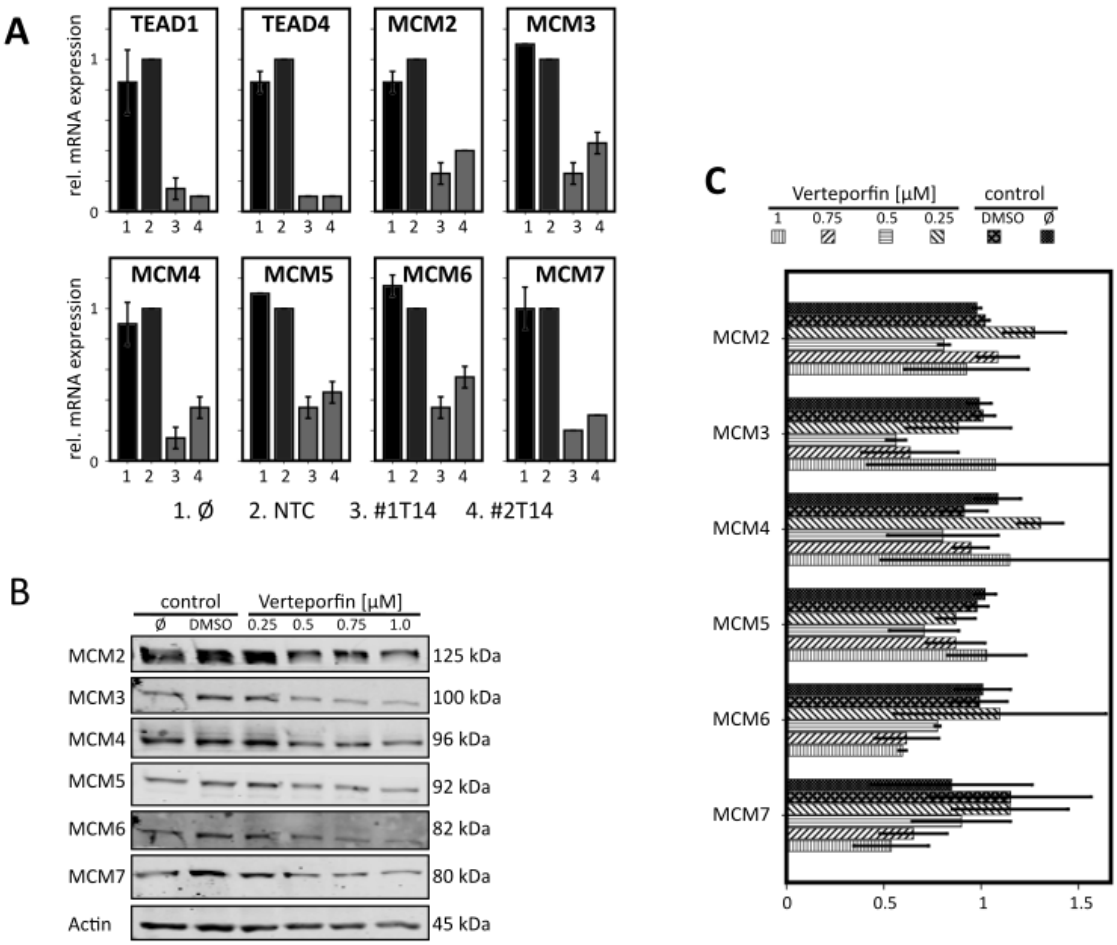

Figure 7: Verteporfin and the transcription factors TEAD1 and TEAD4 regulate MCM gene expression *in vitro*.
(A) Transient transfection of two TEAD1 and TEAD4-specific siRNAs reduced expression levels of MCM genes, as illustrated by real-time PCR. Mean±SD of two independent experiments in Sk-Hep1 cells is shown. Untreated (Ø) and nonsense siRNA (NTC) transfected cells served as controls. Data were normalized to NTC controls. Comparable results were achieved for HLF cells (not shown). (B) Treatment with Verteporfin for 48 hours reduced MCM protein levels in HLF cells. Untreated (Ø) and DMSO-treated cells served as controls. β-Actin was used as a loading control. (C) Quantification of MCM proteins relative to Actin expression of two independent experiments. Comparable results were achieved for Sk-Hep1 and HepG2 cells (not shown).

These data strongly suggested partial YAP/TAZ/TEAD-dependency of MCM protein expression in liver cancer cells. To substantiate this mechanistic connection, the FDA-approved substance

Verteporfin was administered to HCC cells. This drug is a photosensitizer used to treat macular degeneration but has also sensitizer-independent properties, including the inhibition of the YAP/TAZ/TEAD interaction followed by YAP/TAZ degradation (81).

Quantitative immunoblotting analysis of Verteporfin-treated HLF cells is displayed in Figure 7BC showing a clear gradual decrease of MCM6 and MCM7 protein level with increasing drug concentration compared to the respective controls. For MCM2-5, a moderate protein reduction was detectable. However, the simultaneous decrease of the house-keeper β-Actin complicated the analysis of these MCM family members at the protein level. Nevertheless, these data further supported the YAP- and TEAD-dependent transcriptional regulation of MCMs in liver cancer cells.

To further confirm the physical interaction of YAP/TAZ and TEAD4 with the promoter regions of the MCM genes, additional ChIP and luciferase assays experiments were performed. Therefore, the gene promoter sequences of all MCM family genes (defined as -2 kbp to +1 kbp) were analyzed using the software JASPAR to predict possible TEAD4 binding sites. Various potential TEAD4 binding sites were detected and scored by the binding probability, with a score of 5-8 representing medium binding probability. Within the predicted binding sites scored higher than 8, primer pairs were designed around the potential binding sites closest to the transcription starting site (PCR product smaller than 200 bp). The ChIP-primer pairs surrounding the predicted TEAD4 binding sites were validated on total genomic DNA and shown in Figure 8A. Within the MCM4 promoter region, no suitable primer pair could be found due to the GC-rich character of this genomic region.

The real-time PCR analysis of DNA precipitated from HLF cells is shown in Figure 8 B, illustrating the specific binding of YAP, TAZ, and TEAD4 to the predicted MCM promoter regions (with exception of MCM4). TEAD4-ChIPs showed higher amounts of precipitated DNA compared to YAP-ChIP and TAZ-ChIP due to the indirect binding of YAP and TAZ to DNA. Following YAP-IP, 0.16% to 0.34% of input DNA covering analyzed MCM3 and MCM6 promotor regions were precipitated, respectively. Similar, but partly weaker effects could be observed upon TAZ-IP with 0.05% (MCM5) to 0.32% (MCM3) of precipitated input-DNA. TEAD4-IP bound almost twice the amount of DNA with 0.23% for MCM5 and 0.56% for MCM3. ChIP analysis in HepG2 cell confirmed these findings and showed a reproducible precipitation of 0.4% (MCM2) to 1.8% (MCM3) of all MCM promoter regions upon TEAD4-IP. These results confirmed the direct interaction of YAP, TAZ with TEAD4 to the predicted binding sites within the MCM gene promoter regions.

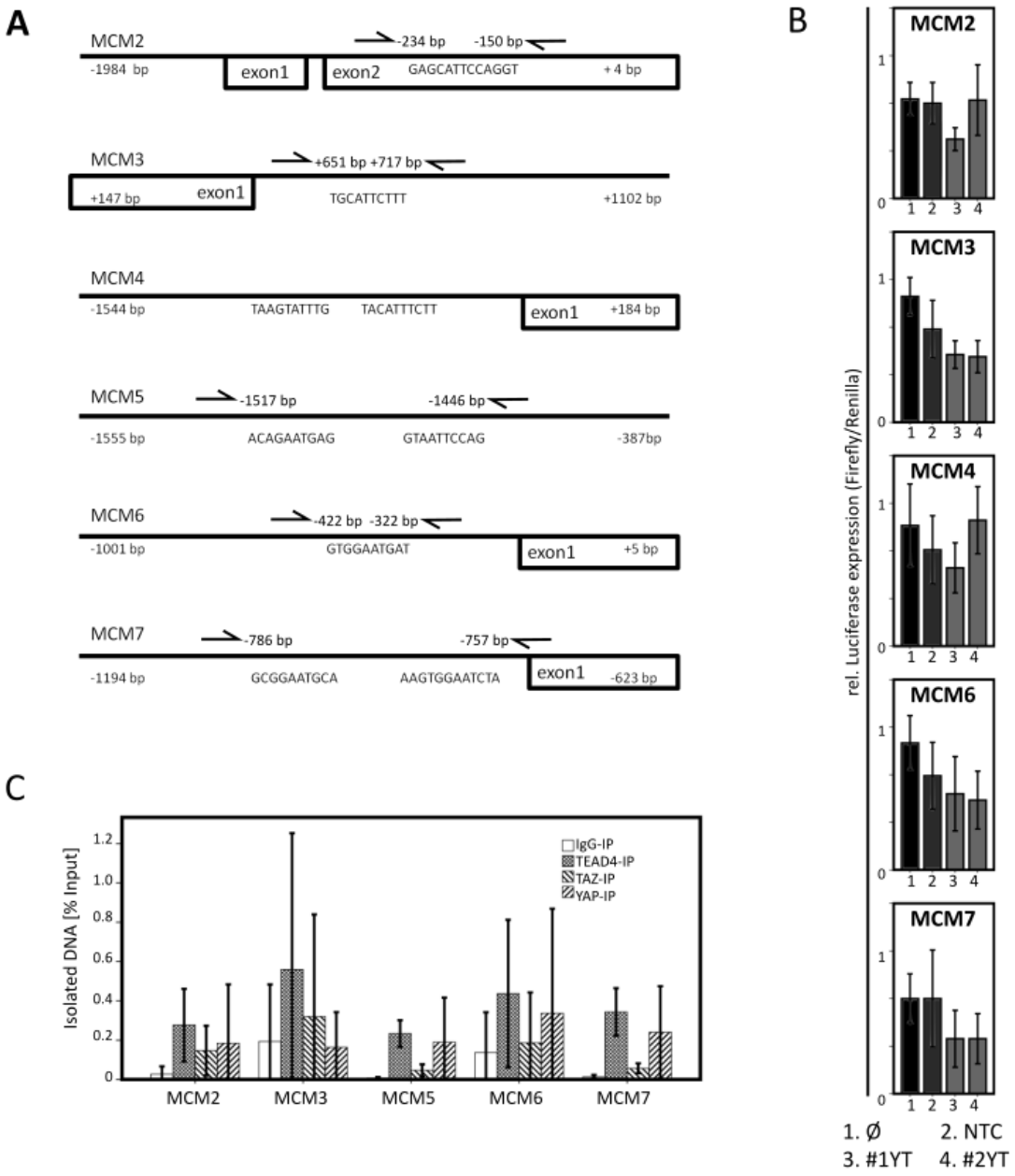

Figure 8: YAP, TAZ, and TEAD4 physically bind to MCM gene promoters.
(A) Schemes illustrate promoter regions fused to Firefly luciferase for luciferase assays with TEAD4 binding sites targeted by ChIP assay-primers (location indicated by arrows). (B) ChIP with YAP, TAZ, TEAD4 and IgG control confirmed binding to the predicted promoter positions in HLF. Similar results were obtained for HepG2 cells (not shown). IP = Immunoprecipitation. (C) Combined siRNA-inhibition of YAP and TAZ reduced MCM promoter activity measured by Firefly luciferase activity normalized to Renilla luciferase activity. Untreated (Ø) and nonsense siRNA (NTC) transfection served as controls. Mean±SD of three independent experiments in HLF cells is shown. Comparable results were achieved for HepG2 cells.

To verify the functional relevance of YAP and TAZ on MCM expression in HLF cells, luciferase assays were performed using plasmids containing MCM promoter regions. Therefore the respective promoter regions, containing the TEAD4 binding sites, which were shown in the previous ChIP assays, were cloned upstream of a plasmid-based Firefly luciferase gene (Figure

8A). Due to technical problems in cloning, only vector constructs for MCM2-4 and 6-7 promoters have been generated and verified by sequencing. The Firefly luciferase constructs were transiently co-transfected into HepG2 and HLF cells with a Renilla luciferase plasmid used for normalization 8 h prior to siRNA treatment. Luciferase activity was measured 48 h after plasmid transfection. The normalized luminescence intensities illustrated an obvious reduction for the MCM3, MCM6, and MCM7 reporters after YAP/TAZ inhibition (between 10 and 40%; Figure 8C). For MCM2 and MCM4, one siRNA combination showed a reproducible signal decrease, while the other combination led to a moderate (for MCM2, second siRNA combination) or no (for MCM4, second siRNA combination) reduction of Luciferase activity compared to the controls.

In summary, expression data analysis after genetic manipulation and treatment with a YAP/TAZ/TEAD inhibitor, protein binding studies as well as activity assays illustrate that both Hippo pathway effectors YAP and TAZ directly regulate the transcription of MCM helicase genes in different liver cancer cell lines in a TEAD-dependent manner.

5.2.2 YAP Regulates MCM mRNA Expression *in vivo*

Following up on the above demonstrated regulation of MCMs by YAP *in vitro*, a transgenic mouse model with inducible and hepatocyte-specific overexpression of constitutively active human YAP^{S127A} was employed (Figure 9A)(50). In this model, the liver activator protein (LAP) is controlling the tetracycline transactivator (tTA) expression. The tTA protein is interacting with doxycycline, which is administered with the drinking water, leading to its inactivation (TET-off system). Upon doxycycline withdrawal, the tTA activates the tetracycline-inducible promoter, controlling the expression of the mutant YAP^{S127A} gene. After 8 – 12 weeks of YAP^{S127A} overexpression, mice develop a severe increase in liver size (hepatomegaly, 8 weeks) and eventually tumor formation (12 weeks), with exemplary livers shown in Figure 9B.

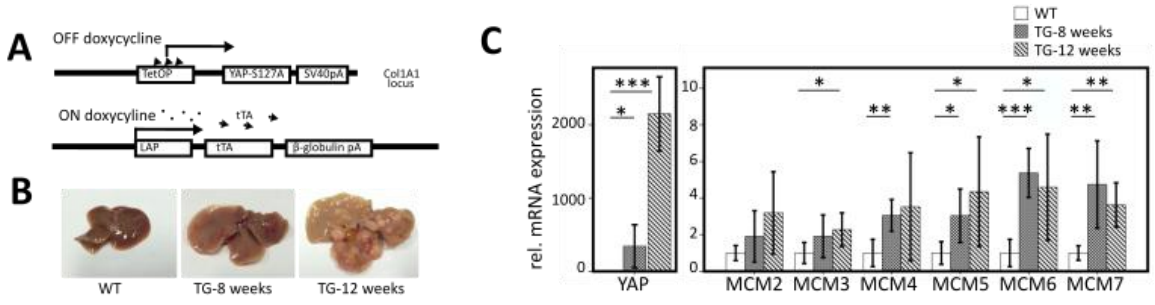

Figure 9: Confirmation of YAP-dependent MCM expression in a transgenic mouse model.
(A) Illustration of liver-specific and doxycycline-dependent YAP^{S127A} overexpression as described by Camargo (50). The liver activator protein (LAP) promoter controlling the expression of tetracycline transactivator (tTA) ensures tissue-specificity. The mutant YAP gene expression is regulated by a Tet-promoter located downstream of the *collagen type I alpha 1 chain* locus (Col1A1). (B) Withdrawal of doxycyclin induces the hepatocyte-specific expression of the mutant YAP gene (YAP^{S127A}). Induction of the transgene for 8 - 12 weeks increased the liver size and first macroscopic tumors are detectable. (C) Expression levels of YAP and murine MCM2-7 mRNAs were analyzed in livers of wildtype (WT; 5 mice) and YAPtg mice after 8 and 12 weeks (5 and 4 mice respectively) of YAP^{S127A} induction. (* $p < 0.05$; ** $p < 0.01$; *** $p < 0.001$)

The mRNA levels of all murine MCM family members in transgenic mouse livers after 8 (without macroscopic tumors; n = 5) or 12 (with macroscopic tumors; n = 4) weeks of transgene induction was compared with wildtype mouse livers (n = 5). Real-time PCR analysis revealed 2 to 5-fold elevated MCM2-7 expression levels upon YAP^{S127A} induction (Figure 9C). Tumor-bearing mice had significantly higher MCM3, MCM5, MCM6, and MCM7 expression levels after 12 weeks of doxycycline-withdrawal. Importantly, 8 weeks after YAP^{S127A} overexpression (malignant transformation), transgenic mouse livers already showed a 3 to 5-fold increase of MCM4, MCM5, MCM6, and MCM7 mRNA levels compared to the control group.

In summary, these results further illustrate that elevated MCM2-7 levels are regulated by YAP in primary murine hepatocytes. Importantly, this MCM overexpression is already detectable in pre-malignant livers, illustrating that these elevated MCM amounts are not due to malignant transformation.

5.2.3 MCM Family Members Regulate HCC Cell Proliferation

To assess the relevance of the MCM family members in HCC cells, different functional assays were performed. For this purpose, siRNA inhibitions for individual MCM family members were established (exemplary immunoblots shown in Figure 10A). Efficient reduction was confirmed at the protein levels with a reduction of individual MCMs below 25%. Cell viability assays were performed 48 h after siRNA treatment in Sk-Hep1 and HepG2. Targeting different MCMs, no consistent or reproducible reduction of cell viability could be observed, as exemplary shown for MCM2, MCM6 and MCM7 (Figure 10B).

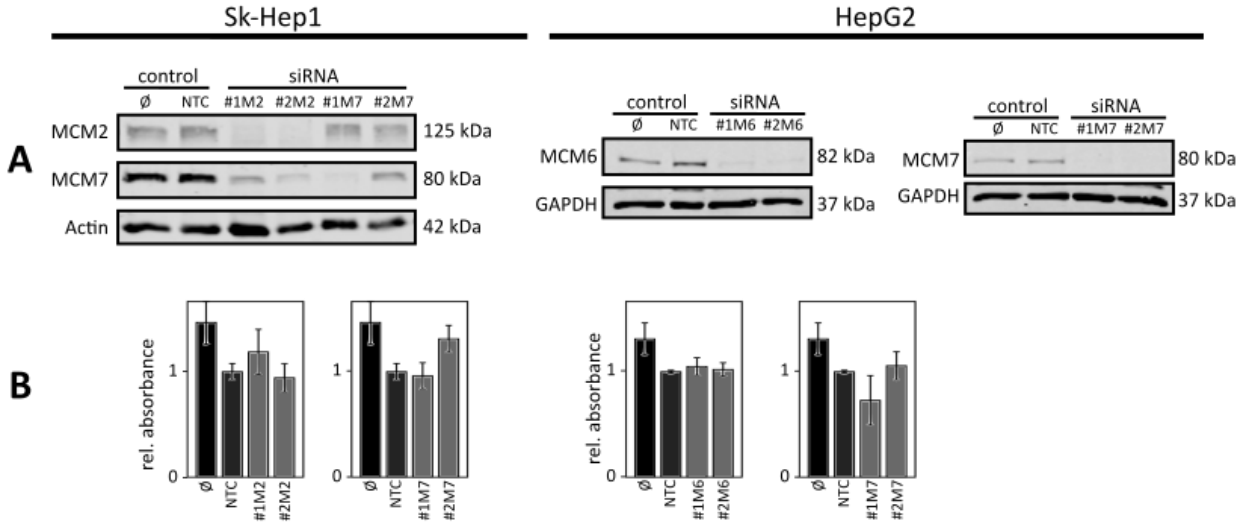

Figure 10: Individual MCM inhibition has no influence on cell viability.
(A) Transient knockdown of MCM2, MCM6 or MCM7 with specific siRNAs led to reduced protein levels of the respective MCMs after 48h, as illustrated by Western Blot analysis in HepG2 and Sk-Hep1 cells. (B) Cell viability-assay: Transient knockdown of MCM2, MCM6 or MCM7 had no consistent effect on cell-viability after 48h of inhibition. Untreated (Ø) and nonsense siRNA (NTC) transfection served as controls. Mean±SD of two independent experiments in HepG2 and Sk-Hep1 cells is shown.

It was hypothesized that the lack of change in cell viability was either due to a low sensitivity of the applied test or the residual amount of the respective amount was sufficient to ensure DNA replication. In order to overcome these obstacles, one approach was to totally delete MCMs employing the CRISPR/Cas9 system.

Therefore, plasmids were cloned that contained GFP, a single guide RNA (sgRNA) targeting MCM2 and the *pac* gene, encoding *N*-acetyl-transferase for puromycin-resistance. HepG2 cells stably expressing Cas9 (HepG2-Cas9) were generated and transfected, but no homozygous MCM2-deleted stable cells could be obtained. This led to the conclusion, that complete silencing of MCM2 is essential for proliferation. To further define the temporal impact of MCM2 on cell viability a competitor assay was established as illustrated in Figure 11A.

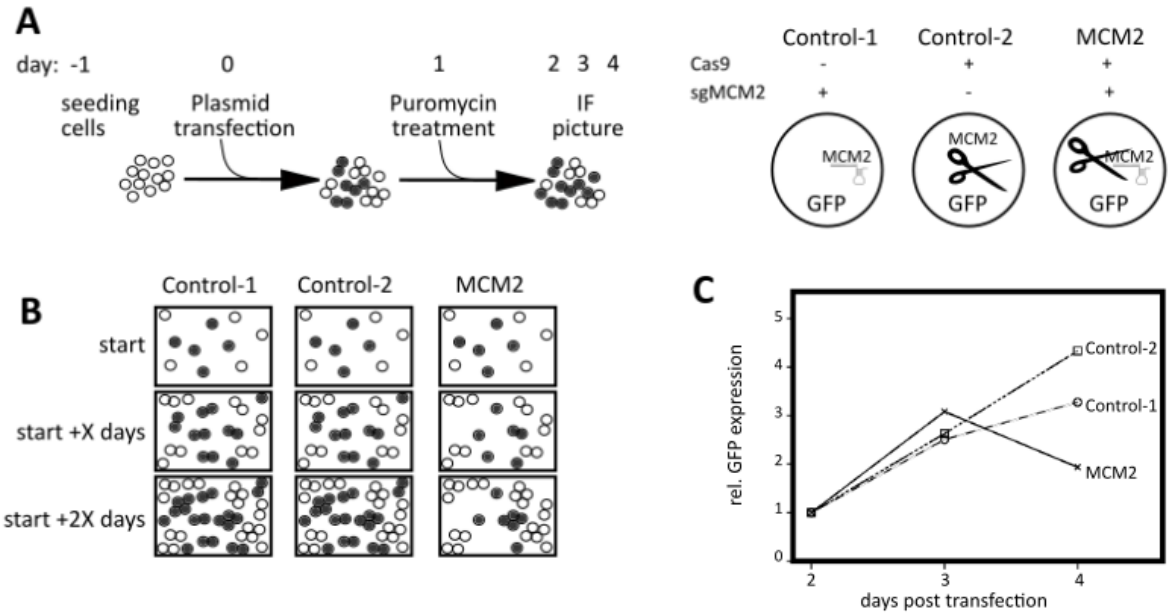

Figure 11: Competitor assay.
(A) Scheme illustrating CRISPR/Cas9-based competitor assay and enzymes and RNA present in successfully transfected cells. (B) Anticipated course of the experiment with effectively transfected cells expressing GFP in gray and untransfected cells in white. (C) Competitor assay: Transfection of HepG2 and HepG2-Cas9 cells, with sgRNA-coding or empty CRISPR-plasmids. The green fluorescent area was measured and normalized to day 2 and the mean of 3 independent experiments is depicted in the graph.

Therefore, HepG2-Cas9 cells were transfected with the plasmid coding for the sgRNA targeting *MCM2*, selected with puromycin and immunofluorescene pictures were taken. HepG2 cells transfected with the MCM2 targeting vector (Control-1) and HepG2-Cas9 cells transfected with an empty vector (Control-2) served as controls (Figure 11B). The green fluorescent area represented an indicator for the number of cells with sgRNA-mediated MCM2 inhibition (MCM2) or transfected cells with intact MCM2 (Control-1 and Control-2). The GFP-positive area per picture was measured and normalized to the data obtained at day two after transfection. Therefore, in this assay the GFP-positive area could be associated with the amount of cell proliferation and the cumulative result of three independent experiments illustrated in Figure

11C. The results showed a steady increase of green areas (proliferating cells) in both control groups on day 3 and 4. On the contrary, cells lacking MCM2 (HepG2-Cas9 sgMCM2) showed reduced proliferation 4 days after transfection.

Another approach to investigate the impact of MCMs on liver cancer cell proliferation was to reduce the protein expression of all MCM family members (MCM2-7) at once. It was assumed that the combined RNAi treatment would reduce the stochastic probability of individual cells expressing all MCM proteins and thus masking possible effects. Therefore, combined siRNA inhibitions combining all siRNAs that target all MCM family members were established and a reduction of each MCM within a single treatment to below 25% was considered as efficient (Figure 12AB).

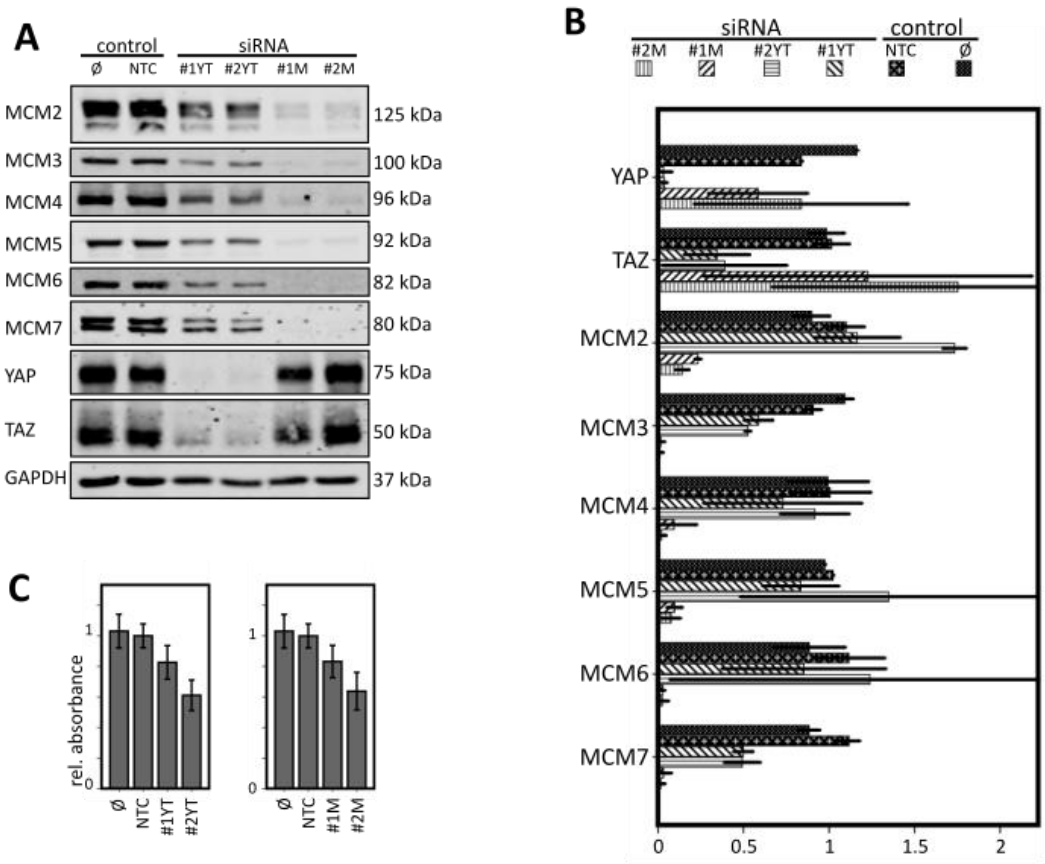

Figure 12: YAP and TAZ influence proliferation via MCM regulation.
(A) Transient knockdown of YAP/TAZ and all MCM family members with specific siRNAs led to reduced protein levels of the respective proteins as illustrated by Western Blot analysis in HLF cells. GAPDH was used as a loading control. (B) Quantification of two independent experiments as described in (A) normalized to GAPDH expression. Comparable results were achieved for HepG2 cells (not shown). (C) BrdU-assay: Transient knockdown of YAP/TAZ and all MCMs led to reduced BrdU incorporated into genomic DNA, 48 hours after inhibition. Untreated (Ø) and nonsense siRNA (NTC) transfection served as controls. Mean±SD of three independent experiments in HLF cells is shown. Comparable results were achieved for HepG2 cells (not shown).

The relevance of all MCM family members on proliferation was examined using a BrdU assay after combined siRNA-mediated silencing of all MCMs in HepG2 and HLF cells. Inhibition of YAP

and TAZ was performed as a positive control. The thymidine analog BrdU was subjected to the medium 48 h after RNAi treatment for 1 h of incubation, and incorporated by proliferating cells stochastically into duplicating DNA. Efficient, combined MCM2-7 knockdown has similar effects as combined YAP and TAZ knockdown on BrdU incorporation in HLF cells. In total, the BrdU-incorporation assay illustrated that proliferation is reduced about 20-40% after MCM2-7, YAP and TAZ knockdown in HepG2 and HLF cells (Figure 12C and data not shown) confirmed that efficient, combined MCM2-7 knockdown has similar effects as YAP and TAZ.

Taken together, these results demonstrate that only the efficient and rapid knockdown of MCM-helicase in liver cancer cell lines leads to reduced cell proliferation visible in BrdU ELISA assay. The more sensitive assay confirmed the pro-proliferative role of an individual MCM (here MCM2) in cell proliferation (competitor assay).

5.2.4 MCM2-7 Expression Correlates to Poor Clinical Prognosis in Human HCC

The previous results demonstrated that YAP positively correlated with MCM2-7 expression, *in vitro* and *in vivo*, and that YAP/TAZ directly regulated MCM transcription. In order to validate these findings in independent human HCC cohorts, mRNA expression data derived from 242 HCC patients (cohort 1) (72) and 370 liver cancer patients (cohort 2) (27) were analyzed. The comparison of mRNA levels in tumor with the corresponding non-tumorous liver tissue showed that all MCM helicase components were significantly overexpressed in HCC tissues (Figure 13).

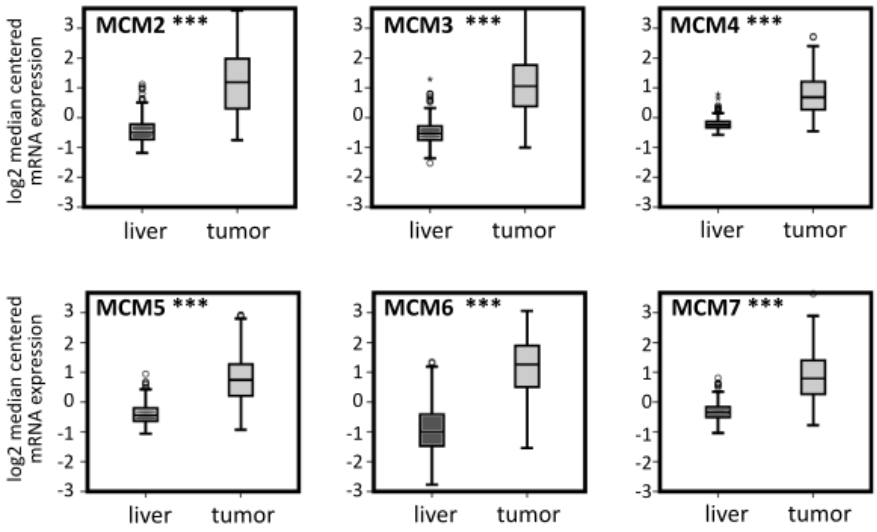

Figure 13: Elevated expression of MCMs in human HCCs.
MCM2-7 mRNA is overexpressed in a cohort of 242 liver cancer patients compared to surrounding liver tissue (cohort 1). (*** $p < 0.001$)

To correlate the amounts of individual MCM mRNA levels with clinical outcome of HCC patients, Kaplan-Meier plots were generated. Therefore, data from HCC patients were divided into equal groups (threshold: median) according to their MCM2-7 mRNA expression levels. HCC patients

with higher MCM helicase expression had significantly worse overall survival and earlier cancer recurrence as compared to patients with lower MCM expression (Figure 14).

In order to determine whether clinicopathological features were associated with the general expression of all MCM helicase family members in HCC patients (cohort 2), the individual MCM mRNA expression data were combined and summed up to a score. The MCM score was then used to divide the patients into three groups of high (34%), medium (33%) and low (33%) helicase expression. Patient characteristics including age and tumor grading were analyzed with respect to the MCM classification and the numbers of patients with a certain characteristic were quantified. Data analysis revealed no significant enrichment of female or male patients in groups with high-medium, or low MCM expression scores (Table 32).

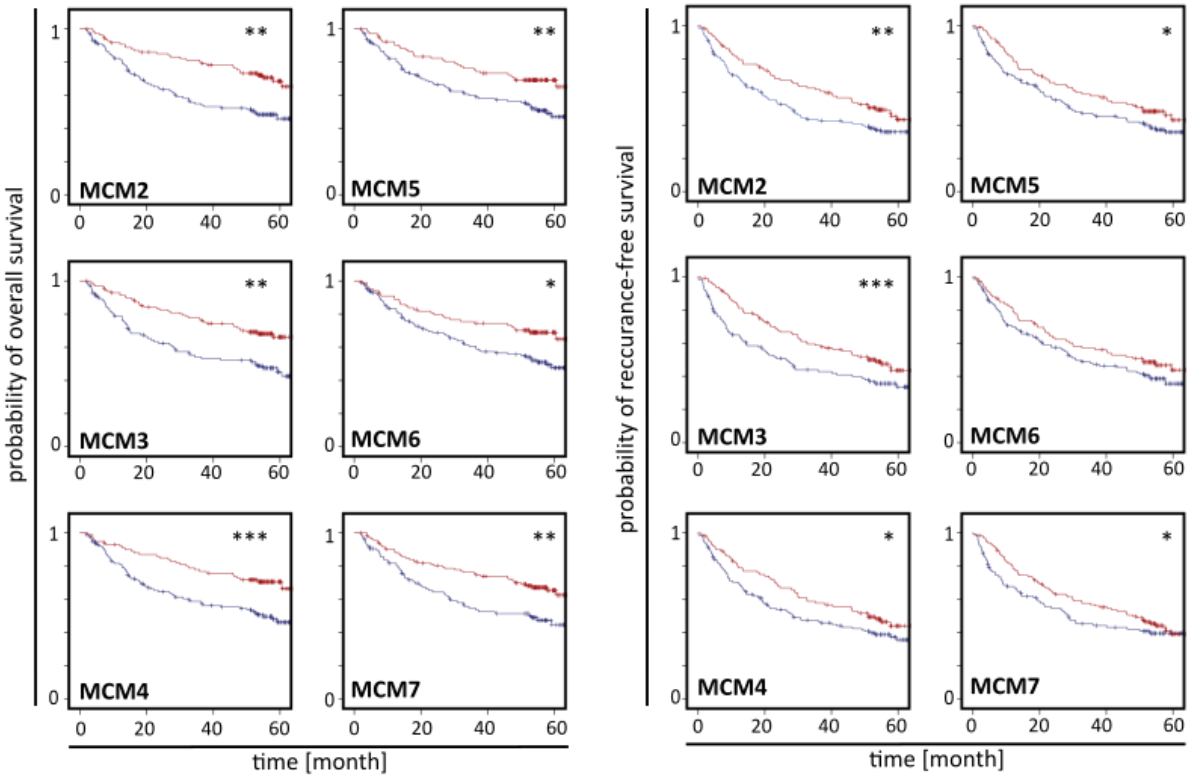

Figure 14: Elevated expression of MCMs correlates with poor prognosis in HCC patients.
Kaplan-Meier analysis of MCM2-7 for overall and recurrence-free survival in cohort 1 with blue indicating high and red low expression levels. High MCM transcript levels significantly correlate with earlier tumor recurrence and disease-free survival (Wilcoxon-test). Comparable results were achieved for the TCGA LIHC cohort (not shown). (* $p < 0.05$; ** $p < 0.01$; *** $p < 0.001$)

Furthermore, the age of patients, vascular invasion, and inflammation did not statistically correlate with the amount of MCMs mRNA levels in this cohort. Asian and Caucasian patients were equally represented in the dataset. However, the Caucasian patients were significantly enriched in the group with low MCM abundance. In addition, the parameter 'family history', which represents cancer diagnosis of genetically related family members, was significantly

associated with a higher expression of MCM helicases. Patients with a high body mass index (BMI >30) were significantly overrepresented within the low MCM patient cluster. In agreement with the analyzed survival data, TNM stage and tumor grade at diagnosis significantly correlated with higher MCM expression.

Together, these findings indicate that all MCM helicase family members are overexpressed at mRNA level in human HCC and that elevated MCM2-7 expression is associated with tumor dedifferentiation and poor clinical outcome of HCC patients.

Table 32: Elevated expression of MCMs correlate with clinicopathological features.
An MCM score was used to divide patients into groups with high, medium and low MCM expression, by summing the mRNA expression values for MCM2-7 in cohort2. Additionally, patients were divided into groups for each feature, followed by the quantification of the number of patients in each group. The median value was used to assign for the analysis of age. The numbers of patients with the respective clinicopathological feature are listed in the table together with the p-value of the statistical test (Chi-squared test). n.s.=not significant

		MCM cluster				
		High	Medium	Low	SUM	sig.
gender	female	43	41	37	121	n.s.
	male	80	83	87	250	
family history	yes	75	75	58	208	0.006
	no	30	31	51	112	
race	asian	65	59	34	158	0.000
	caucasian	51	56	77	184	
tumor grade	G1+G2	58	72	102	232	0.000
	G3+G4	65	49	20	134	
TNM stage	T1+T2	82	96	97	275	0.040
	T3+T4	41	27	25	93	
vascular invasion	no	64	68	74	206	n.s.
	yes	35	39	35	109	
BMI	normal	83	87	65	235	0.014
	obese	24	16	32	72	
inflammation	no	30	41	46	117	n.s.
	yes	38	37	42	117	
age	≥ 61	53	57	69	179	n.s.
	< 61	70	67	55	192	

5.2.5 YAP Expression Correlates to MCM Expression in Human HCC

To further confirm the overexpression of individual MCMs on protein levels and to associate their abundance with the subcellular localization of YAP in tumor cells, immunohistochemical stains of TMA containing 105 HCCs and 7 normal liver tissues were performed.

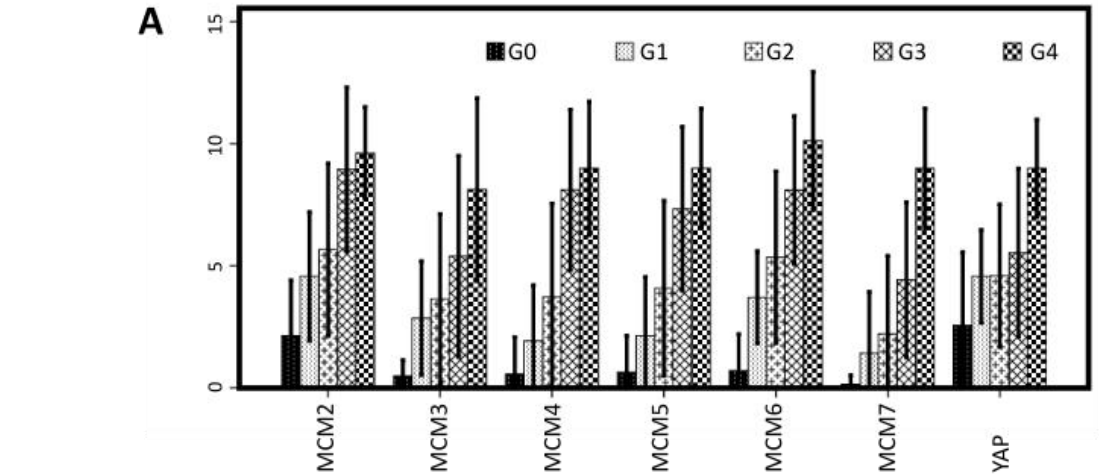
A
15
10
5
0
G0
G1
G2
G3
G4
MCM2
MCM3
MCM4
MCM5
MCM6
MCM7
YAP

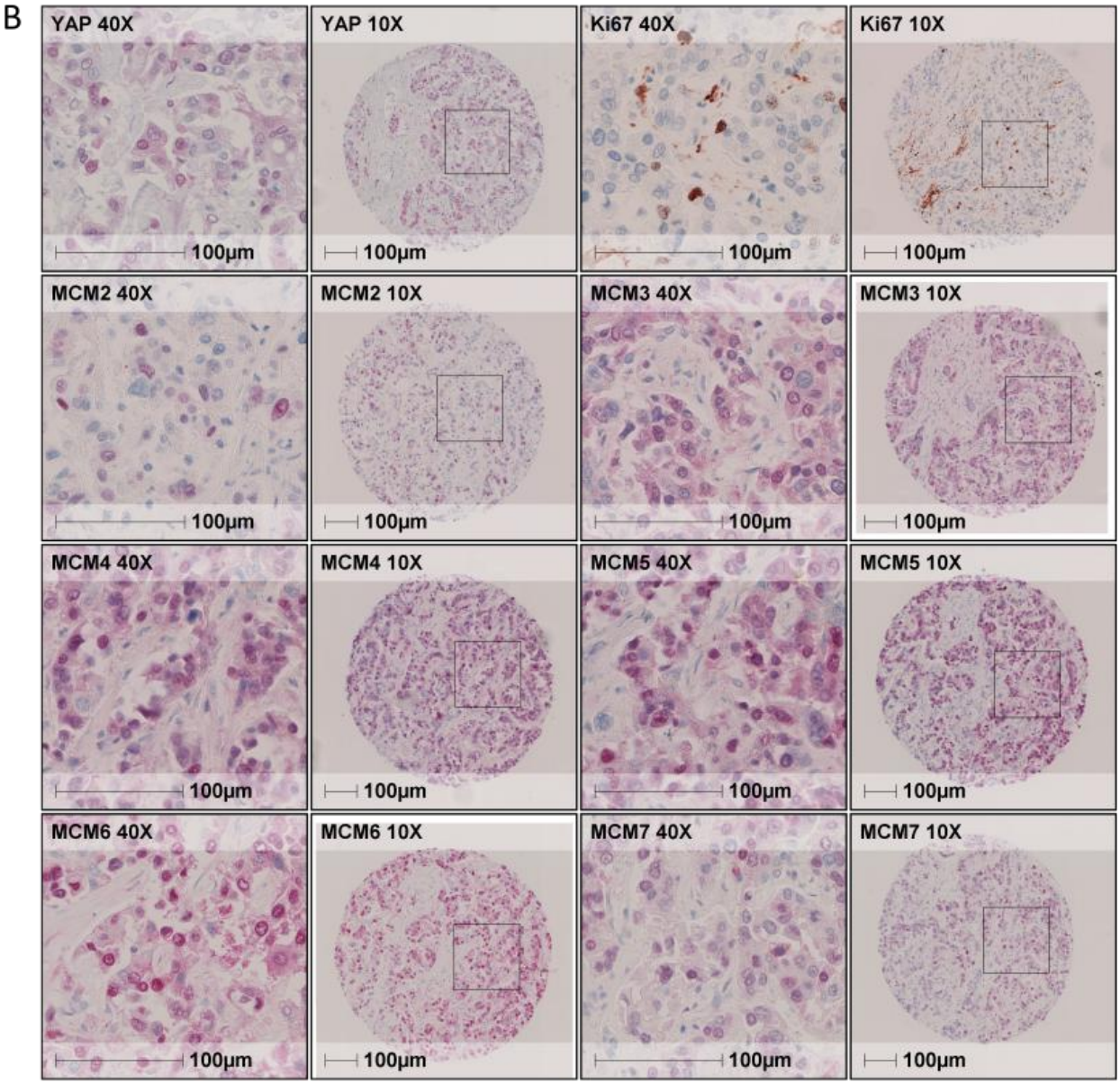
B
YAP 40X
YAP 10X
Ki67 40X
Ki67 10X
MCM2 40X
MCM2 10X
MCM3 40X
MCM3 10X
MCM4 40X
MCM4 10X
MCM5 40X
MCM5 10X
MCM6 40X
MCM6 10X
MCM7 40X
MCM7 10X
100µm

Figure 15: YAP expression correlates with MCM-helicase expression and histological grading in HCC patients.
(A) TMA evaluation shows a significant correlation between YAP and MCM2-7 levels with tumor gradings (G1-G4) as illustrated by the bar graph. G0 = healthy liver. (B) Exemplary immunohistochemical stains of YAP and Ki67 positive human HCC tissue stained for Ki67, YAP and MCM2-7, respectively.

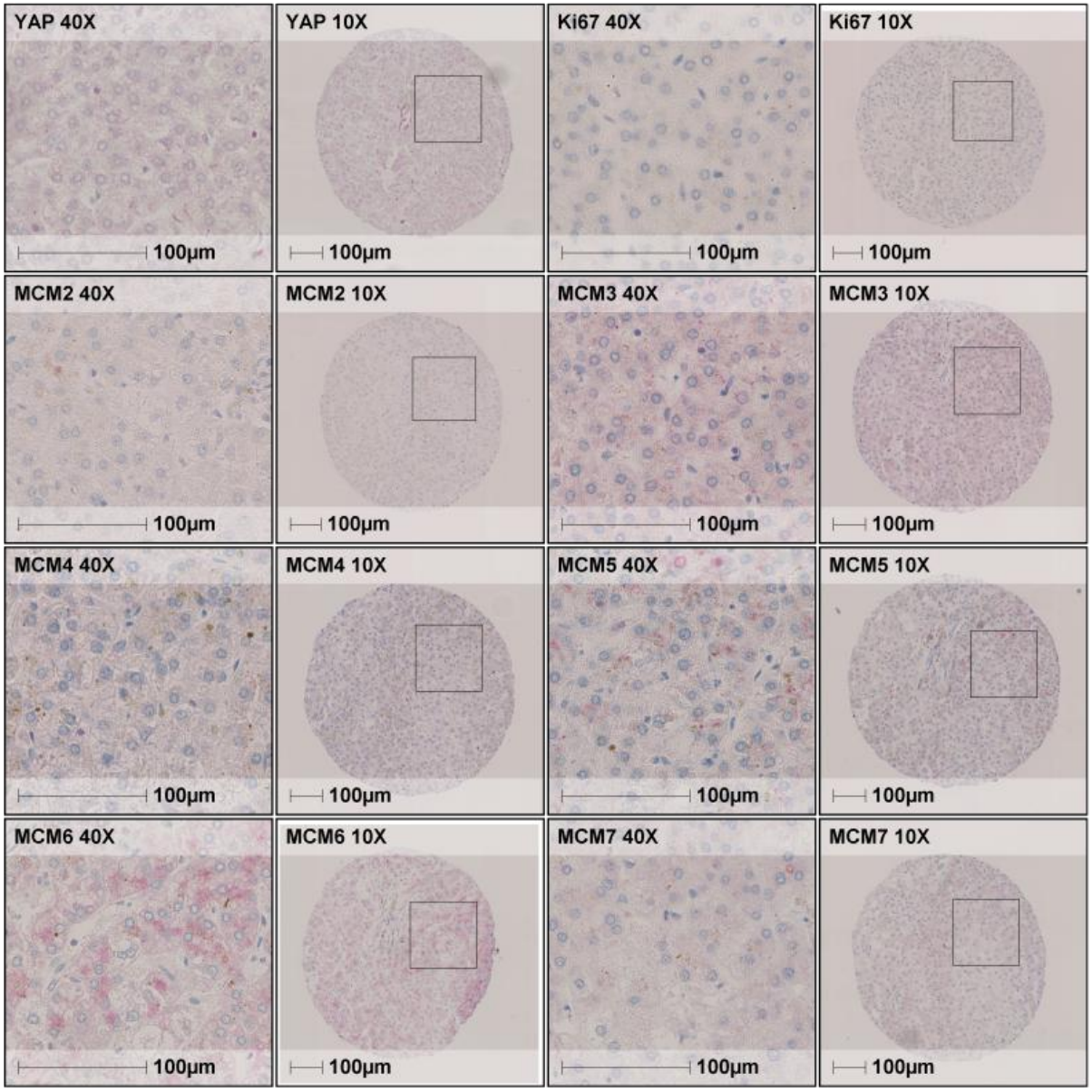

Figure 16: YAP and Ki67 negative human HCC samples (TMA analysis).
Exemplary immunohistochemical stain of YAP and Ki67 negative human HCC tissue stained for Ki67, YAP and MCM2-7.

For this purpose, respective staining protocols for YAP, the proliferation marker KI67, and MCM2-7 were established. Systematic evaluation of all TMAs revealed a strong correlation of YAP and MCM2-7 protein expression with tumor grading, which further validated the previous

findings of the expression analysis (Figure 15A; Table 33). Exemplary stains for YAP and Ki67 double positive and negative HCC tissues are shown in Figure 15B and Figure 16, respectively. Hence MCMs are functionally related proteins, comparable protein staining levels in individual HCC tissue samples were expected. Indeed, statistical comparison of MCM stains revealed a highly significant and positive correlation of MCMs with each other (Table 33).

As expected from the literature, Spearman analysis of TMA evaluation showed a significant correlation of nuclear YAP expression with the proliferation marker Ki67 (61). In addition, YAP and Ki67 showed a significant positive association with all MCM helicase members in HCC tissues (Table 33).

Table 33: YAP and Ki67 expression correlate with MCM2-7 expression and histological grading in HCC patients.
Spearman correlation analysis of evaluated TMAs illustrates a significant correlation between YAP and Ki67 with MCM2-7 levels and tumor gradings (G). (* $p < 0.1$; ** $p < 0.01$).

	YAP	MCM2	MCM3	MCM4	MCM5	MCM6	MCM7	G
Ki67	0.383**	0.713**	0.588**	0.595**	0.549**	0.540**	0.593**	0.437**
YAP	1	0.480**	0.389**	0.476**	0.467**	0.404**	0.480**	0.318**
MCM2		1	0.724**	0.753**	0.755**	0.784**	0.692**	0.446**
MCM3			1	0.810**	0.792**	0.734**	0.753**	0.382**
MCM4				1	0.929**	0.835**	0.850**	0.483**
MCM5					1	0.864**	0.822**	0.304**
MCM6						1	0.719**	0.512**
MCM7							1	0.435**

To further support the association of Hippo pathway effectors and MCM family members, Spearman analysis of the mRNA expression data in cohort 2 has been performed (Table 34). As expected from the TMA analysis, YAP mRNA expression significantly correlated with the mRNA expression of all MCM family members. Moreover, a moderate but significant correlation of the two Hippo effectors YAP and TAZ with each other became apparent in cohort 2. In line with this observation, TAZ expression showed moderate correlation to MCM3, MCM5, MCM6, and MCM7 and no significant correlation to MCM2 and MCM4 expression.

Together, these findings show that all MCM helicase family members correlate strongly with YAP, Ki67 and moderately with TAZ expression in human HCC. Additionally, elevated MCM2-7 levels are associated with high tumor dedifferentiation.

Table 34: YAP and TAZ mRNA expression correlate with MCM helicase mRNA expression in human HCC.
(cohort2; * $p < 0.1$; ** $p < 0.01$).

	YAP	MCM2	MCM3	MCM4	MCM5	MCM6	MCM7
YAP	1	0.351**	0.446**	0.401**	0.423**	0.415**	0.382**
TAZ	0.216**	0.083	0.127**	0.037	0.148**	0.182**	0.116*

5.3 PRC2

5.3.1 YAP Regulates PRC2 Component Expression via TEAD

Because in the initial screen, some PRC2 complex family members were differentially regulated after YAP inhibition (Figure 5), the impact of YAP on these factors was further investigated in the second part of the project. In order to confirm the positive regulatory effects of YAP on PRC2 components in section 5.1.1, immunoblot analysis was performed after YAP silencing in liver cancer cells. Therefore, HepG2, Sk-Hep1 and HLF cells were transfected with two YAP-specific siRNA for 48 h and the protein expression was analyzed (Exemplary shown for HLF cells in Figure 17. Due to weak effects of YAP inhibition on mRNA expression, EZH1 was excluded from further analyses. In addition, and due to limited antibody availability, RBBP4 and EED protein expression could not be further analyzed. However, for the remaining factors (EZH2, SUZ12 and RBBP7), immunoblot quantification showed that efficient YAP knockdown was associated with reduced PRC2 protein expression in HLF cells.

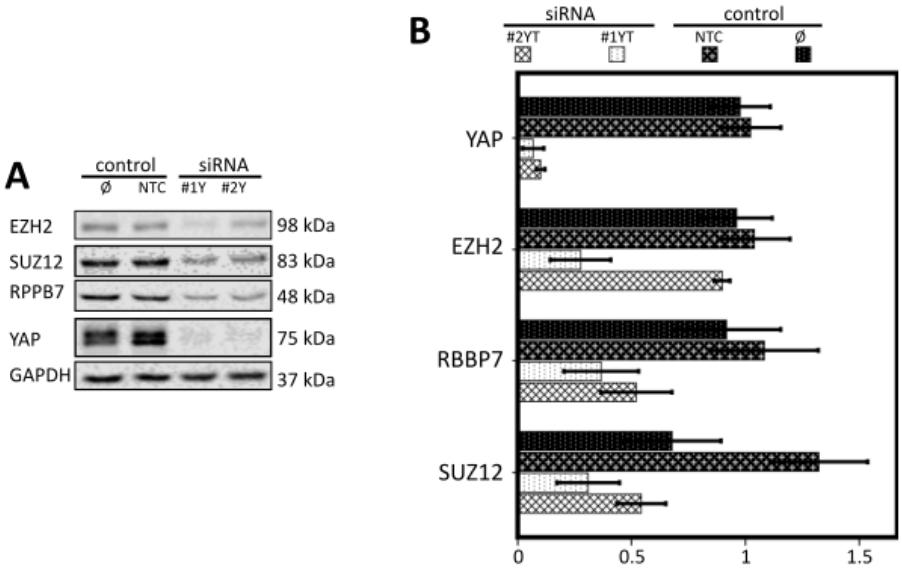

Figure 17: The transcriptional co-activator YAP regulates PRC2 component expression *in vitro*.
(A) Transient transfection with YAP-specific siRNAs led to reduced levels of EZH2, SUZ12 and RBBP7 proteins as exemplarily illustrated by Western Blot analysis in HLF cells. (B) Protein quantification of PRC2 components relative to GAPDH expression of two independent experiments. Untreated (Ø) and nonsense siRNA (NTC) transfection served as controls. GAPDH was used as a loading control. Comparable results were achieved for Sk-Hep1 and HepG2 cells (not shown).

As for the MCMs, the involved transcription factor interacting with YAP and regulating PRC2 components had to be identified. For this, Sk-Hep1 cells were treated with TEAD1 and TEAD4-specific siRNA for 48 h and analyzed via real-time PCR. Figure 18A shows that a reduction of TEAD mRNA to 10-20% led to a reduction of the analyzed PRC2 components by 25 to 75% at the mRNA level in Sk-Hep1, suggesting that these TEAD family members are involved in the YAP-dependent regulation of EZH2, SU12, RBBP7.

To further analyze the YAP/TEAD-dependency of the PRC2 protein expression, HLF and HepG2 cells were treated with different concentrations of the YAP/TEAD inhibitor Verteporfin. Even though a decreased expression of EZH2, SUZ12, and RBBP7 by 10 to 40% compared to the DMSO-control was detected when treated with Verteporfin, no dose dependent change in protein abundance could be observed (Figure 18BC). Hence mRNA analysis of Verteporfin treated HepG2 and Sk-Hep1 cells showed a gradually decreased expression of EZH2, SUZ12 and RBBP7 to 20-40% (data not shown). This data further support the relevance of the YAP/TEAD transcription complex for the regulation of the analyzed PRC2 components in HepG2 and Sk-Hep1.

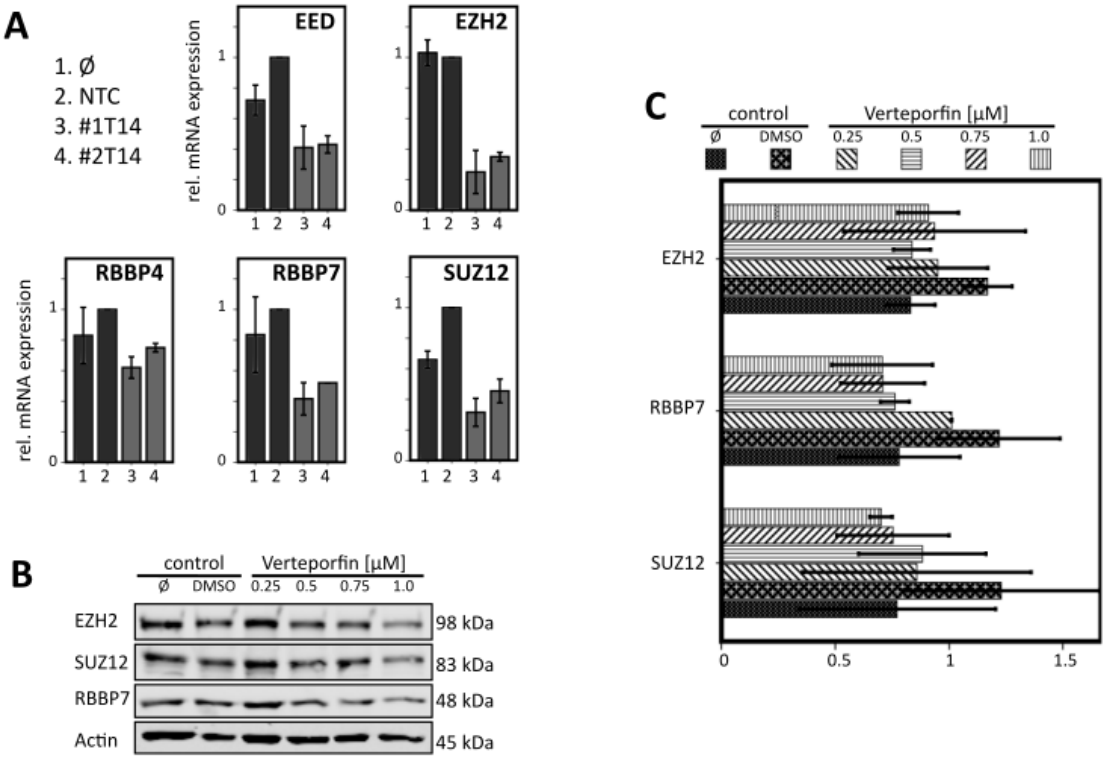

Figure 18: Effects of Verteporfin and the transcription factors TEAD1 and TEAD4 on PRC2 components *in vitro*.
(A) Transient transfection of two TEAD1 and TEAD4-specific siRNAs reduced expression levels of PRC2 components, as illustrated by real-time PCR. Mean±SD of two independent experiments in Sk-Hep1 cells is shown. Untreated (Ø) and nonsense siRNA (NTC) transfected cells served as controls. Data were normalized to NTC controls. (B) Treatment with Verteporfin for 48 h reduced EZH2, SUZ12 and RBBP7 levels in HLF cells. Untreated (Ø) and DMSO-treated cells served as controls. β-Actin was used as a loading control. (C) Quantification of PRC2 complex proteins relative to β-Actin levels of two independent experiments is shown. Comparable results were achieved for HepG2 cells (not shown).

To validate these findings by ChIP, the human promoter sequences of EZH2, SUZ12, and RBBP7 (-2 kbp until +1 kbp) were subjected to online software analysis tool JASPAR, which predicted various potential TEAD4 binding sites. The predicted TEAD4 binding sites with a binding score of 8 or higher were considered for primer design. ChIP-primer pairs were designed focusing on the predicted binding sites closest to the transcription start of each gene (predicted PCR product smaller than 200 bp). The primers functionally validated on total genomic DNA are shown in

Figure 19A. DNA precipitated from HLF cells using TEAD4-antibody was analyzed by real-time PCR and shown in Figure 19B. TEAD4-ChIPs could precipitate 0.07% to 0.11% of input-DNA covering RBBP7 and EZH2 promoter regions respectively, whereas IgG-IP did not precipitate any detectable DNA. Additional ChIP analysis in HepG2 cells showed a precipitation of EZH2 and SUZ12 promoter regions of 0.8-0.9% input-DNA, respectively.

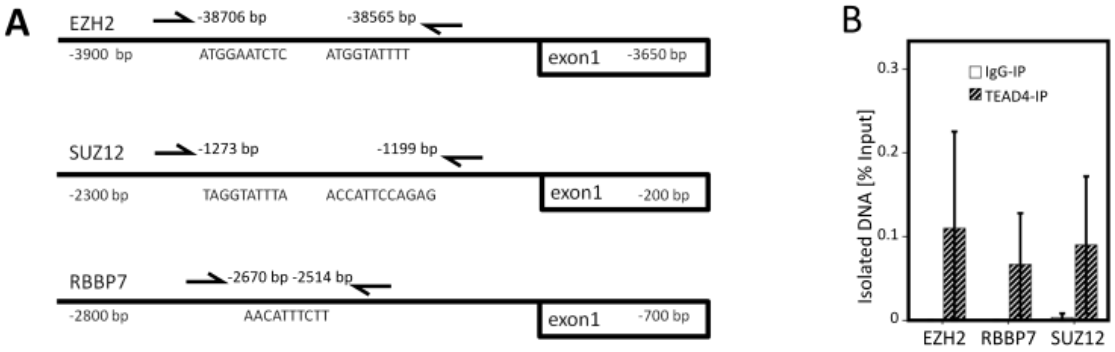

Figure 19: TEAD4 physically binds to PRC2 gene promoters.
(A) Schemes illustrate promoter regions fused to Firefly luciferase with TEAD4 binding sites targeted by ChIP-primers (location indicated by arrows). (B) ChIP with YAP, TAZ, and TEAD4 confirmed binding to the analyzed consensus sites in HLF. Similar results were obtained for HepG2 cells (not shown). IP = Immunoprecipitation.

Together, these results indicate an interaction of a YAP/TEAD4 complex that directly regulates the transcription of PRC2 components through promoter binding in different liver cancer cell lines.

5.3.2 YAP Regulates PRC2 mRNA Expression *in vivo*

Having established that YAP regulates the expression of PRC2 components at the transcriptional level *in vitro*, it was intended to confirm these observations in the YAP^{S127A} mouse model (Figure 13A). Therefore, primary hepatocytes isolated from 6 wildtype mice were compared to YAP^{S127A}-positive hepatocytes isolated from 4 mice, 8 weeks after transgene induction. Real-time PCR analysis illustrated a 1.3-fold induction for SUZ12 and an up to 3.6-fold increase for EZH2 upon YAP induction (Figure 20).

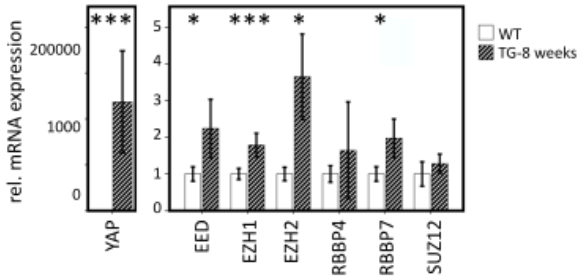

Figure 20: YAP-transgenic mouse model.
Expression levels of YAP and PRC2 components mRNA (EED, EZH1, EZH2, RBBP4, RBBP7, and SUZ12) were analyzed from isolated hepatocytes of wildtype (WT; n=6) and YAPtg (n=4) mice after 8 weeks of YAP^{S127A} induction. (*** $p < 0.001$; * $p < 0.05$)

These results further illustrated that elevated levels of these PRC2 components correlated with YAP overexpression already in primary hepatocytes isolated from pre-malignant murine livers with YAP-induced hyperplasia.

5.3.3 YAP Regulates Histone H3 Trimethylation via PRC2 Expression

Having established that YAP directly regulates the expression of PRC2 components, the next step was to determine whether the biological effects of PRC2 may be influenced by YAP activity. PRC2 is catalysing the trimethylation of lysine 27 of histone H3 (H3K27me3), an epigenetic mark silencing gene transcription (82). In order to test whether the absence of YAP reduces the abundance of this epigenetic mark, siRNA-mediated knockdown of YAP was repeated in different liver cancer cell lines. Figure 21 shows a decrease of SUZ12, EZH2 and RBBP7 levels and a subsequent reduction of H3K27me3 by 60-80% upon YAP silencing. To ascertain if the observed effect is mediated by PRC2, HLF cells were treated with an EZH2-specific kinase inhibitor (Tazemetostat) for 48 h. Tazemetostat is intended to exclusively inhibit the methyltransferase activity of PRC2 without affecting protein expression (83). Compared to DMSO treated cells, Tazemetostat had no conclusive effects on the protein abundance of EZH2, SUZ12, and RBBP7 as depicted in Figure 21. On the other hand, H3K27me3 was reduced to 27% in HLF and 23% in HepG2 cells upon drug treatment for 48 h compared to the respective controls.

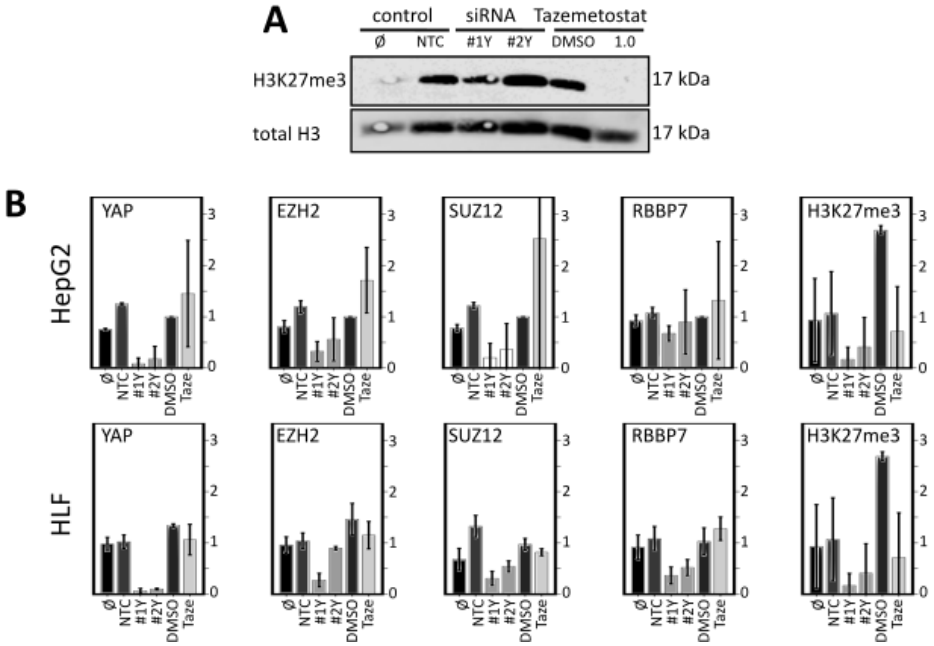

Figure 21: Trimethylation of histone H3 regulated by YAP via PRC2.
(A) Exemplary Immunolot displaying total histone H3 and H3K27me3 after Tazemetostat treatment and RNAi knockdown of YAP in HLF cells. (B) Immunoblot quantification of two independent RNAi knockdown experiments illustrating PRC2 components and H3K27me3 upon Tazemetostat treatment and RNAi knockdown of YAP in HLF and HepG2 cells. Untreated (Ø), DMSO and nonsense siRNA (NTC) transfection served as controls. GAPDH and total histone H3 were used as a loading control.

These findings demonstrate that the expression of the epigenetic marker H3K27me3 was reduced upon YAP inhibition and EZH2 kinase inhibition.

5.3.4 Comparison of YAP and PRC2 Target Genes in HCC Cells

The previous data indicated that YAP may regulate histone methylation via the transcriptional control of essential PRC2 complex constituents. However, it is unknown which negatively regulated YAP target genes might be affected by this molecular mechanism. A comparative expression profiling analysis of HCC cells was performed to define genes, which are inversely controlled by PRC2-histone methylation and thereby represent indirect YAP target genes. For this reason, YAP as well as the PRC2 constituents EZH2 and SUZ12, were inhibited by two independent siRNAs in HepG2 cells. Total mRNA was isolated 48 hours after inhibition and subjected to expression profiling analysis (Affymetrix platform). Biological replicates of HepG2 cells transfected with two siRNAs were compared with nonsense siRNA treated cells. As depicted in Figure 22A, the working hypothesis for target gene analysis was that nuclear YAP positivity is associated with increased PRC2/H3K27me3 abundance and gene inhibition. Figure 22B shows the workflow from the identification of significantly regulated genes in the array up to the identification of possibly regulated pathways and target genes using Ingenuity Pathway Analysis (IPA) software.

In total, 1,311, 1,124 and 686 genes were significantly regulated by both siRNAs targeting EZH2, SUZ12, and YAP, respectively. The VENN diagram in Figure 22C shows that 133 of all significantly regulated genes (n=2,324) are coregulated by all three analyzed proteins. To narrow down the number of genes presumably regulated by the mechanism depicted in Figure 22A, the transcriptome data was filtered for significantly up-regulated genes upon YAP, SUZ12 or EZH2 knockdown. In total, 1,147 genes were significantly and consistently elevated in these arrays with 5.8% (66 genes) regulated by YAP and both PRC2 complex constituents (Table 37; Table 38).

In the next step, regulated pathways associated with these transcriptionally modified genes were examined using the IPA software. Each siRNA treatment consisting of two independent siRNAs was analyzed separately by subjecting the whole panel of significantly regulated genes to IPA core analysis. Each core analysis assigns activation z-scores to each pathway, which predicts an association for the functional impact on a pathway. The top canonical pathways activated in 4 out of 6 core analysis include FXR/RXR-activation ($p = 4x10^{-4}$ to $9x10^{-14}$), a signalling pathway that is involved in several liver specific processes as bile acid regulation and lipoprotein, lipid, and glucose metabolism. Additionally, acute phase response signaling is activated in 5 out of six core analysis ($p=2x10^{-3}$ to $5x10^{-15}$), part of the early-defense system triggered by neoplasia amongst other stimuli and the proteins involved partly overlap with proteins in IL6- or PI3K/AKT signaling. These results were merged using IPA comparison analysis and the z-scores of the 20 strongest regulated pathways (activation and inactivation) are shown in Figure 23A. This list of

pathways with potential impact on tumor cell biology include degradation of serotonin (z-score = 2.6 – 2.8), TGF-β-signaling (z-score = 0.8 – 2.6) and five pathways associated with cholesterol metabolism, like cholesterol biosynthesis (z-score = -1.3 – -2.5) and LXR/RXR activation (z-score = 2.8 – 3.7).

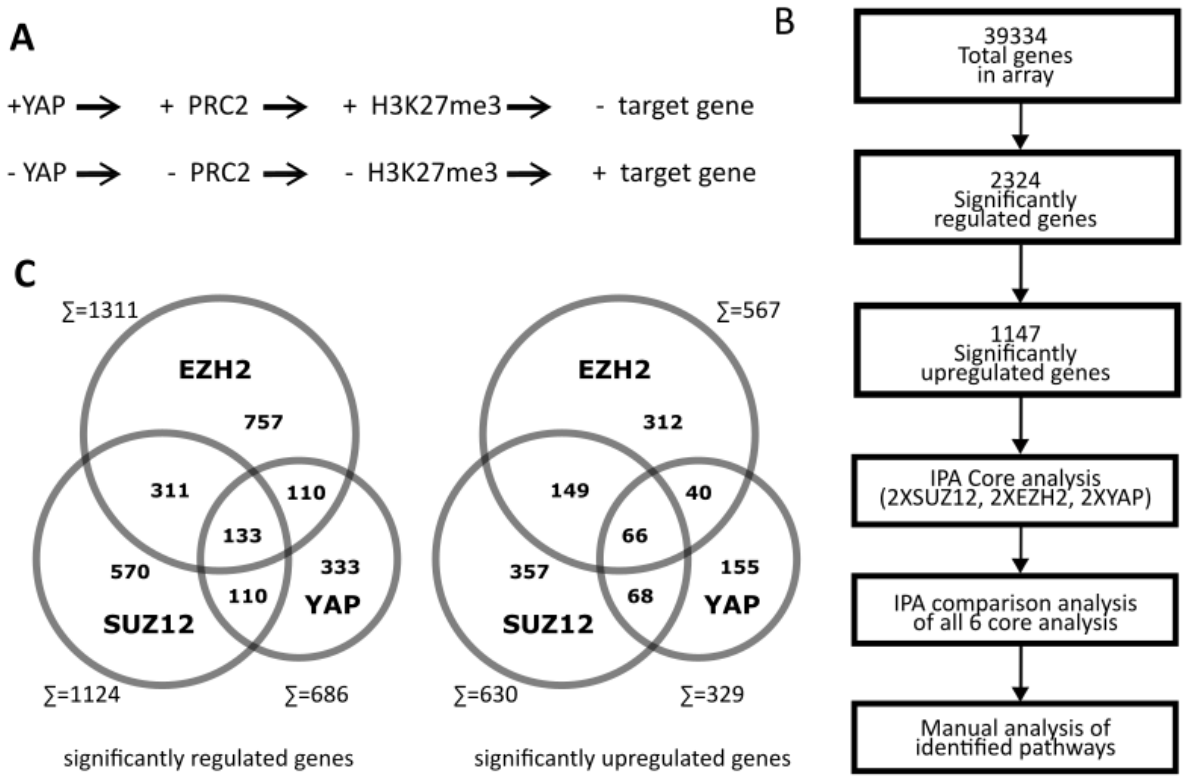

Figure 22: Transcriptome analysis upon YAP, EZH2 and SUZ12 knockdown.
(A) Scheme depicting the working hypothesis where nuclear YAP localization increases PRC2 levels and trimethylation of H3K27 resulting in target gene repression. (B) Scheme depicting microarray evaluation and IPA analysis. (B) VENN diagram of significantly (up)-regulated genes by RNAi knockdown of YAP, SUZ12, and EZH2 compared to nonsense siRNA treatment in HepG2 cells.

Interestingly, this comparison revealed LXR/RXR-activation as highest induced pathway after all types of inhibitions ($p = 3x10^{-5}$ to $3x10^{-10}$), which has many similarities to the FXR/RXR pathway. The heatmap in Figure 23B shows the genes associated with LXR/RXR activation after YAP, SUZ12, or EZH2 silencing and their expression values normalized to the NTC control. To confirm whether the regulated genes were affected by the PRC2 upstream regulator YAP, real-time PCR was performed after YAP and TAZ-inhibition in HepG2 cells for 48 h analyzing some LXR/RXR associated genes (84).

The mRNA expression data revealed that *ATP binding cassette subfamily A member* 1 (ABCA1) and *apolipoprotein C3* (APOC3) were indeed induced as predicted by the expression profiling data (Figure 23C).The results for ABCA1 and APOE were inconsistent since only one siRNA combination for YAP and TAZ affected these genes (Figure 23C). These results indicate that YAP could negatively regulate the transcription of a target gene subgroup probably through the

induction of PRC2 components, which silence gene transcription via histone methylation. First bioinformatic analysis of high-throughput data revealed that the LXR/RXR activation has been revealed as a downstream effector of YAP reduction. This suggests that YAP-positive tumors inactivate the LXR/RXR-pathway via PRC2 induction, preventing apoptosis in tumor cells (85).

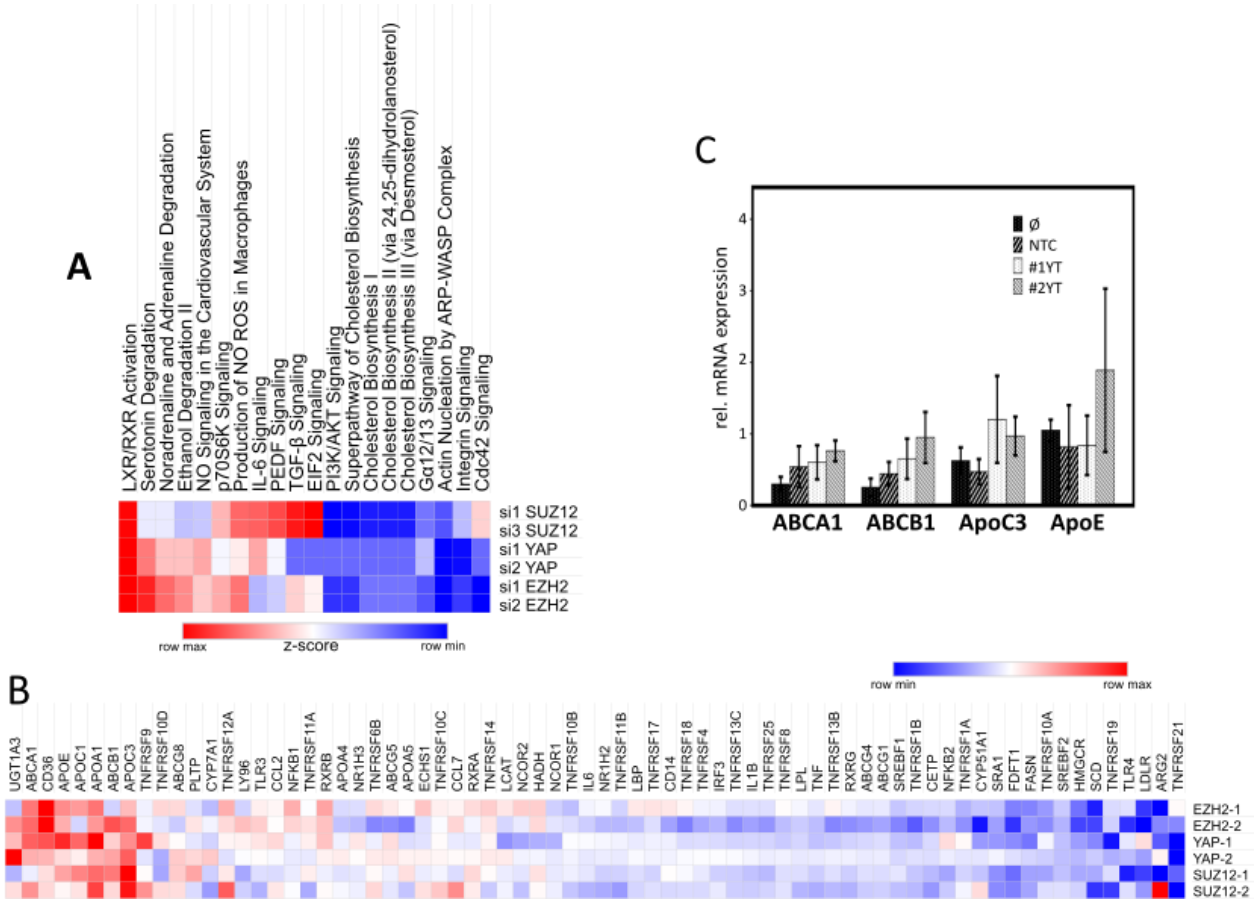

Figure 23: IPA analysis after transcriptome analysis.
(A) Heatmap of IPA comparison analysis showing z-scores (max. = 3,74; min. = -3,32) of top 20 canonical pathways activated and deactivated within analyzed transcriptomic data. (B) Expression profiling of LXR/RXR activation-associated genes after RNAi knockdown of YAP, SUZ12, and EZH2 normalized to nonsense siRNA treatment in HepG2 cells. (C) Transient transfection of each two YAP and TAZ-specific siRNAs increased expression levels of some LXR/RXR activation-associated genes, as illustrated by real-time PCR. The mean±SD of three independent experiments in HepG2 cells is shown. Untreated (Ø) and nonsense siRNA (NTC) transfected cells served as controls. Data were normalized to NTC controls.

5.3.5 YAP Expression Correlates to SUZ12 and EZH2 Expression in Human HCC

Given that YAP positively correlates with PRC2 component expression *in vitro* and *in vivo* and that the YAP-associated transcription factor TEAD4 directly bound to the promoter regions of EZH2, RBBP7 and SUZ12, the next aim was to confirm this association in human HCC tissues. Therefore, mRNA expression data of 242 HCC patients (cohort 1) (72) and 370 liver cancer patients (cohort 2) (27) was analyzed. Figure 24 shows the comparison of mRNA expression levels of liver tumors compared to surrounding tissue, illustrating a significant overexpression of the PRC2 components EED, EZH2, RBBP4, RBBP7, and SUZ12 in HCC. No such induction was

detectable for EZH1.

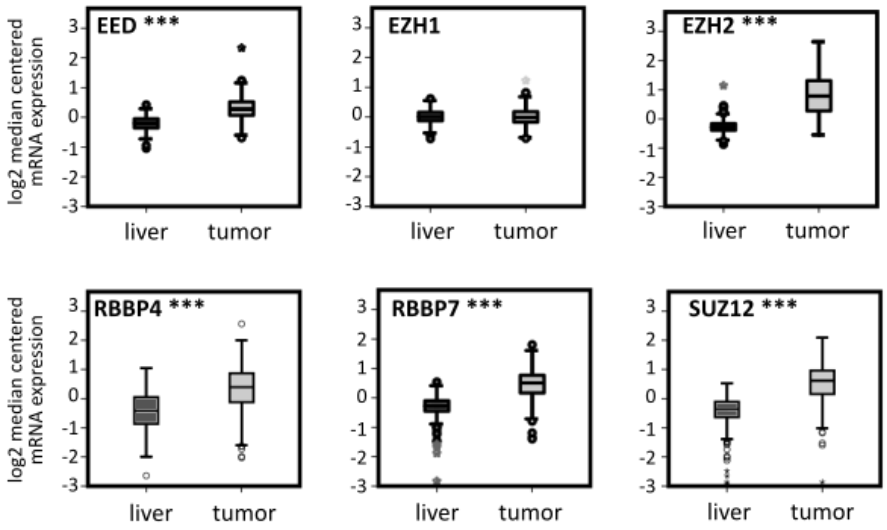

Figure 24: Elevated expression of PRC2 components in human HCCs.
EZH2, RBBP7, and SUZ12 mRNA is overexpressed in HCC samples compared to surrounding tissue in a cohort of 242 liver cancer patients (cohort 1). (*** $p < 0.001$)

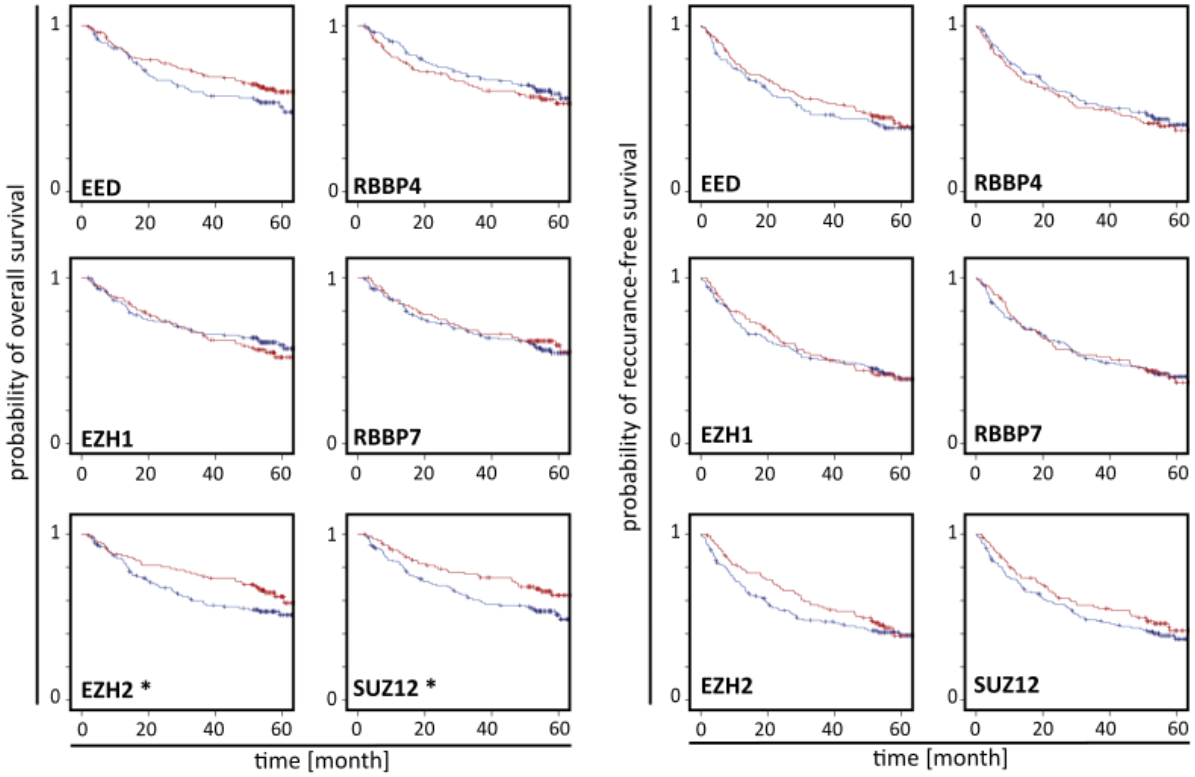

Figure 25: Elevated expression of PRC2 components correlate with poor prognosis in HCC patients.
Kaplan-Meier analysis of EED, EZH1, EZH2, RBBP4, RBBP7, and SUZ12 in cohort 1 with blue indicating high and red low expression levels. High transcript levels of EZH2 and SUZ12 significantly correlate with a worse survival probability (Wilcoxon-test). (* $p < 0.05$)

For Kaplan-Meier analysis, patients were divided into two groups with high and low transkript expression of the respective PRC2 complex gene (threshold: median) (Figure 25). HCC patients with high EZH2, SUZ12, and EED mRNA expression tend to have shorter overall survival. Most PRC2 core components had no statistical impact on patient survival in the analyzed data set. Because only elevated SUZ12 and EZH2 levels associated significantly with patient prognosis, all further analysis on human samples focused on either EZH2 or SUZ12 or both.

Table 35: Elevated expression of EZH2 correlate with clinicopathological features.
EZH2 was used to divide patients into groups with high, medium and low expression, using mRNA expression data from cohort 2. Additionally, patients were divided into groups for each feature, followed by the quantification of the number of patients in each group. The median value was used to assign for the analysis of age. The numbers of patients with the respective clinicopathological feature are listed in the table together with the p-value of the statistical test (Chi-squared test). n.s.=not significant

		EZH2 cluster				
		High	Medium	Low	SUM	sig
gender	female	38	43	40	121	n.s.
	male	86	80	84	250	
family history	yes	73	73	62	208	n.s.
	no	34	36	42	112	
race	asian	66	51	41	158	0.010
	caucasian	52	59	73	184	
tumor grade	G1+G2	61	70	101	232	0.000
	G3+G4	62	51	21	134	
TNM stage	T1+T2	83	94	98	275	0.035
	T3+T4	41	29	23	93	
vascular invasion	no	57	68	81	206	n.s.
	yes	36	41	32	109	
BMI	normal	81	79	75	235	n.s.
	obese	26	20	26	72	
inflammation	no	29	42	46	117	n.s.
	yes	33	40	44	117	
age	≥ 61	46	67	66	179	0.009
	< 61	78	56	58	192	

In the next step, the clinicopathological features of cohort 2 were compared with EZH2 expression, which was consistently regulated by YAP in all previous *in vitro* and *in vivo* experiments. Table 35 shows the contingency tables, displaying the interrelation between EZH2 expression [high (34%), medium (33%) and low (33%)] and patient characteristics such as age and tumor grading. This analysis revealed that Asian patients tended to enrich in clusters with higher EZH2 expression, while Caucasian patients tended to have lower EZH2 levels. The development of well-differentiated tumors (G1/G2) correlated with low EZH2 abundance. Patients with increased inflammation or vascular invasion of tumor tissue were evenly distributed within the EZH2 clusters. However, the patient age of 61 years and older at diagnosis was associated with lower EZH2 expression, whereas younger patients significantly expressed higher EZH2 levels. Gender, body mass index and family history didn't show any association with

EZH2 expression levels.

Together, these findings show that PRC2 is overexpressed in human HCC and that the expression of some PRC2 complex proteins such as EZH2 and SUZ12 significantly correlates with poor clinical outcome of HCC patients.

5.3.6 YAP Expression Correlates to PRC2 Expression in Human HCC

Finally, the protein abundance and its correlation with YAP levels was analyzed using an HCC-TMA (105 HCCs and 7 normal liver tissues). Figure 26 shows exemplary YAP-positive and YAP-negative IHC stains as well as corresponding EZH2 and SUZ12 stains.

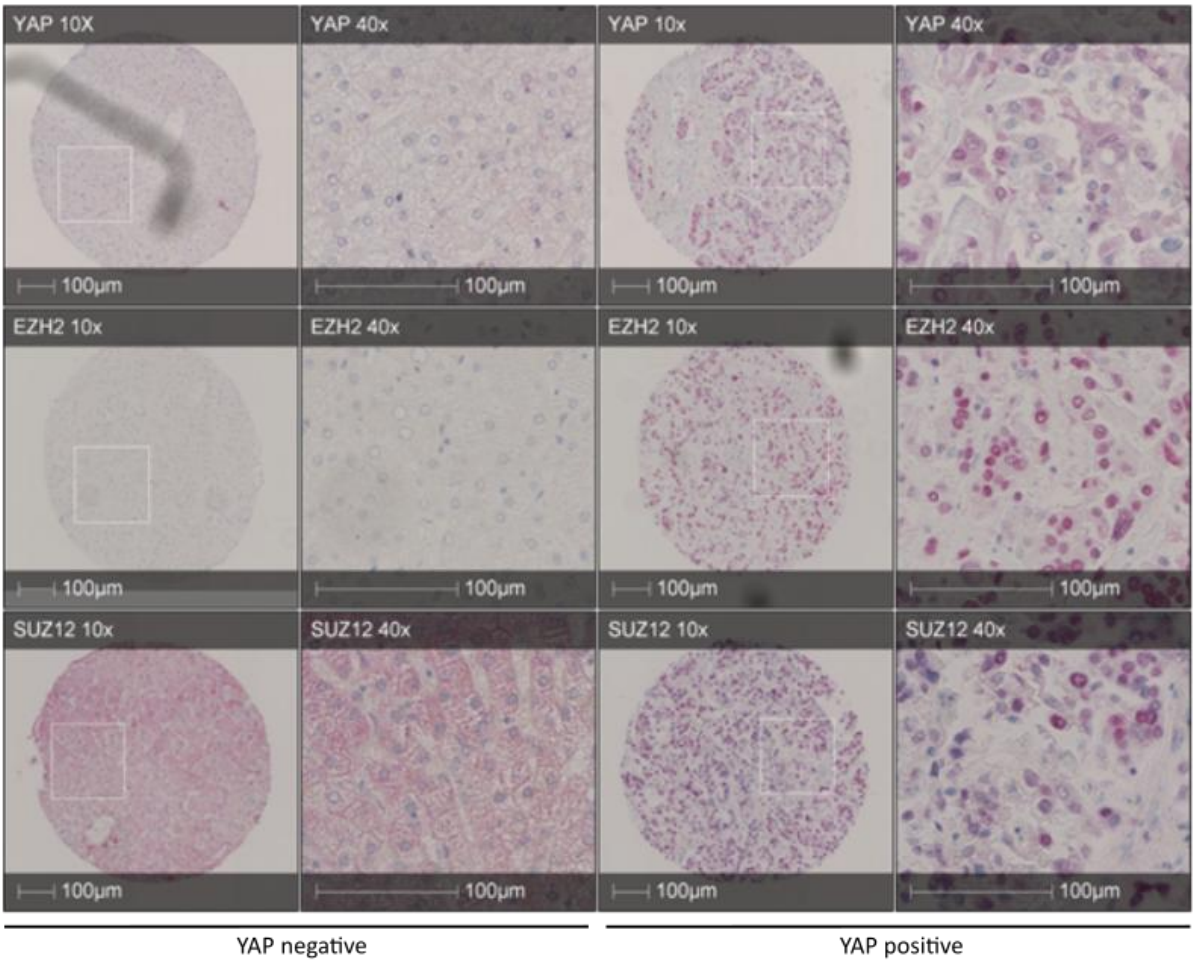

Figure 26: YAP expression correlates with EZH2 and SUZ12 expression in HCC patients.
Exemplary immunohistochemical stains of YAP positive and negative human HCC tissue stained for YAP, EZH2 and SUZ12.

In accordance with the Kaplan-Meier analysis and the correlation data of EZH2 mRNA expression with tumor grading, the TMA evaluation showed a significant correlation of YAP, SUZ12 and EZH2 protein expression with tumor grading (Figure 27; Table 36). The systematic evaluation of all TMAs also revealed a significant correlation of nuclear YAP expression with the analyzed PRC2 components SUZ12 and EZH2 as illustrated in Table 36.

In summary, these findings emphasize that PRC2 components EZH2 and SUZ12 strongly correlate with nuclear YAP expression in human HCC

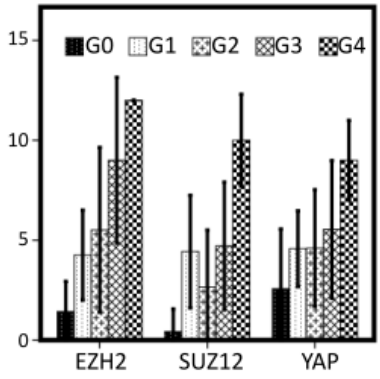

Figure 27: YAP, EZH2, and SUZ12 expression correlate with tumor grading in HCC patients.
TMA evaluation shows a significant correlation between YAP, EZH2 and SUZ12 levels with tumor gradings (G1-G4) as illustrated by the bar graph. G0 = healthy liver.

Table 36: YAP and Ki67 expression correlate with EZH2 and SUZ12 levels and histological grading in HCC patients.
Spearman correlation analysis of evaluated TMAs illustrates a significant correlation between YAP and Ki67 with EZH2 and SUZ12 levels and tumor gradings (G). (* $p < 0.5$; ** $p < 0.01$).

	Ki67	YAP	SUZ12	EZH2
G	0.427**	0.236*	0.320**	0.436**
Ki67		0.379**	0.507**	0.717**
YAP			0.255*	0.406**
SUZ12				0.516**

6 Discussion

Hippo pathway and its effectors are frequently deregulated in the context of liver cancer development. This study identified novel target gene families with the potential to mediate the oncogenic properties of YAP and TAZ (Figure 28).

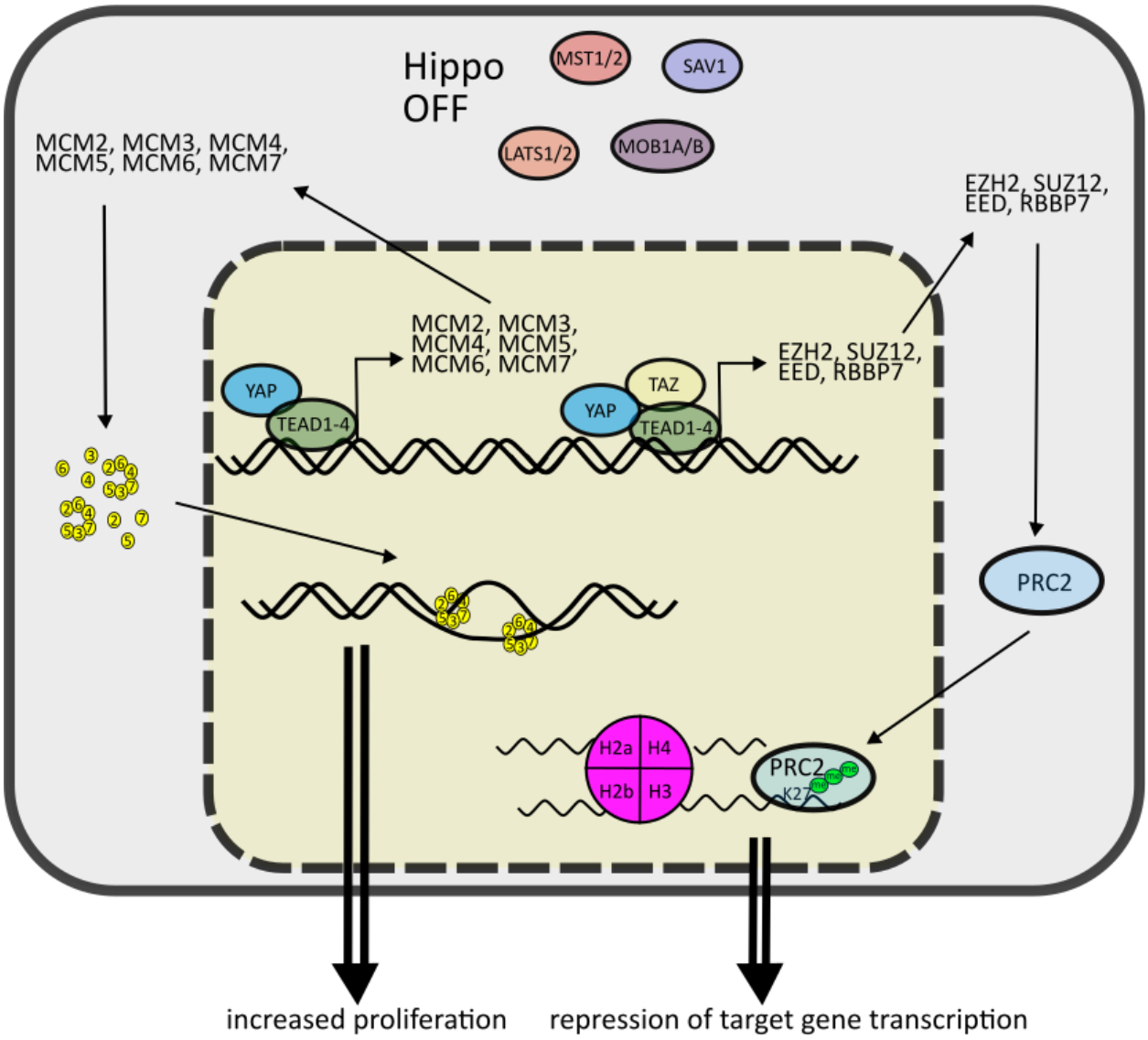

Figure 28: Overview depicting the mechanism of YAP depended MCM helicase and PRC2 induction.
Turning off the Hippo pathway results in nuclear YAP and TAZ accumulation inducing the transcription of target genes (MCM2-7, EED, EZH2, SUZ12 and RBBP7). Increased amount of MCM proteins (yellow circles) leads to elevated MCM helicase abundance and increased proliferation. Target gene transcription was repressed upon increased PRC2 mediated H3K27me3.

In this study, it could be determined that, YAP and TAZ induce the transcription of MCM helicase, which is necessary for DNA replication. The overexpression of MCM helicase constituents has also been observed in human HCC tumor tissue and correlates with poor

clinical outcome of HCC patients. Furthermore, this study provides first evidence of YAP induced gene silencing by transcriptional regulation of PRC2 components, a functionally related group of proteins involved in epigenetic silencing of gene transcription. Taken together these data pinpoint novel YAP/TAZ target genes induced in human HCCs, which might represent interesting therapeutic target structures for the treatment of YAP-driven liver tumors.

6.1 MCM Helicase

6.1.1 Dysregulation of MCM Helicase Subunits in Hepatocarcinogenesis

overexpressed during carcinogenesis in a Hippo pathway-dependent manner. In this study, elevated levels of MCM helicase subunits have been identified as novel YAP/TAZ-regulated gene family in hepatocarcinogenesis. Moreover, increased MCM expression was linked with poor clinical outcome of HCC patients, which corresponds with the pro-tumorigenic properties of YAP and TAZ in tumorigenesis.

The naming minichromosome maintenance (MCM) of the MCM genes originates from a mutation screen performed in budding yeast (86). Based on these results, the authors hypothesized, that only a small number of proteins is responsible for the initiation of a large number of replication origins (86). Amongst the identified proteins, six factors share a high degree of structural and functional similarities and were called the MCM protein family or MCM helicase (MCM2, MCM3, MCM4, MCM5, MCM6, and MCM7). Genes coding for MCMs are located on different chromosomes and share structural similarities with regard to the so-called MCM-box and a zink finger motif, presented in Figure 29 (87). Additionally to the shared functional characteristics, the human MCM proteins share 31-38% identical amino acids with each other.

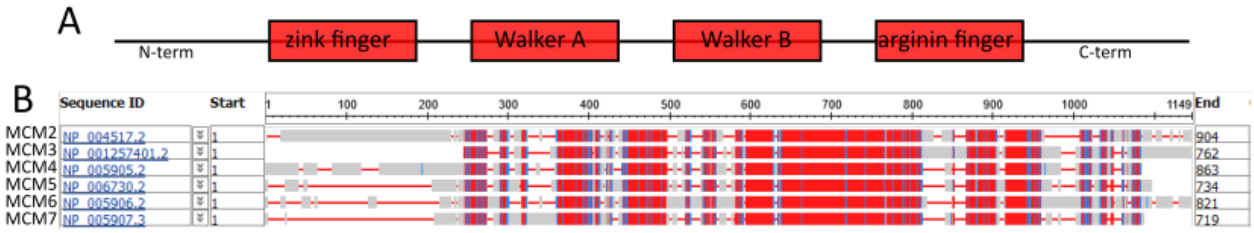

Figure 29: MCM helicase sequence homology.
(A) Scheme showing the conserved domain structure of MCM proteins. (B) To obtain shared motifs among the human MCM helicase, protein sequences were aligned with COBALT-software. Residues conserved among the six sequences in the alignment are shaded in red.

Each MCM-box consists of three functional amino acid sequences. The Walker A and B ATPase motifs, which are responsible for the binding and hydrolysis of ATP, and the arginin finger motif, binding the γ-phosphate and facilitates its cleavage (87). The energy of ATP hydrolysis is used to separate the strands of the DNA double helix. Since the discovery of MCM helicase in the context of impaired proliferation, several attempts have been made to analyze the role of these

proteins in carcinogenesis. Freeman et al. performed immunohistochemical analysis to evaluate the expression of MCM2, MCM5, and Ki67 in 210 healthy and matched tumor tissues including lung, colon, skin and bladder tissues (88). In tumor samples, the authors detected a high correlation between MCM expression and Ki67 levels, linking MCM expression to the proliferative activity of tumor cells in different cancer types. Moreover, the amount of MCM2 and MCM5 positive nuclei gradually increased with tumor dedifferentiation, with approximately 20% positive nuclei in normal tissue to 100% in poorly differentiated tumors (88).

Interestingly, the study presented here does not only show an elevated abundance of MCM2, MCM6, and MCM7 proteins in HCC tissues, but also revealed a statistical association between all analyzed MCM helicase members with increasing tumor grade/dedifferentiation. Additionally, a highly significant correlation between the proliferation marker Ki67 and MCM helicase protein abundance in HCC tumor tissue was confirmed. For hepatocarcinogenesis, the present study confirmed similar reports with immunohistochemical analysis revealing elevated expression of MCM2 (89), MCM6 (90) and MCM7 (91) in HCCs compared to normal liver tissues.

Furthermore, elevated mRNA expression levels of different MCM genes in human HCCs compared to normal and cirrhotic livers have been detected in this study. The analysis of two published HCC cohorts (27, 72) showed high mRNA expression of each MCM family member correlating with poor overall and disease-free survival. Moreover, an MCM score, calculated to rank the MCM helicase expression within each HCC sample, could link elevated MCM expression to several clinicopathological features and etiologic factors as race, age and tumor progression. These results are in line with the IHC analysis of Liu et al. (90) and the recently published analysis of these cohorts by Liao et al. (92).

In summary, the results from this study and published literature illustrate that individual MCM proteins represent reliable markers of physiological and pathologicall hepatocyte and HCC cell proliferation. Moreover, high mRNA expression of MCM helicase in HCC patients is a useful marker to predict a worse clinical outcome.

6.1.2 MCM Helicase is a Downstream Target of YAP, TAZ, and TEAD4

All ten known human MCM proteins are associated with cell cycle progression. Six of them, MCM2-7, form a ring-shaped hexameric complex during the G1 cell cycle phase, named the MCM helicase (78). As discussed in chapter 6.1.1, MCM helicase overexpression correlates with proliferation and tumor progression in HCC. However, the mechanistic reason for increased MCM expression in HCC cells is poorly understood.

Chromosomal alterations of MCM genes in the context of cancer progression have been rarely described in different tumor types. For example, array comparative genomic hybridization (aCGH) of 23 non-small cell lung cancer tumors revealed chromosomal amplification of MCM2 and MCM6 (93). Additionally genome-wide copy number and microarray mRNA expression

analysis of 25 paired healthy/tumorous gastric tissues showed amplification of the MCM3 and MCM4 genes (94). Furthermore, previous studies demonstrated that a chromosomal amplification of the chromosomal region 7q21-22 frequently occurred in gastric cancer, including the MCM7 gene (95). Interestingly, this report also showed that mir-25 can suppress the tumor suppressor p53, thereby providing an additional oncogenic stimulus for hepatocytes (95). MCM proteins are evolutionary highly conserved throughout eukaryotes, but the individual genes are located on different chromosomal regions suggesting that each single MCM protein may have specific roles in DNA replication (87, 96). Nevertheless, publications only report the amplification of individual MCM genes so far but not simultaneous genomic gains and so far no reports focusing on the situation of MCMs in liver cancer have been published. This indicates that other molecular mechanisms might be responsible for the cooperative overexpression of MCM observed in HCC cells.

In order to ensure proper DNA replication, all six MCM proteins must be present at specific cell cycle phases. This suggests that overexpression of MCM helicase constituents has to be collectively induced by higher level mechanisms such as common transcriptional regulation. For example, Petrocca et al. analyzed gastric cancer cell lines and detected the expression of MCM7 and a cluster of microRNAs regulated by the cell-cycle associated transcription factor *E2F transcription factor 1* (E2F1) (97). Additionally, E2F1 has also been shown to induce MCM5 and MCM6 transcription in rat embryonic fibroblast REF52 cells (98). Another member of the E2F family, E2F2, was identified by ChIP analysis, to interact with *cAMP responsive element binding protein* (CREB) and to cooperatively repress MCM5 transcription (99). It is therefore tempting to speculate that transcriptional regulation is the most important mechanism for the cooperative overexpression of all MCM family members. This is supported by results from our laboratory, illustrating that YAP and TAZ together with the transcription factor FOXM1 induce the expression of the so-called chromosome instability (CIN) gene signature in liver cancer cells with MCM2 and MCM7 being part of CIN70 (38).

Inhibition of the Hippo pathway or YAP activation is known to induce proliferation, as was shown in different cell lines and transgenic mouse models (61, 100). Moreover, expression data analysis showed repression of cell cycle-associated genes upon YAP inhibition (38, 101). In line with published data, we found all individual MCMs being downregulated upon YAP inhibition in liver cancer cells (5.2.1). Furthermore, we determined that combined YAP and TAZ reduction led to an even stronger decrease of all MCM helicase components. The direct physical relevance of YAP, TAZ, and TEAD4 was proven by ChIP and reporter gene assays for most of the MCM helicase promoters. Nevertheless, further experiments need to be conducted to substantiate that the Hippo pathway is one of the major drivers for the regulation of MCM helicase expression. Moreover, it would be interesting to investigate if and how YAP, TAZ, and TEAD4 physically interact in the transcriptional regulation of target genes.

Together these results demonstrate that the Hippo/YAP/TAZ pathway is involved in the regulation of the complete MCM protein family, which might be critical for tumor cells to facilitate fast and efficient DNA replication and cell proliferation.

6.1.3 YAP Supports Proliferation via the MCM Helicase

Proliferation is characterized by increased cell growth as well as fast and frequent mitosis. Cell cycle progression is tightly regulated by hormones and growth factors modifying the expression and activation of cyclins, CDKs, and replisome proteins. Indeed, the Hippo/YAP/TAZ pathway has been frequently associated with the regulation of proliferation and cell cycle progression. Recently, it has been shown that YAP regulates the expression of the CIN gene signature involving several cell cycle-associated genes including MCM2 and MCM7 (38). To ensure proper proliferation, functionally related groups of genes have to be regulated and coordinated.

In order to ensure error-free DNA duplication, thousands of DNA replication origins have to fire simultaneously during S-Phase. Therefore all replication origins are already licensed in the G1 cell cycle phase which allows their immediate response to activating stimuli. Origin licensing is the initial step in DNA duplication where the pre-replicative complex (pre-RC) is loaded on the DNA. The pre-RC forms when the origin recognition complex subunit (ORC) 1-6, chromatin licensing and DNA replication factor 1 (CDT1), cell division cycle (CDC) 6, and the MCM helicase, duplet's, are loaded onto double-stranded DNA (102).

G1/S cell cycle transition is eventually initialized by the assembly of the so-called CMG-helicase, CDC45, MCM2-7, and GINS complex (GINS complex subunit 1-4), and phosphorylation of MCMs by activated cyclin dependent kinases (CDK) and Dbf4-dependent kinase (DDK). About 50,000 to 100,000 activated replication origins per cell have been identified in different cell lines (103). Interestingly, the present study stated on one hand that RNAi-mediated inhibition of individual MCM proteins had no effect on cell viability and on the other hand that the disruption of MCM2 gene using CRISPR/Cas9 reduced proliferation. This might be explained by the excess of origins licensed during the G1 cell cycle phase. The licensed but not initially firing origins are called 'silent' or 'dormant origins' and get activated upon replication fork stalling and improper DNA replication, serving as back-up origins to ensure proper DNA duplication. This shows that much more pre-RC proteins exist than needed during cell cycle progression. In order to prevent re-replication when two replication forks meet, the activity of CMG-helicases has to be stopped. Amongst other mechanisms, Moreno et al. reported polyubiquitinylation of MCM7 followed by degradation during replication fork termination in *xenopus laevis* egg extract (104). Upon S/G2 cell cycle transition, MCMs get modified and thereby subsequently degraded, enforcing new MCM transcription and nuclear translocation (105).

In this study it could be determined that YAP can induce cell proliferation partly through the regulation of MCM expression. YAP and MCM2-7 inhibition in liver cancer cells led to reduced

proliferation rate as demonstrated by diminished BrdU incorporation (Figure 12). The anti-proliferative effects were comparable between both approaches, even though MCM helicase reduction upon YAP inhibition was less effective than targeted MCM2-7 inhibition. This suggests that YAP partly mediates its functional properties regarding replication and proliferation through the MCM helicase. However, it is likely that also other cell cycle-associated genes are critical downstream effectors of YAP. Indeed, a recent publication showed the regulation of cell cycle-associated genes as *cyclin B1*, *CDC2*, and *CDC45* by YAP (38). Still, it remains to be elucidated, whether all of these genes are direct YAP target genes and if their upregulation can mimic YAP-mediated proliferation.

In summary, the results complement previous studies, both demonstrating that deregulation of YAP expression has direct effects on cell proliferation partly mediated by the transcriptional regulation of MCMs. It is tempting to speculate that MCM helicase presence and activity could represent a potential marker for YAP-dependent HCC proliferation or a therapeutic target structure.

6.2 PRC2

6.2.1 Dysregulation of PRC2 in HCC Development

Considering the hepatocarcinogenesis process, epigenetic changes have been frequently observed in chronic liver damage caused by different etiologies (106). Epigenetics is currently defined as ‘the study of changes in gene function that are mitotically and/or meiotically heritable and that do not entail a change in DNA sequence’ (107). Thus, epigenetic imprints are passed to daughter cells during cell division, which is not only important for embryonic development but also for carcinogenesis in case of dysregulation (108).

The most common cellular tools to adjust epigenetic-dependent gene expression are posttranslational modifications of histones or DNA bases (109). In this study on hepatocarcinogenesis, YAP/TAZ-dependent expression changes of several histone modifying proteins have been observed. Covalent N-terminal modifications of histones are introduced and removed by a variety of enzymes and protein complexes, with direct impact on gene transcription. The protein complex found to be regulated by YAP and TAZ in this study is a member of the Polycomb group (PcG), known to repress target gene expression by histone methylation. PcG proteins have been first identified in D*rosophila melanogaster*, regulating the expression of *HOX* genes and ensuring the proper segment identity during embryonal development (110). In total, three complex families have been identified containing PcG proteins, namely PhoRC, polycomb repressive complex 1 and 2.

All identified PcG proteins deregulated upon YAP inhibition in this study are members of PRC2, which is composed of the core components EZH1/2, SUZ12, RBBP4/7, EED and several variable proteins (111). The relevance of PRC2 in embryonic development has been proven by different

transgenic mouse models. Since EZH1 is ubiquitously and continuously expressed and EZH2 is highly associated with cell proliferation in wildtype mice, the major focus of this study lies on EZH2 (112). Mouse embryos lacking SUZ12, EED or EZH2 showed developmental and proliferative defects and were not viable (79, 113). Interestingly, even though the proteins SUZ12 (79) and EED (114) are essential to PRC2 function, protein expression data in human cancer tissue is scarce. In contrast, the overexpression of the catalytic subunit EZH2 in human cancers has frequently been described, as is the case for breast cancer (115), prostate cancer (116) and lymphomas (117). In this study, an overexpression of SUZ12 and EZH2 in human HCC samples could be demonstrated, which is supported by findings of Au SL et al. in 2012 (118). Additionally, this project showed that increasing EZH2 expression correlates with poor tumor differentiation of HCCs, as previously shown by Sasaki et al. (119). All these data underline the relevance of EZH2 in carcinogenesis at least as a marker for cancer progression. Cai et al. found increased expression of 3meK27H3, the epigenetic mark of the PRC2 complex, in human HCC tissues (120). Furthermore, Xu K et al. and Kim J et al. found a PRC2-independent role of EZH2 in carcinogenesis, showing that EZH2 and *androgen receptor* (AR) cooperate in target gene activation (121, 122). This might explain the frequent dysregulation of EZH2 in comparison to other PRC2 components.

In summary, this study illustrated an increased expression of PRC2 components, especially EZH2, in HCCs and a correlation with worse clinical outcome of liver cancer patients.

6.2.2 PRC2 is a Downstream Target of YAP and TEAD4

The Hippo pathway effector YAP is known to interact with TEAD4 in the induction of target gene transcription associated with cell cycle progression and induction of cell growth (34). Several novel YAP target genes have been identified, amongst them are genes associated with poor clinical outcome like MCM proteins and the PRC2 member EZH2 (38).

It has been shown that the PRC2 complex is crucial to embryonic development and individual components are frequently overexpressed in different tumor entities. In line with the poor clinical outcome of patients with increased EZH2 expression, an imbalance in PRC2 composition and activity could contribute to tumor formation and progression. The relevance of PRC2 components in carcinogenesis has been further supported by RNAi experiments, showing cell growth inhibition (123) and reduced cell proliferation (116) upon EZH2 withdrawal. For this reason, it is crucial to understand mechanisms regulating the expression of PRC2 components. The relevance of PRC2 components for cell growth, identified in this study as YAP-dependent, has been confirmed by at least two independent publications. Bracken et al. described a direct pRB/E2F-dependent regulation of EZH2 and EED expression during cell growth (124). They showed that the promoter regions of EED and EZH2 are responsive to the transcription factors E2F1, E2F2, and E2F3 in reporter gene assays and confirmed the physical binding of E2F3 and E2F4 to the EZH2 promoter by ChIP assays. Another study illustrated not only the binding of β-

catenin to the SUZ12 promoter but also an increased binding in colon cancer compared to healthy colon tissue, thereby suggesting a role of PRC2 in cancer progression (125). Furthermore, PRC2 may provide cancer cells with a growth advantage since it is involved in cancer cell resistance to conventional chemotherapeutics or irradiation therapy. In this case, EZH2, SUZ12, and EED are actively recruited to DNA damage sites, while depletion of EZH2 leads to a less efficient double-strand break repair and increased sensitivity to gamma irradiation (126).

The results of this study illustrate that the Hippo/YAP pathway may directly affect PRC2 activity via regulation of PRC2 constituent expression. Indeed, first evidence for a connection of the Hippo pathway with PRC2 activity in regulating target gene transcription has recently been reported. Wang et al. showed in breast cancer cells that YAP directly binds to EZH2 at promoters, thereby repressing gene expression (127). Data provided in the present study could not only demonstrate that YAP levels effect the expression of EZH2 and other PRC2 components, but also a direct physical binding of YAP and TEAD4 to the promoter sites of EZH2 and SUZ12. Together, these data illustrate the existence of multiple regulatory mechanisms connecting the Hippo pathway with PRC2 complex activity. Irrespective of the mechanism, the Hippo/YAP axis seems to be the superior regulator controlling PRC2 abundance and activity.

6.2.3 YAP Represses Target Genes Using PRC2

It has been shown, that YAP and TEAD4 can repress gene expression, thereby inducing cell survival (128). Even though different mechanisms regulating YAP mediated target gene induction are known, the repressed genes and the underlying mechanism remain poorly studied. This study identified members of the transcriptional repression complex PRC2 as a direct YAP and TEAD4 target gene, which might represent an additional molecular mechanism of how the Hippo pathway could diminishes gene expression.

Epigenetic regulation of gene expression is involved in different physiological and pathological processes such as stem cell differentiation and tumorigenesis (129, 130). Among different epigenetic marks, covalent histone modifications were found to modify chromatin density and the accessibility of DNA by other proteins, which was called the histone code hypothesis (131). N-terminal histone modifications, including methylation, acetylation, ADP ribosylation, ubiquitination, citrullination, and phosphorylation, are introduced and removed by a variety of enzymes and protein complexes (132). Especially, acetylation of histones is usually associated with transcriptional activation (e.g. H3K9, H3K14, H3K18, H3K23, H4K5, H4K8, H4K12, and H4K16), while histone methylation, depending on location and extent of the modification, can inhibit (H3K9, H3K27, and H4K20) as well as activate (H3K4, H3K36, and H3K79) gene transcription (109).

The repressive mark H3K27me3 is introduced by the complex PRC2 leading to chromosomal condensation and eventually HOX repression (133). *Vice versa*, RNAi-mediated silencing of EZH2, EED, or SUZ12 de-repressed different target genes in human embryonic fibroblasts (134). The present study delineates that YAP inhibition results in increased target gene expression, as the ABC transporter components ABCA1 and ABCB1, while reducing the transcription of PRC2 components. A recently identified target gene of PRC2 is EPCAM, which is re-expressed in HBV-positive cells upon SUZ12 knockdown and represents a marker for hepatic cancer stem cells (135). Additionally, the present study illustrates a YAP-dependent EZH2 and SUZ12 transcription, which led to the assumption that YAP overexpression might represses EPCAM expression *via* PRC2 induction. Another possibility might be a non-transcriptional interaction between YAP and PRC2, since such a mechanism has been described in breast cancer cells (127).

This study shows direct binding of TEAD4 to EZH2, RBBP7 and SUZ12 promoter regions, indicating that the Hippo pathway regulates PRC2 abundance and activity to repress target gene expression. Indeed, the microarray data show that 19% of the significantly upregulated genes after YAP inhibition are identical to genes effected by SUZ12 and EZH2 inhibition. This indicates that besides direct transcriptional regulation, YAP could indirectly repress the expression of target genes by highjacking the PRC2 complex. This is in line with data from Kim and colleagues, who identified target genes repressed by YAP and TEAD4, which are not affected by EZH2 depletion (128). These data underline the importance for the identification of direct and indirect YAP target genes in order to develop pharmaceutical approaches to repress oncogenic YAP activity without interfering with regenerative capabilities.

Altogether these results illustrate that YAP can not only induce target gene expression but also repress gene transcription. In the light of published data, the results presented here indicate that YAP represses PRC2 target genes, which might lead to the identification of novel Hippo pathway regulatory feedback loops.

6.3 Therapeutic approaches

HCC exhibits a poor survival rate and few therapeutic options, as described in 1.1.2. Since HCCs have different molecular features (1.1.3) and current systemic treatment options only include multi-kinase inhibitors and tyrosin kinase inhibitors, research focuses on identifying more specific approaches. Given that the Hippo pathway is important for carcinogenesis (1.2.2), first perturbation approaches targeting this pathway have been developed. Verteporfin, which is also used as pharmacological inhibitor in this study, is known to disrupt the YAP-TEAD interaction leading to the proteasomal degradation of YAP and TEAD (37). Indeed, Verteporfin treatment of liver cancer cells in this study showed a dose-dependent decrease of YAP-target gene expression, which is in line with previous publications (38, 136). However, the total blockage of the Hippo pathway might also hava adverse effects, since it is required for liver regeneration as illustrated by partial hepatectomy in adult mice, where the omitted YAP/TAZ-

mediated effects could not be compensated by other pro-proliferative pathways (137). These data suggests that a more specific approach is needed to target downstream effects of YAP and TAZ with the aim to find druggable oncogenic targets without preventing liver regeneration upon treatment.

As discussed in section 6.1.2, the MCM helicase was identified as a direct YAP and TAZ target gene, which is directly involved in cell proliferation. Already during physiological cell proliferation, an excess amount of MCMs compared to the theoretically minimal requirement for sufficient DNA duplication can be detected (138). Even more, MCM proteins are detectable in precancerous lesions and cancer tissue, as shown in sections 5.2.2 and 5.2.5. These facts imply that a change in cell viability upon suboptimal MCM reduction could not be expected, which was acertained in Figure 10. Theoretically, the therapeutic abolishment of MCMs would result in a replication block leading to senescence or apoptosis. Initial CRISPR/Cas9 experiments presented in this study show the expected reduction in cell proliferation (Figure 11), which would be a valuable approach for cancer treatment of HCC patients, though it might be fatal for the surrounding regenerative and chronically damaged liver. Therefore, the MCM helicase does not appear to be a suitable target for drug development, but MCMs could serve as proliferation and prognostic marker as discussed in section 6.1.1.

Another YAP target identified in this study is PRC2, a complex responsible for epigenetic repression of gene transcription (6.2.3). Due to the frequent deregulations of PRC2 components in different cancers, several pharmaceutical approaches to inhibit the function of EZH2, the key enzyme of the complex, have been developed (139). First approaches to inhibit PRC2 effects in breast cancer were made using S-adenosylhomocysteine hydrolase inhibitor 3-Deazaneplanocin A (DZNep), which efficiently induced apoptotic cell death in cancer cells but not in normal cells (140). Several EZH2 inhibitors are currently in clinical trials (141), with Tazemetostat presenting a highly potent and selective inhibitor directly binding EZH2 (83). In the course of this study, it could be shown that Tazemetostat could efficiently reduce H3K27me3 in different liver cancer cell lines, supporting the results that led to the initiation of a clinical trial. First recent data show a favorable safety profile and antitumor activity in advanced solid tumors and lymphomas (142). In addition to targeting the enzymatic activity of PRC2, the disruption of the complex was explored by targeting EED. The H3K27me3-binding function of EED is blocked by newly developed small molecules, like EED226, which allosterically inhibit EZH2 enzymatic activity and disrupt the complex (143, 144). A comparable inhibitor, A-395, demonstrates even superior effects on tumor growth inhibition *in vivo* relative to the mentioned EZH2 inhibitors (145). The recent increase in availability of PRC2-inhibiting drugs provides novel interesting tool for further investigation to disrupt oncogenic PRC2/YAP feedback loops.

In summary, the Hippo pathway is a major regulator of cell proliferation, equally important for liver regeneration as well as cancer progression. Therefore, downstream effectors of YAP and

TAZ had to be evaluated for target potential. Especially the PRC2 components EZH2, EED and SUZ12, target genes identified in this study proved to be promising targets for further evaluation.

.

7 Publications

“Oncogenic transcriptional co-activators YAP and TAZ regulate the expression of MCM helicase constituents in hepatocellular carcinoma” – poster

33. Jahrestagung der German Association of the Study of the Liver (GASL), Essen 2017

“YAP (Yes-Associated Protein) induces PRC2 (Polycomb Repressive Complex 2) complex proteins to regulate histone methylation” – poster

34. Jahrestagung der German Association of the Study of the Liver (GASL), Hamburg 2018

“YAP and TAZ induce MCM protein expression to facilitate tumor-supporting properties in liver cancer” – poster

American Association for Cancer Research (AACR) Annual Meeting, Chicago (USA) 2018

8 Literature

1. Rappaport AM. Hepatic blood flow: morphologic aspects and physiologic regulation. International review of physiology. 1980;21:1-63.
2. Irwin M. Arias (Editor) AWWC-E, James L. Boyer (Co-Editor), David A. Shafritz (Co-Editor), Nelson Fausto (Co-Editor), Harvey J. Alter (Co-Editor), David E. Cohen (Co-Editor). The Liver: Biology and Pathobiology: Wiley; 2009. 1216 p.
3. Tsukada N, Ackerley CA, Phillips MJ. The structure and organization of the bile canalicular cytoskeleton with special reference to actin and actin-binding proteins. Hepatology (Baltimore, Md). 1995;21(4):1106-13.
4. Bray F, Ferlay J, Soerjomataram I, Siegel RL, Torre LA, Jemal A. Global cancer statistics 2018: GLOBOCAN estimates of incidence and mortality worldwide for 36 cancers in 185 countries. CA: a cancer journal for clinicians. 2018;68(6):394-424.
5. El-Serag HB. Hepatocellular carcinoma. The New England journal of medicine. 2011;365(12):1118-27.
6. Su TH, Chen PJ. Emerging hepatitis B virus infection in vaccinated populations: a rising concern? Emerging microbes & infections. 2012;1(9):e27.
7. Carter W, Connelly S, Struble K. Reinventing HCV Treatment: Past and Future Perspectives. Journal of clinical pharmacology. 2017;57(3):287-96.
8. McGlynn KA, Petrick JL, London WT. Global epidemiology of hepatocellular carcinoma: an emphasis on demographic and regional variability. Clinics in liver disease. 2015;19(2):223-38.
9. Balogh J, Victor D, 3rd, Asham EH, Burroughs SG, Boktour M, Saharia A, et al. Hepatocellular carcinoma: a review. Journal of hepatocellular carcinoma. 2016;3:41-53.
10. Mathurin P, Bataller R. Trends in the management and burden of alcoholic liver disease. Journal of hepatology. 2015;62(1 Suppl):S38-46.
11. Wu MY, Yiang GT, Cheng PW, Chu PY, Li CJ. Molecular Targets in Hepatocarcinogenesis and Implications for Therapy. Journal of clinical medicine. 2018;7(8).
12. El-Serag HB, Rudolph KL. Hepatocellular carcinoma: epidemiology and molecular carcinogenesis. Gastroenterology. 2007;132(7):2557-76.
13. Gaillard H, Garcia-Muse T, Aguilera A. Replication stress and cancer. Nature reviews Cancer. 2015;15(5):276-89.
14. Ferlay J, Soerjomataram I, Dikshit R, Eser S, Mathers C, Rebelo M, et al. Cancer incidence and mortality worldwide: sources, methods and major patterns in GLOBOCAN 2012. International journal of cancer Journal international du cancer. 2015;136(5):E359-86.
15. Desai JR, Ochoa S, Prins PA, He AR. Systemic therapy for advanced hepatocellular carcinoma: an update. Journal of gastrointestinal oncology. 2017;8(2):243-55.
16. Hiraoka A, Kumada T, Kariyama K, Takaguchi K, Itobayashi E, Shimada N, et al. Therapeutic potential of lenvatinib for unresectable hepatocellular carcinoma in clinical practice: Multicenter analysis. Hepatology research : the official journal of the Japan Society of Hepatology. 2019;49(1):111-7.
17. Abou-Alfa GK, Meyer T, Cheng AL, El-Khoueiry AB, Rimassa L, Ryoo BY, et al. Cabozantinib in Patients with Advanced and Progressing Hepatocellular Carcinoma. The New England journal of medicine. 2018;379(1):54-63.
18. El-Khoueiry AB, Sangro B, Yau T, Crocenzi TS, Kudo M, Hsu C, et al. Nivolumab in patients with advanced hepatocellular carcinoma (CheckMate 040): an open-label, non-comparative, phase 1/2 dose escalation and expansion trial. Lancet (London, England). 2017;389(10088):2492-502.

19. Spangenberg HC, Thimme R, Blum HE. Targeted therapy for hepatocellular carcinoma. Nature reviews Gastroenterology & hepatology. 2009;6(7):423-32.
20. Dhanasekaran R, Bandoh S, Roberts LR. Molecular pathogenesis of hepatocellular carcinoma and impact of therapeutic advances. F1000Research. 2016;5.
21. Boyault S, Rickman DS, de Reynies A, Balabaud C, Rebouissou S, Jeannot E, et al. Transcriptome classification of HCC is related to gene alterations and to new therapeutic targets. Hepatology (Baltimore, Md). 2007;45(1):42-52.
22. Calderaro J, Couchy G, Imbeaud S, Amaddeo G, Letouze E, Blanc JF, et al. Histological subtypes of hepatocellular carcinoma are related to gene mutations and molecular tumour classification. Journal of hepatology. 2017;67(4):727-38.
23. Staib F, Hussain SP, Hofseth LJ, Wang XW, Harris CC. TP53 and liver carcinogenesis. Human mutation. 2003;21(3):201-16.
24. Newell P, Toffanin S, Villanueva A, Chiang DY, Minguez B, Cabellos L, et al. Ras pathway activation in hepatocellular carcinoma and anti-tumoral effect of combined sorafenib and rapamycin in vivo. Journal of hepatology. 2009;51(4):725-33.
25. Matter MS, Decaens T, Andersen JB, Thorgeirsson SS. Targeting the mTOR pathway in hepatocellular carcinoma: current state and future trends. Journal of hepatology. 2014;60(4):855-65.
26. Zhu AX, Duda DG, Sahani DV, Jain RK. HCC and angiogenesis: possible targets and future directions. Nature reviews Clinical oncology. 2011;8(5):292-301.
27. Cancer Genome Atlas Research Network. Electronic address wbe, Cancer Genome Atlas Research N. Comprehensive and Integrative Genomic Characterization of Hepatocellular Carcinoma. Cell. 2017;169(7):1327-41 e23.
28. Luedde T, Schwabe RF. NF-kappaB in the liver--linking injury, fibrosis and hepatocellular carcinoma. Nature reviews Gastroenterology & hepatology. 2011;8(2):108-18.
29. Justice RW, Zilian O, Woods DF, Noll M, Bryant PJ. The Drosophila tumor suppressor gene warts encodes a homolog of human myotonic dystrophy kinase and is required for the control of cell shape and proliferation. Genes Dev. 1995;9(5):534-46.
30. Dong J, Feldmann G, Huang J, Wu S, Zhang N, Comerford SA, et al. Elucidation of a universal size-control mechanism in Drosophila and mammals. Cell. 2007;130(6):1120-33.
31. Kango-Singh M, Nolo R, Tao C, Verstreken P, Hiesinger PR, Bellen HJ, et al. Shar-pei mediates cell proliferation arrest during imaginal disc growth in Drosophila. Development (Cambridge, England). 2002;129(24):5719-30.
32. Harvey KF, Pfleger CM, Hariharan IK. The Drosophila Mst ortholog, hippo, restricts growth and cell proliferation and promotes apoptosis. Cell. 2003;114(4):457-67.
33. Huang J, Wu S, Barrera J, Matthews K, Pan D. The Hippo signaling pathway coordinately regulates cell proliferation and apoptosis by inactivating Yorkie, the Drosophila Homolog of YAP. Cell. 2005;122(3):421-34.
34. Zhao B, Ye X, Yu J, Li L, Li W, Li S, et al. TEAD mediates YAP-dependent gene induction and growth control. Genes Dev. 2008;22(14):1962-71.
35. Yu FX, Zhao B, Guan KL. Hippo Pathway in Organ Size Control, Tissue Homeostasis, and Cancer. Cell. 2015;163(4):811-28.
36. Zhao B, Li L, Lei Q, Guan KL. The Hippo-YAP pathway in organ size control and tumorigenesis: an updated version. Genes Dev. 2010;24(9):862-74.
37. Liu-Chittenden Y, Huang B, Shim JS, Chen Q, Lee SJ, Anders RA, et al. Genetic and pharmacological disruption of the TEAD-YAP complex suppresses the oncogenic activity of YAP. Genes Dev. 2012;26(12):1300-5.

38. Weiler SME, Pinna F, Wolf T, Lutz T, Geldiyev A, Sticht C, et al. Induction of Chromosome Instability by Activation of Yes-Associated Protein and Forkhead Box M1 in Liver Cancer. Gastroenterology. 2017;152(8):2037-51 e22.
39. Zhao B, Wei X, Li W, Udan RS, Yang Q, Kim J, et al. Inactivation of YAP oncoprotein by the Hippo pathway is involved in cell contact inhibition and tissue growth control. Genes Dev. 2007;21(21):2747-61.
40. Piccolo S, Dupont S, Cordenonsi M. The biology of YAP/TAZ: hippo signaling and beyond. Physiological reviews. 2014;94(4):1287-312.
41. Sorrentino G, Ruggeri N, Specchia V, Cordenonsi M, Mano M, Dupont S, et al. Metabolic control of YAP and TAZ by the mevalonate pathway. Nature cell biology. 2014;16(4):357-66.
42. Makita R, Uchijima Y, Nishiyama K, Amano T, Chen Q, Takeuchi T, et al. Multiple renal cysts, urinary concentration defects, and pulmonary emphysematous changes in mice lacking TAZ. American journal of physiology Renal physiology. 2008;294(3):F542-53.
43. Morin-Kensicki EM, Boone BN, Howell M, Stonebraker JR, Teed J, Alb JG, et al. Defects in yolk sac vasculogenesis, chorioallantoic fusion, and embryonic axis elongation in mice with targeted disruption of Yap65. Molecular and cellular biology. 2006;26(1):77-87.
44. McPherson JP, Tamblyn L, Elia A, Migon E, Shehabeldin A, Matysiak-Zablocki E, et al. Lats2/Kpm is required for embryonic development, proliferation control and genomic integrity. The EMBO journal. 2004;23(18):3677-88.
45. Nishio M, Hamada K, Kawahara K, Sasaki M, Noguchi F, Chiba S, et al. Cancer susceptibility and embryonic lethality in Mob1a/1b double-mutant mice. The Journal of clinical investigation. 2012;122(12):4505-18.
46. Lee JH, Kim TS, Yang TH, Koo BK, Oh SP, Lee KP, et al. A crucial role of WW45 in developing epithelial tissues in the mouse. The EMBO journal. 2008;27(8):1231-42.
47. Oh S, Lee D, Kim T, Kim TS, Oh HJ, Hwang CY, et al. Crucial role for Mst1 and Mst2 kinases in early embryonic development of the mouse. Molecular and cellular biology. 2009;29(23):6309-20.
48. Song H, Mak KK, Topol L, Yun K, Hu J, Garrett L, et al. Mammalian Mst1 and Mst2 kinases play essential roles in organ size control and tumor suppression. Proceedings of the National Academy of Sciences of the United States of America. 2010;107(4):1431-6.
49. Zhou D, Conrad C, Xia F, Park JS, Payer B, Yin Y, et al. Mst1 and Mst2 maintain hepatocyte quiescence and suppress hepatocellular carcinoma development through inactivation of the Yap1 oncogene. Cancer Cell. 2009;16(5):425-38.
50. Camargo FD, Gokhale S, Johnnidis JB, Fu D, Bell GW, Jaenisch R, et al. YAP1 increases organ size and expands undifferentiated progenitor cells. Current biology : CB. 2007;17(23):2054-60.
51. Michalopoulos GK. Liver regeneration. Journal of cellular physiology. 2007;213(2):286-300.
52. Grijalva JL, Huizenga M, Mueller K, Rodriguez S, Brazzo J, Camargo F, et al. Dynamic alterations in Hippo signaling pathway and YAP activation during liver regeneration. American journal of physiology Gastrointestinal and liver physiology. 2014;307(2):G196-204.
53. Hanahan D, Weinberg RA. Hallmarks of cancer: the next generation. Cell. 2011;144(5):646-74.
54. Jimenez-Velasco A, Roman-Gomez J, Agirre X, Barrios M, Navarro G, Vazquez I, et al. Downregulation of the large tumor suppressor 2 (LATS2/KPM) gene is associated with poor prognosis in acute lymphoblastic leukemia. Leukemia. 2005;19(12):2347-50.
55. Seidel C, Schagdarsurengin U, Blumke K, Wurl P, Pfeifer GP, Hauptmann S, et al. Frequent hypermethylation of MST1 and MST2 in soft tissue sarcoma. Molecular carcinogenesis. 2007;46(10):865-71.
56. Sasaki H, Kawano O, Endo K, Suzuki E, Yukiue H, Kobayashi Y, et al. Human MOB1 expression in non-small-cell lung cancer. Clinical lung cancer. 2007;8(4):273-6.
57. Kosaka Y, Mimori K, Tanaka F, Inoue H, Watanabe M, Mori M. Clinical significance of the loss of MATS1 mRNA expression in colorectal cancer. International journal of oncology. 2007;31(2):333-8.

58. Zanconato F, Cordenonsi M, Piccolo S. YAP/TAZ at the Roots of Cancer. Cancer Cell. 2016;29(6):783-803.
59. Takahashi Y, Miyoshi Y, Takahata C, Irahara N, Taguchi T, Tamaki Y, et al. Down-regulation of LATS1 and LATS2 mRNA expression by promoter hypermethylation and its association with biologically aggressive phenotype in human breast cancers. Clinical cancer research : an official journal of the American Association for Cancer Research. 2005;11(4):1380-5.
60. Zender L, Spector MS, Xue W, Flemming P, Cordon-Cardo C, Silke J, et al. Identification and validation of oncogenes in liver cancer using an integrative oncogenomic approach. Cell. 2006;125(7):1253-67.
61. Tschaharganeh DF, Chen X, Latzko P, Malz M, Gaida MM, Felix K, et al. Yes-associated protein up-regulates Jagged-1 and activates the Notch pathway in human hepatocellular carcinoma. Gastroenterology. 2013;144(7):1530-42 e12.
62. Steinhardt AA, Gayyed MF, Klein AP, Dong J, Maitra A, Pan D, et al. Expression of Yes-associated protein in common solid tumors. Human pathology. 2008;39(11):1582-9.
63. Chan SW, Lim CJ, Guo K, Ng CP, Lee I, Hunziker W, et al. A role for TAZ in migration, invasion, and tumorigenesis of breast cancer cells. Cancer research. 2008;68(8):2592-8.
64. Cordenonsi M, Zanconato F, Azzolin L, Forcato M, Rosato A, Frasson C, et al. The Hippo transducer TAZ confers cancer stem cell-related traits on breast cancer cells. Cell. 2011;147(4):759-72.
65. Li Z, Wang Y, Zhu Y, Yuan C, Wang D, Zhang W, et al. The Hippo transducer TAZ promotes epithelial to mesenchymal transition and cancer stem cell maintenance in oral cancer. Molecular oncology. 2015;9(6):1091-105.
66. Zhang X, Abdelrahman A, Vollmar B, Zechner D. The Ambivalent Function of YAP in Apoptosis and Cancer. International journal of molecular sciences. 2018;19(12).
67. Wang X, Zheng Z, Caviglia JM, Corey KE, Herfel TM, Cai B, et al. Hepatocyte TAZ/WWTR1 Promotes Inflammation and Fibrosis in Nonalcoholic Steatohepatitis. Cell metabolism. 2016;24(6):848-62.
68. Lee KP, Lee JH, Kim TS, Kim TH, Park HD, Byun JS, et al. The Hippo-Salvador pathway restrains hepatic oval cell proliferation, liver size, and liver tumorigenesis. Proceedings of the National Academy of Sciences of the United States of America. 2010;107(18):8248-53.
69. Stemmer M, Thumberger T, Del Sol Keyer M, Wittbrodt J, Mateo JL. CCTop: An Intuitive, Flexible and Reliable CRISPR/Cas9 Target Prediction Tool. PloS one. 2015;10(4):e0124633.
70. Papadopoulos JS, Agarwala R. COBALT: constraint-based alignment tool for multiple protein sequences. Bioinformatics (Oxford, England). 2007;23(9):1073-9.
71. Khan A, Fornes O, Stigliani A, Gheorghe M, Castro-Mondragon JA, van der Lee R, et al. JASPAR 2018: update of the open-access database of transcription factor binding profiles and its web framework. Nucleic acids research. 2018;46(D1):D260-D6.
72. Roessler S, Jia HL, Budhu A, Forgues M, Ye QH, Lee JS, et al. A unique metastasis gene signature enables prediction of tumor relapse in early-stage hepatocellular carcinoma patients. Cancer research. 2010;70(24):10202-12.
73. Vandesompele J, De Preter K, Pattyn F, Poppe B, Van Roy N, De Paepe A, et al. Accurate normalization of real-time quantitative RT-PCR data by geometric averaging of multiple internal control genes. Genome biology. 2002;3(7):RESEARCH0034.
74. Sandelin A, Alkema W, Engstrom P, Wasserman WW, Lenhard B. JASPAR: an open-access database for eukaryotic transcription factor binding profiles. Nucleic acids research. 2004;32(Database issue):D91-4.
75. Schindelin J, Arganda-Carreras I, Frise E, Kaynig V, Longair M, Pietzsch T, et al. Fiji: an open-source platform for biological-image analysis. Nature methods. 2012;9(7):676-82.

76. Dai M, Wang P, Boyd AD, Kostov G, Athey B, Jones EG, et al. Evolving gene/transcript definitions significantly alter the interpretation of GeneChip data. Nucleic acids research. 2005;33(20):e175.
77. Badouel C, Garg A, McNeill H. Herding Hippos: regulating growth in flies and man. Current opinion in cell biology. 2009;21(6):837-43.
78. Bell SD, Botchan MR. The minichromosome maintenance replicative helicase. Cold Spring Harbor perspectives in biology. 2013;5(11):a012807.
79. Pasini D, Bracken AP, Jensen MR, Lazzerini Denchi E, Helin K. Suz12 is essential for mouse development and for EZH2 histone methyltransferase activity. The EMBO journal. 2004;23(20):4061-71.
80. Kodaka M, Hata Y. The mammalian Hippo pathway: regulation and function of YAP1 and TAZ. Cellular and molecular life sciences : CMLS. 2015;72(2):285-306.
81. Gibault F, Corvaisier M, Bailly F, Huet G, Melnyk P, Cotelle P. Non-Photoinduced Biological Properties of Verteporfin. Current medicinal chemistry. 2016;23(11):1171-84.
82. Sauvageau M, Sauvageau G. Polycomb group proteins: multi-faceted regulators of somatic stem cells and cancer. Cell stem cell. 2010;7(3):299-313.
83. Knutson SK, Warholic NM, Wigle TJ, Klaus CR, Allain CJ, Raimondi A, et al. Durable tumor regression in genetically altered malignant rhabdoid tumors by inhibition of methyltransferase EZH2. Proceedings of the National Academy of Sciences of the United States of America. 2013;110(19):7922-7.
84. Zhao C, Dahlman-Wright K. Liver X receptor in cholesterol metabolism. The Journal of endocrinology. 2010;204(3):233-40.
85. Bobin-Dubigeon C, Chauvin A, Brillaud-Meflah V, Boiffard F, Joalland MP, Bard JM. Liver X Receptor (LXR)-regulated Genes of Cholesterol Trafficking and Breast Cancer Severity. Anticancer research. 2017;37(10):5495-8.
86. Maine GT, Sinha P, Tye BK. Mutants of S. cerevisiae defective in the maintenance of minichromosomes. Genetics. 1984;106(3):365-85.
87. Forsburg SL. Eukaryotic MCM proteins: beyond replication initiation. Microbiology and molecular biology reviews : MMBR. 2004;68(1):109-31.
88. Freeman A, Morris LS, Mills AD, Stoeber K, Laskey RA, Williams GH, et al. Minichromosome maintenance proteins as biological markers of dysplasia and malignancy. Clinical cancer research : an official journal of the American Association for Cancer Research. 1999;5(8):2121-32.
89. Quaglia A, McStay M, Stoeber K, Loddo M, Caplin M, Fanshawe T, et al. Novel markers of cell kinetics to evaluate progression from cirrhosis to hepatocellular carcinoma. Liver international : official journal of the International Association for the Study of the Liver. 2006;26(4):424-32.
90. Liu Z, Li J, Chen J, Shan Q, Dai H, Xie H, et al. MCM family in HCC: MCM6 indicates adverse tumor features and poor outcomes and promotes S/G2 cell cycle progression. BMC cancer. 2018;18(1):200.
91. Zhou YM, Zhang XF, Cao L, Li B, Sui CJ, Li YM, et al. MCM7 expression predicts post-operative prognosis for hepatocellular carcinoma. Liver international : official journal of the International Association for the Study of the Liver. 2012;32(10):1505-9.
92. Liao X, Liu X, Yang C, Wang X, Yu T, Han C, et al. Distinct Diagnostic and Prognostic Values of Minichromosome Maintenance Gene Expression in Patients with Hepatocellular Carcinoma. Journal of Cancer. 2018;9(13):2357-73.
93. Dehan E, Ben-Dor A, Liao W, Lipson D, Frimer H, Rienstein S, et al. Chromosomal aberrations and gene expression profiles in non-small cell lung cancer. Lung cancer (Amsterdam, Netherlands). 2007;56(2):175-84.
94. Cheng L, Wang P, Yang S, Yang Y, Zhang Q, Zhang W, et al. Identification of genes with a correlation between copy number and expression in gastric cancer. BMC medical genomics. 2012;5:14.
95. Tamilzhalagan S, Rathinam D, Ganesan K. Amplified 7q21-22 gene MCM7 and its intronic miR-25 suppress COL1A2 associated genes to sustain intestinal gastric cancer features. Molecular carcinogenesis. 2017;56(6):1590-602.

96. Liu Y, Richards TA, Aves SJ. Ancient diversification of eukaryotic MCM DNA replication proteins. BMC evolutionary biology. 2009;9:60.
97. Petrocca F, Visone R, Onelli MR, Shah MH, Nicoloso MS, de Martino I, et al. E2F1-regulated microRNAs impair TGFbeta-dependent cell-cycle arrest and apoptosis in gastric cancer. Cancer Cell. 2008;13(3):272-86.
98. Ohtani K, Iwanaga R, Nakamura M, Ikeda M, Yabuta N, Tsuruga H, et al. Cell growth-regulated expression of mammalian MCM5 and MCM6 genes mediated by the transcription factor E2F. Oncogene. 1999;18(14):2299-309.
99. Laresgoiti U, Apraiz A, Olea M, Mitxelena J, Osinalde N, Rodriguez JA, et al. E2F2 and CREB cooperatively regulate transcriptional activity of cell cycle genes. Nucleic acids research. 2013;41(22):10185-98.
100. Ehmer U, Sage J. Control of Proliferation and Cancer Growth by the Hippo Signaling Pathway. Molecular cancer research : MCR. 2016;14(2):127-40.
101. Carter SL, Eklund AC, Kohane IS, Harris LN, Szallasi Z. A signature of chromosomal instability inferred from gene expression profiles predicts clinical outcome in multiple human cancers. Nature genetics. 2006;38(9):1043-8.
102. Fragkos M, Ganier O, Coulombe P, Mechali M. DNA replication origin activation in space and time. Nat Rev Mol Cell Biol. 2015;16(6):360-74.
103. Picard F, Cadoret JC, Audit B, Arneodo A, Alberti A, Battail C, et al. The spatiotemporal program of DNA replication is associated with specific combinations of chromatin marks in human cells. PLoS genetics. 2014;10(5):e1004282.
104. Moreno SP, Bailey R, Campion N, Herron S, Gambus A. Polyubiquitylation drives replisome disassembly at the termination of DNA replication. Science (New York, NY). 2014;346(6208):477-81.
105. Braun KA, Breeden LL. Nascent transcription of MCM2-7 is important for nuclear localization of the minichromosome maintenance complex in G1. Molecular biology of the cell. 2007;18(4):1447-56.
106. Hardy T, Mann DA. Epigenetics in liver disease: from biology to therapeutics. Gut. 2016;65(11):1895-905.
107. Wu C, Morris JR. Genes, genetics, and epigenetics: a correspondence. Science (New York, NY). 2001;293(5532):1103-5.
108. Egger G, Liang G, Aparicio A, Jones PA. Epigenetics in human disease and prospects for epigenetic therapy. Nature. 2004;429(6990):457-63.
109. Dupont C, Armant DR, Brenner CA. Epigenetics: definition, mechanisms and clinical perspective. Seminars in reproductive medicine. 2009;27(5):351-7.
110. Kassis JA, Kennison JA, Tamkun JW. Polycomb and Trithorax Group Genes in Drosophila. Genetics. 2017;206(4):1699-725.
111. Schuettengruber B, Chourrout D, Vervoort M, Leblanc B, Cavalli G. Genome regulation by polycomb and trithorax proteins. Cell. 2007;128(4):735-45.
112. Margueron R, Li G, Sarma K, Blais A, Zavadil J, Woodcock CL, et al. Ezh1 and Ezh2 maintain repressive chromatin through different mechanisms. Molecular cell. 2008;32(4):503-18.
113. O'Carroll D, Erhardt S, Pagani M, Barton SC, Surani MA, Jenuwein T. The polycomb-group gene Ezh2 is required for early mouse development. Molecular and cellular biology. 2001;21(13):4330-6.
114. Yu W, Zhang F, Wang S, Fu Y, Chen J, Liang X, et al. Depletion of polycomb repressive complex 2 core component EED impairs fetal hematopoiesis. Cell death & disease. 2017;8(4):e2744.
115. Raaphorst FM, Meijer CJ, Fieret E, Blokzijl T, Mommers E, Buerger H, et al. Poorly differentiated breast carcinoma is associated with increased expression of the human polycomb group EZH2 gene. Neoplasia (New York, NY). 2003;5(6):481-8.

116. Varambally S, Dhanasekaran SM, Zhou M, Barrette TR, Kumar-Sinha C, Sanda MG, et al. The polycomb group protein EZH2 is involved in progression of prostate cancer. Nature. 2002;419(6907):624-9.
117. Dukers DF, van Galen JC, Giroth C, Jansen P, Sewalt RG, Otte AP, et al. Unique polycomb gene expression pattern in Hodgkin's lymphoma and Hodgkin's lymphoma-derived cell lines. The American journal of pathology. 2004;164(3):873-81.
118. Au SL, Wong CC, Lee JM, Fan DN, Tsang FH, Ng IO, et al. Enhancer of zeste homolog 2 epigenetically silences multiple tumor suppressor microRNAs to promote liver cancer metastasis. Hepatology (Baltimore, Md). 2012;56(2):622-31.
119. Sasaki M, Ikeda H, Itatsu K, Yamaguchi J, Sawada S, Minato H, et al. The overexpression of polycomb group proteins Bmi1 and EZH2 is associated with the progression and aggressive biological behavior of hepatocellular carcinoma. Laboratory investigation; a journal of technical methods and pathology. 2008;88(8):873-82.
120. Cai MY, Hou JH, Rao HL, Luo RZ, Li M, Pei XQ, et al. High expression of H3K27me3 in human hepatocellular carcinomas correlates closely with vascular invasion and predicts worse prognosis in patients. Molecular medicine (Cambridge, Mass). 2011;17(1-2):12-20.
121. Xu K, Wu ZJ, Groner AC, He HH, Cai C, Lis RT, et al. EZH2 oncogenic activity in castration-resistant prostate cancer cells is Polycomb-independent. Science (New York, NY). 2012;338(6113):1465-9.
122. Kim J, Lee Y, Lu X, Song B, Fong KW, Cao Q, et al. Polycomb- and Methylation-Independent Roles of EZH2 as a Transcription Activator. Cell reports. 2018;25(10):2808-20.e4.
123. Chen Y, Lin MC, Yao H, Wang H, Zhang AQ, Yu J, et al. Lentivirus-mediated RNA interference targeting enhancer of zeste homolog 2 inhibits hepatocellular carcinoma growth through down-regulation of stathmin. Hepatology (Baltimore, Md). 2007;46(1):200-8.
124. Bracken AP, Pasini D, Capra M, Prosperini E, Colli E, Helin K. EZH2 is downstream of the pRB-E2F pathway, essential for proliferation and amplified in cancer. The EMBO journal. 2003;22(20):5323-35.
125. Kirmizis A, Bartley SM, Farnham PJ. Identification of the polycomb group protein SU(Z)12 as a potential molecular target for human cancer therapy. Molecular cancer therapeutics. 2003;2(1):113-21.
126. Campbell S, Ismail IH, Young LC, Poirier GG, Hendzel MJ. Polycomb repressive complex 2 contributes to DNA double-strand break repair. Cell cycle (Georgetown, Tex). 2013;12(16):2675-83.
127. Wang T, Mao B, Cheng C, Zou Z, Gao J, Yang Y, et al. YAP promotes breast cancer metastasis by repressing growth differentiation factor-15. Biochimica et biophysica acta Molecular basis of disease. 2018;1864(5 Pt A):1744-53.
128. Kim M, Kim T, Johnson RL, Lim DS. Transcriptional co-repressor function of the hippo pathway transducers YAP and TAZ. Cell reports. 2015;11(2):270-82.
129. Atlasi Y, Stunnenberg HG. The interplay of epigenetic marks during stem cell differentiation and development. Nature reviews Genetics. 2017;18(11):643-58.
130. Kanwal R, Gupta K, Gupta S. Cancer epigenetics: an introduction. Methods in molecular biology (Clifton, NJ). 2015;1238:3-25.
131. Strahl BD, Allis CD. The language of covalent histone modifications. Nature. 2000;403(6765):41-5.
132. Marmorstein R, Trievel RC. Histone modifying enzymes: structures, mechanisms, and specificities. Biochimica et biophysica acta. 2009;1789(1):58-68.
133. Kirmizis A, Bartley SM, Kuzmichev A, Margueron R, Reinberg D, Green R, et al. Silencing of human polycomb target genes is associated with methylation of histone H3 Lys 27. Genes Dev. 2004;18(13):1592-605.
134. Bracken AP, Dietrich N, Pasini D, Hansen KH, Helin K. Genome-wide mapping of Polycomb target genes unravels their roles in cell fate transitions. Genes Dev. 2006;20(9):1123-36.

135. Mani SK, Zhang H, Diab A, Pascuzzi PE, Lefrancois L, Fares N, et al. EpCAM-regulated intramembrane proteolysis induces a cancer stem cell-like gene signature in hepatitis B virus-infected hepatocytes. Journal of hepatology. 2016;65(5):888-98.
136. Brodowska K, Al-Moujahed A, Marmalidou A, Meyer Zu Horste M, Cichy J, Miller JW, et al. The clinically used photosensitizer Verteporfin (VP) inhibits YAP-TEAD and human retinoblastoma cell growth in vitro without light activation. Experimental eye research. 2014;124:67-73.
137. Lu L, Finegold MJ, Johnson RL. Hippo pathway coactivators Yap and Taz are required to coordinate mammalian liver regeneration. Experimental & molecular medicine. 2018;50(1):e423.
138. Ge XQ, Jackson DA, Blow JJ. Dormant origins licensed by excess Mcm2-7 are required for human cells to survive replicative stress. Genes Dev. 2007;21(24):3331-41.
139. Fioravanti R, Stazi G, Zwergel C, Valente S, Mai A. Six Years (2012-2018) of Researches on Catalytic EZH2 Inhibitors: The Boom of the 2-Pyridone Compounds. Chemical record (New York, NY). 2018;18(12):1818-32.
140. Tan J, Yang X, Zhuang L, Jiang X, Chen W, Lee PL, et al. Pharmacologic disruption of Polycomb-repressive complex 2-mediated gene repression selectively induces apoptosis in cancer cells. Genes Dev. 2007;21(9):1050-63.
141. Kim KH, Roberts CW. Targeting EZH2 in cancer. Nat Med. 2016;22(2):128-34.
142. Italiano A, Soria JC, Toulmonde M, Michot JM, Lucchesi C, Varga A, et al. Tazemetostat, an EZH2 inhibitor, in relapsed or refractory B-cell non-Hodgkin lymphoma and advanced solid tumours: a first-in-human, open-label, phase 1 study. The Lancet Oncology. 2018;19(5):649-59.
143. Qi W, Zhao K, Gu J, Huang Y, Wang Y, Zhang H, et al. An allosteric PRC2 inhibitor targeting the H3K27me3 binding pocket of EED. Nature chemical biology. 2017;13(4):381-8.
144. Li L, Zhang H, Zhang M, Zhao M, Feng L, Luo X, et al. Discovery and Molecular Basis of a Diverse Set of Polycomb Repressive Complex 2 Inhibitors Recognition by EED. PloS one. 2017;12(1):e0169855.
145. He Y, Selvaraju S, Curtin ML, Jakob CG, Zhu H, Comess KM, et al. The EED protein-protein interaction inhibitor A-395 inactivates the PRC2 complex. Nature chemical biology. 2017;13(4):389-95.

9 Acknowledgements

Für die Möglichkeit die vorliegende Arbeit am Pathologischen Institut des Universitätsklinikums Heidelberg anfertigen zu dürfen, möchte ich mich bei dem Institutsleiter Prof. Dr. Peter Schirmacher und dem Arbeitsgruppenleiter Prof. Dr. Kai Breuhahn herzlich bedanken.

Mein besonderer Dank gilt Prof. Dr. Kai Breuhahn, der mir dieses interessante Projekt ermöglicht und diese Dissertation begutachtet hat. Besonders dankbar bin ich für die konstruktiven Ratschläge, die produktive Arbeitsumgebung und das in mich gesetzte Vertrauen.

Mein weiterer Dank gilt meinem Doktorvater Prof. Dr. Ralf Bartenschlager für seine Bereitschaft, diese Dissertation zu begutachten und vor der Biowissenschaftlichen Fakultät der Universität Heidelberg zu vertreten. Die konstruktiven Anregungen während der TAC-Meetings haben wesentlich zum Gelingen dieser Arbeit beigetragen.

Weiterhin möchte ich mich bei Prof. Dr. Alwin Krämer bedanken, der mich als Mitglied meines TAC-Komitees bei dem Fortschritt dieser Arbeit unterstützt hat.

Bei Frau Prof. Dr. Michaela Frye und Herrn Prof. Dr. Stefan Wölfl möchte ich danken für ihre Bereitschaft als Prüfer in meiner Disputation zu fungieren.

Außerdem danke ich dem Team von HBIGS für die Fortbildungen und organisatorische Unterstützung.

Für die Durchführung und Auswertung der Microarrays möchte ich mich bei Dr. Carolina de la Torre und Dr. Carsten Sticht bedanken. Für die unkomplizierte Zusammenarbeit bei den IHC-Färbungen danke ich Heike Conrad und dem IHC-Team.

Ohne die Unterstützung und die unkomplizierte Zusammenarbeit im Labor hätte sich mein Thema nicht zu diesem Projekt entwickeln können. Danken möchte ich Michaela für die konstante Unterstützung und die hilfreichen Ratschläge. Außerdem möchte ich Sarah für die Begleitung speziell im CRISPR/Cas Projekt danken. Jenny, Christina und Georg danke ich für die unermüdliche Unterstützung bei den MCM-Klonierungen. Danken möchte ich auch Anna und Clemens für das in mich gesetzte Vertrauen und die Möglichkeit zu unterrichten. Besonders möchte ich mich bei meinen Weggefährten bedanken, insbesondere Sofia, Stefan, Margarita, Shan, Lisi, Caro, Sarah und Feli, die mich immer mit Rat und Tat unterstützt haben. Außerdem danke ich Ariane, Eva, Geli und allen anderen Labormitgliedern der AG Roessler, AG Singer, AG Longerich und AG Tschaharganeh. Weiterhin möchte ich mich bei Clarissa, Minakshi und allen Freunden bedanken, die mich auch außerhalb des Laboralltags auf meinem Weg begleitet und unterstützt haben.

Acknowledgements

Ein ganz besonderer Dank gilt meinen Eltern und meiner Schwester Anna, die mich unermüdlich und selbstlos in allen Lebenslagen unterstützt haben. Ohne diesen bedingungslosen Rückhalt wäre diese Arbeit nicht möglich gewesen.

10 Appendix

Table 37: 66 genes significantly upregulated upon SUZ12, EZH2 and YAP inhibition.

Gene Symbol	Gene name	CHR	REFSEQ-ID
A1CF	APOBEC1 complementation factor	10	NM_001198818
AHSG	alpha 2-HS glycoprotein	3	NM_001354571
ALB	albumin	4	NM_000477
ALCAM	activated leukocyte cell adhesion molecule	3	NM_001243280
ALDH2	aldehyde dehydrogenase 2 family	12	NM_000690
AMBP	alpha-1-microglobulin/bikunin precursor	9	NM_001633
APOH	apolipoprotein H	17	NM_000042
ATF2	activating transcription factor 2	2	NM_001256090
ATP11C	ATPase phospholipid transporting 11C	X	NM_001010986
ATP7B	ATPase copper transporting beta	13	NM_000053
ATRN	attractin	20	NM_001207047
C11orf54	chromosome 11 open reading frame 54	11	NM_001286067
C1S	complement C1s	12	NM_001346850
C2	complement C2	6	NM_000063
C5	complement C5	9	NM_001317163
C6orf62	chromosome 6 open reading frame 62	6	NM_030939
CASK	calcium/calmodulin dependent serine prot	X	NM_001126054
CLOCK	clock circadian regulator	4	NM_001267843
CPQ	carboxypeptidase Q	8	NM_016134
CYP27A1	cytochrome P450 family 27 subfamily A member 1	2	NM_000784
DHRS3	dehydrogenase/reductase 3	1	NM_001319225
EML6	echinoderm microtubule associated protein 6	2	NM_001039753
EMSY	EMSY, BRCA2 interacting transcriptional	11	NM_001300942
ERAP1	endoplasmic reticulum aminopeptidase 1	5	NM_001040458
F10	coagulation factor X	13	NM_000504
F5	coagulation factor V	1	NM_000130
FAM3B	family with sequence similarity 3 member B	21	NM_058186
FST	follistatin	5	NM_006350
GPR160	G protein-coupled receptor 160	3	NM_014373
IGSF1	immunoglobulin superfamily member 1	X	NM_001170961
INPP5A	inositol polyphosphate-5-phosphatase A	10	NM_001321042
ITIH2	inter-alpha-trypsin inhibitor heavy chai	10	NM_002216
KANK4	KN motif and ankyrin repeat domains 4	1	NM_001320269
LRP1	LDL receptor related protein 1	12	NM_002332

MAPK8	mitogen-activated protein kinase 8	10	NM_001278547
MGC12916	uncharacterized protein MGC12916	17	NM_032729
MTTP	microsomal triglyceride transfer protein	4	NM_000253
NDST1	N-deacetylase and N-sulfotransferase 1	5	NM_001301063
NFE2L2	nuclear factor, erythroid 2 like 2	2	NM_001145412
ORM1	orosomucoid 1	9	NM_000607
ORM2	orosomucoid 2	9	NM_000608
PALMD	palmdelphin	1	NM_017734
PIP4K2B	phosphatidylinositol-5-phosphate 4-kinase type 2 beta	17	NM_003559
PTPRF	protein tyrosine phosphatase receptor type	1	NM_001329137
RALGAPA2	Ral GTPase activating protein catalytic	20	NM_020343
RAPGEF1	Rap guanine nucleotide exchange factor 1	9	NM_001304275
RMND5A	required for meiotic nuclear division 5	2	NM_022780
ROBO1	roundabout guidance receptor 1	3	NM_001145845
SCARNA9	small Cajal body-specific RNA 9	11	NR_002569
SEC11C	SEC11 homolog C, signal peptidase complex subunit	18	NM_001307941
SERPINA4	serpin family A member 4	14	NM_001289032
SERPIND1	serpin family D member 1	22	NM_000185
SERPINF1	serpin family F member 1	17	NM_001329903
SERPINI1	serpin family I member 1	3	NM_001122752
SLC5A9	solute carrier family 5 member 9	1	NM_001011547
SMLR1	small leucine rich protein 1	6	NM_001195597
SNORA47	small nucleolar RNA, H/ACA box 47	5	NR_003014
SNORA49	small nucleolar RNA, H/ACA box 49	12	NR_002979
STK38L	serine/threonine kinase 38 like	12	NM_015000
TAF11	TATA-box binding protein associated fact	6	NM_001270488
TEX2	testis expressed 2	17	NM_001288732
TF	transferrin	3	NM_001063
TTC3	tetratricopeptide repeat domain 3	21	NM_001001894
VEGFA	vascular endothelial growth factor A	6	NM_001025366
WASF3	WAS protein family member 3	13	NM_001291965
ZNF217	zinc finger protein 217	20	NM_006526

Table 38: Fold-change and adjusted p-values (FDP) of 66 significantly upregulated genes.

	#1 EZH2		#2 EZH2		#1 SUZ12		#2 SUZ12		#1 YAP		#2 YAP	
Gene Symbol	fold-change	FDR	fold-change	FDR	fold-change	FDR	fold-change	FDR	fold-change	FDR	fold-change	FDR
A1CF	1,05	0,000	1,12	0,000	1,08	0,000	1,06	0,000	1,06	0,000	1,17	0,000
AHSG	1,01	0,031	1,05	0,000	1,03	0,000	1,03	0,000	1,03	0,000	1,06	0,000
ALB	1,05	0,000	1,08	0,000	1,11	0,000	1,03	0,000	1,04	0,000	1,08	0,000
ALCAM	1,06	0,000	1,09	0,000	1,11	0,000	1,08	0,000	1,07	0,000	1,14	0,000
ALDH2	1,02	0,037	1,10	0,000	1,07	0,000	1,04	0,000	1,02	0,009	1,03	0,001
AMBP	1,06	0,000	1,03	0,001	1,07	0,000	1,03	0,002	1,02	0,045	1,09	0,000
APOH	1,05	0,000	1,06	0,000	1,04	0,000	1,04	0,000	1,03	0,000	1,07	0,000
ATF2	1,05	0,000	1,05	0,000	1,05	0,000	1,03	0,001	1,03	0,003	1,06	0,000
ATP11C	1,03	0,019	1,04	0,002	1,07	0,000	1,04	0,002	1,06	0,000	1,04	0,003
ATP7B	1,02	0,027	1,08	0,000	1,03	0,002	1,04	0,000	1,02	0,007	1,07	0,000
ATRN	1,03	0,000	1,02	0,002	1,03	0,001	1,03	0,002	1,02	0,018	1,04	0,000
C11orf54	1,07	0,000	1,08	0,000	1,08	0,000	1,04	0,018	1,06	0,001	1,08	0,000
C1S	1,07	0,000	1,30	0,000	1,39	0,000	1,12	0,000	1,04	0,015	1,10	0,000
C2	1,05	0,000	1,12	0,000	1,10	0,000	1,06	0,000	1,04	0,001	1,10	0,000
C5	1,15	0,000	1,09	0,000	1,19	0,000	1,08	0,000	1,07	0,001	1,10	0,000
C6orf62	1,05	0,000	1,04	0,000	1,05	0,000	1,06	0,000	1,04	0,000	1,02	0,002
CASK	1,05	0,000	1,05	0,000	1,04	0,000	1,10	0,000	1,04	0,001	1,05	0,000
CLOCK	1,02	0,007	1,04	0,000	1,06	0,000	1,02	0,010	1,05	0,000	1,02	0,012
CPQ	1,02	0,029	1,05	0,000	1,05	0,000	1,03	0,002	1,02	0,029	1,05	0,000
CYP27A1	1,04	0,002	1,10	0,000	1,11	0,000	1,04	0,001	1,05	0,000	1,10	0,000
DHRS3	1,04	0,000	1,03	0,008	1,08	0,000	1,04	0,001	1,03	0,018	1,04	0,000
EML6	1,03	0,006	1,15	0,000	1,17	0,000	1,08	0,000	1,04	0,001	1,10	0,000
EMSY	1,06	0,000	1,04	0,016	1,07	0,000	1,05	0,001	1,04	0,002	1,05	0,001
ERAP1	1,04	0,003	1,06	0,000	1,04	0,003	1,04	0,002	1,04	0,005	1,05	0,000
F10	1,05	0,002	1,10	0,000	1,06	0,000	1,04	0,020	1,06	0,000	1,17	0,000

F5	1,04	0,001	1,07	0,000	1,04	0,001	1,04	0,000	1,02	0,034	1,13	0,000
FAM3B	1,06	0,006	1,09	0,000	1,07	0,001	1,06	0,003	1,06	0,004	1,17	0,000
FST	1,13	0,000	1,16	0,000	1,16	0,000	1,11	0,000	1,09	0,000	1,12	0,000
GPR160	1,06	0,000	1,03	0,031	1,06	0,000	1,05	0,000	1,03	0,031	1,04	0,004
IGSF1	1,13	0,000	1,17	0,000	1,18	0,000	1,12	0,000	1,09	0,000	1,26	0,000
INPP5A	1,06	0,000	1,06	0,000	1,06	0,000	1,08	0,000	1,04	0,000	1,07	0,000
ITIH2	1,07	0,000	1,07	0,000	1,08	0,000	1,03	0,000	1,06	0,000	1,06	0,000
KANK4	1,06	0,000	1,16	0,000	1,05	0,001	1,06	0,000	1,04	0,008	1,08	0,000
LRP1	1,04	0,006	1,10	0,000	1,03	0,014	1,05	0,000	1,03	0,037	1,07	0,000
MAPK8	1,07	0,000	1,08	0,000	1,06	0,000	1,08	0,000	1,07	0,000	1,06	0,000
MGC12916	1,06	0,001	1,11	0,000	1,09	0,000	1,09	0,000	1,08	0,000	1,05	0,002
MTTP	1,12	0,000	1,20	0,000	1,10	0,001	1,14	0,000	1,15	0,000	1,37	0,000
NDST1	1,05	0,000	1,05	0,000	1,03	0,002	1,02	0,008	1,04	0,000	1,04	0,000
NFE2L2	1,04	0,000	1,06	0,000	1,03	0,000	1,02	0,018	1,02	0,019	1,04	0,000
ORM1	1,04	0,000	1,06	0,000	1,05	0,000	1,05	0,000	1,02	0,008	1,03	0,000
ORM2	1,06	0,000	1,07	0,000	1,07	0,000	1,07	0,000	1,04	0,000	1,06	0,000
PALMD	1,06	0,000	1,06	0,000	1,13	0,000	1,05	0,000	1,03	0,014	1,15	0,000
PIP4K2B	1,02	0,031	1,02	0,003	1,02	0,039	1,04	0,000	1,03	0,000	1,03	0,000
PTPRF	1,04	0,000	1,04	0,001	1,03	0,008	1,05	0,000	1,02	0,033	1,03	0,008
RALGAPA2	1,06	0,000	1,03	0,012	1,04	0,000	1,07	0,000	1,03	0,004	1,03	0,001
RAPGEF1	1,02	0,022	1,04	0,000	1,04	0,000	1,05	0,000	1,03	0,005	1,04	0,000
RMND5A	1,11	0,000	1,08	0,000	1,02	0,046	1,07	0,000	1,05	0,000	1,08	0,000
ROBO1	1,08	0,000	1,08	0,000	1,05	0,000	1,08	0,000	1,06	0,000	1,07	0,000
SCARNA9	1,12	0,000	1,10	0,000	1,16	0,000	1,08	0,004	1,08	0,005	1,09	0,001
SEC11C	1,04	0,023	1,09	0,000	1,05	0,006	1,06	0,000	1,05	0,002	1,09	0,000
SERPINA4	1,09	0,000	1,05	0,000	1,11	0,000	1,05	0,000	1,04	0,001	1,08	0,000
SERPIND1	1,07	0,000	1,06	0,000	1,12	0,000	1,03	0,010	1,03	0,001	1,11	0,000
SERPINF1	1,05	0,000	1,05	0,000	1,06	0,000	1,04	0,000	1,02	0,014	1,05	0,000

SERPINI1	1,05	0,029	1,15	0,000	1,17	0,000	1,05	0,025	1,06	0,003	1,20	0,000
SLC5A9	1,07	0,000	1,12	0,000	1,07	0,000	1,07	0,000	1,04	0,011	1,11	0,000
SMLR1	1,06	0,003	1,08	0,000	1,16	0,000	1,04	0,030	1,05	0,007	1,18	0,000
SNORA47	1,06	0,000	1,06	0,001	1,07	0,000	1,04	0,010	1,03	0,032	1,06	0,000
SNORA49	1,08	0,000	1,05	0,001	1,09	0,000	1,06	0,001	1,05	0,001	1,06	0,000
STK38L	1,06	0,000	1,05	0,001	1,08	0,000	1,08	0,000	1,08	0,000	1,08	0,000
TAF11	1,08	0,000	1,06	0,000	1,04	0,000	1,07	0,000	1,05	0,000	1,06	0,000
TEX2	1,04	0,000	1,05	0,000	1,03	0,002	1,06	0,000	1,04	0,000	1,06	0,000
TF	1,04	0,000	1,08	0,000	1,07	0,000	1,04	0,000	1,04	0,000	1,04	0,000
TTC3	1,05	0,000	1,04	0,002	1,04	0,001	1,04	0,000	1,04	0,002	1,04	0,002
VEGFA	1,02	0,009	1,06	0,000	1,03	0,001	1,02	0,031	1,03	0,002	1,02	0,029
WASF3	1,07	0,000	1,05	0,000	1,03	0,015	1,05	0,000	1,03	0,012	1,04	0,000
ZNF217	1,04	0,000	1,07	0,000	1,05	0,000	1,04	0,000	1,02	0,013	1,03	0,001

ERKLÄRUNG GEMÄß §8 (3b,c) DER PROMOTIONSORDNUNG

Hiermit erkläre ich, dass ich die vorgelegte Dissertation “Molecular downstream mechanisms of the oncogenic transcriptional regulators YAP/TAZ in hepatocarcinogenesis“ selbstständig verfasst und keine anderen als die angegebenen Quellen und Hilfsmittel benutzt habe. Des Weiteren bestätige ich, dass ich an keiner anderen Stelle ein Prüfungsverfahren beantragt bzw. die Dissertation in dieser oder einer anderen Form bereits als Prüfungsarbeit verwendet oder einer anderen Fakultät als Dissertation vorgelegt habe.

Heidelberg, den 02. Juni 2019

Maria Knaub